HURRICANE LOSS MITIGATION PROGRAM 2023 ANNUAL REPORT

January 1, 2024

Prepared by
Florida Division of Emergency Management

DIVISION HEADQUARTERS
2555 Shumard Oak Boulevard
Tallahassee, FL 32399-2100

Telephone: 850-815-4000
www.FloridaDisaster.org

STATE LOGISTICS RESPONSE CENTER
2702 Directors Row
Orlando, FL 32809-5631

TABLE OF CONTENTS

DIVISION HEADQUARTERS
2555 Shumard Oak Boulevard
Tallahassee, FL 32399-2100

Telephone: 850-815-4000
www.FloridaDisaster.org

STATE LOGISTICS RESPONSE CENTER
2702 Directors Row
Orlando, FL 32809-5631

EXECUTIVE SUMMARY

Pursuant to Subsection 215.559 (6), Florida Statutes (F.S.), this document provides a full report and accounting of activities and evaluation of such activities conducted by the Hurricane Loss Mitigation Program (HLMP). The period covered by this report is July 1, 2022, through June 20, 2023, or State Fiscal Year (FY) 2023. Section 215.559 (1), F.S., establishes the Hurricane Loss Mitigation Program in the Division of Emergency Management (Division). The Division receives an annual appropriation of $10 million from the investment income of the Florida Hurricane Catastrophe Fund, authorized under the Florida General Appropriation Act and section 215.555 (7) (c), F.S. The Shelter Development Program, Gulf Coast State College's (GCSC) Mobile Home Tie-Down Program, and Florida International University's (FIU) Hurricane Research Program account for a combined $6.5 million, or sixty-five (65%) percent of the FY 2023 $10 million appropriation. The remaining thirty-five (35%) percent distributed a community mitigation grant that includes flood and wind mitigation of Florida residences and public outreach and education about retrofits to citizens, local government officials, and their staff.

The Shelter Development Program and GCSC's Mobile Home Tie-Down Program have separate reporting requirements under Section 252.385, F.S., and Section 215.559(2)(a), F.S., respectively. This report includes a project analysis of the Shelter Development Program, an annual report for the GCSC Mobile Home Tie-Down Program, a detailed summary of FIU's Hurricane Research Program progress, and a programmatic analysis of the Hurricane Loss Mitigation Program.

DIVISION HEADQUARTERS
2555 Shumard Oak Boulevard
Tallahassee, FL 32399-2100

Telephone: 850-815-4000
www.FloridaDisaster.org

STATE LOGISTICS RESPONSE CENTER
2702 Directors Row
Orlando, FL 32809-5631

BACKGROUND

In the aftermath of Hurricane Andrew, the Florida Legislature created a series of programs to stabilize the economy and insurance industry. These programs consist of the following:

- Citizens Property Insurance Corporation (formed from a merger of the Florida Windstorm Underwriting Association and the Florida Residential Property and Casualty Joint Underwriting Association), the state insurance plan for residents unable to obtain a conventional homeowner's insurance policy;
- The Florida Hurricane Catastrophe Fund, Section 215.555 F.S., a re-insurance fund established to limit insurance exposure after a storm;
- The Bill Williams Residential Safety and Preparedness Act, which in 1999 created the Hurricane Loss Mitigation Program, Section 215.559 F. S., with an annual appropriation of $10 million.

Section 215.559 (1), F.S., establishes the Hurricane Loss Mitigation Program in the Division of Emergency Management (Division). The Division receives an annual appropriation of $10 million from the investment income of the Florida Hurricane Catastrophe Fund authorized under the Florida General Appropriation Act and Section 215.555 (7) (c) F. S. The annual appropriation provides funding to local governments, state agencies, public and private educational institutions, and non-profit organizations to support programs improving hurricane preparedness, reducing potential losses in the event of a hurricane, and providing research and education to reduce hurricane losses.

Specific Program Areas and Funding Levels

Shelter Development – Pursuant to Section 215.559(2)(a), F. S., $3 million of the annual $10 million appropriation for the Hurricane Loss Mitigation Program directs retrofits to existing facilities and construction of new facilities to enable them for use as public shelters. A report of the state's shelter development program, entitled the Shelter Development Report, is prepared annually and separately submitted to the Governor and the Legislature pursuant to Section 252.385, F.S. The remaining $7 million of the appropriation is allocated according to different subsections in Section 215.559, F. S., as described below.

Gulf Coast State College – Pursuant to Section 215.559(2)(a), F. S., GCSC receives an annual allocation of $2.8 million, or forty (40%) percent of the remaining $7 million. GCSC administers these funds and uses them to mitigate future losses for mobile homes and to provide tie-downs for mobile homes in communities throughout Florida. See Appendix A for GCSC'S FY 2023 Annual Report.

DIVISION HEADQUARTERS
2555 Shumard Oak Boulevard
Tallahassee, FL 32399-2100

Telephone: 850-815-4000
www.FloridaDisaster.org

STATE LOGISTICS RESPONSE CENTER
2702 Directors Row
Orlando, FL 32809-5631

Florida International University (FIU) – Pursuant to Section 215.559(3), F. S., FIU receives $700,000, or ten (10%) percent, of the remaining $7 million. FIU administers these funds and dedicates them to hurricane research at the Type I Center of the State University System to support hurricane loss reduction devices and techniques. See Appendix B for FIU's FY 2023 Final Report.

Hurricane Loss Mitigation Program (HLMP) – The remaining $3.5 million provides grant funding to governmental entities, non-profit organizations, and qualified for-profit organizations as a means to improve the resiliency of residential, community, and government structures within their communities. HLMP advertises funding through a Request for Proposal (RFP), which utilizes a Benefit-Cost Analysis (BCA) for each of the submitted projects to ensure that the recommended mitigation retrofits remain cost-effective.

DIVISION HEADQUARTERS
2555 Shumard Oak Boulevard
Tallahassee, FL 32399-2100

Telephone: 850-815-4000
www.FloridaDisaster.org

STATE LOGISTICS RESPONSE CENTER
2702 Directors Row
Orlando, FL 32809-5631

HURRICANE LOSS MITIGATION PROGRAM

PROGRAM ACTIVITIES

HLMP Funding Distribution

In June 2022, the Division issued a Request for Proposal (RFP) for Fiscal Year (FY) 2023 projects. A review panel appointed by the Division selected eligible applicants based on priority, need, benefit, and alignment with local mitigation strategy projects. Based on this evaluation process, 18 projects became eligible for funding. However, due to the limitation of funds, 15 of 18 were awarded.

Extensions for projects were granted as needed through December 31, 2022. The extensions were granted due to issues with supply chain issues and weather conditions that caused delays in the continuation construction throughout the year.

HLMP Outreach

In early 2023, multiple online webinars were held ahead of the 2023/2024 Request for Proposal (RFP) for potential applicants to learn more about the program. While scheduling kickoff meetings for the awarded FY 2023-2024 projects, the Division was able to hold several in person for the first time since 2018-2019. In doing so, the HLMP team was able to meet the recipients and some homeowners who had previously been part of the grant program. The team was also able to visit some of the locations and structures to be retrofitted.

The Program Manager of HLMP attended the 2023 Wall of Wind Challenge at FIU and was invited to be a guest judge for the event. This event is a judged competition for students to present strategies demonstrating mitigation concepts against hurricane force winds. The team also attended FIU's Eye of the Storm event, which is a community outreach event focused on presenting hurricane education, mitigation, and preparedness to the public.

Public Outreach efforts were also continued throughout the year utilizing the FloridaDisaster.org website. This site provides citizens and potential recipients with the information and forms required to apply for the HLMP program. It also includes an additional hurricane retrofit guide to help citizens make informed decisions on preparing their homes for potentially hazardous weather.

DIVISION HEADQUARTERS
2555 Shumard Oak Boulevard
Tallahassee, FL 32399-2100

Telephone: 850-815-4000
www.FloridaDisaster.org

STATE LOGISTICS RESPONSE CENTER
2702 Directors Row
Orlando, FL 32809-5631

Program Management

The Division is working toward adopting successful processes that are utilized for the federal grant programs administered by the Mitigation Bureau. HLMP project and grant management training programs are continuously evolving to include the best practices experienced by all programs managed by the Bureau. Additionally, custom scope of work templates have been designed for the newly permissible mitigation project types that HLMP manages. These new scopes are Florida-specific, project-specific, and provide explicit instruction on the compliance requirements set forth by the State of Florida, the Division of Emergency Management, and the Bureau of Mitigation.

DIVISION HEADQUARTERS
2555 Shumard Oak Boulevard
Tallahassee, FL 32399-2100

Telephone: 850-815-4000
www.FloridaDisaster.org

STATE LOGISTICS RESPONSE CENTER
2702 Directors Row
Orlando, FL 32809-5631

HURRICANE LOSS MITIGATION PROGRAM

PROGRAM ANALYSIS

FY 2023 Recipients

Figure 1.1 shows the awards and amounts spent to date for FY 2023. Due to supply chain issues, many of these projects were extended through December 31, 2023. Due to the extensions, the current amount spent is lower than in previous years. All currently active projects are proceeding on schedule and are projected to close with most, if not all, funds spent.

Recipient	Award Amount	Spent to Date	Project Type
DEM-HL00063 City of Fellsmere	$194,000.00	$ -	Public Building Wind Mitigation
DEM-HL00064 Lake Support and Emergency Recovery, Inc.	$ 194,000.00	$ 119,911.52	Residential Wind Mitigation
DEM-HL00065 Eckerd College	$ 194,000.00	$ -	Public Building Wind Mitigation
DEM-HL00066 Miami Dade County - Community Action and Human Services Department	$ 194,000.00	$ -	Residential Wind Mitigation
DEM-HL00067 Florida Keys Aqueduct Authority	$ 194,000.00	$ 194,000.00	Public Building Wind Mitigation
DEM-HL00068 Centro Campesino Farmworker Center	$ 194,000.00	$ 194,000.00	Residential Wind Mitigation
DEM-HL00069 Emerald Coast Regional Council	$ 194,000.00	$ 114,686.31	Residential Wind Mitigation
DEM-HL00070 Jefferson County	$ 194,000.00	$ -	Public Building Wind Mitigation
DEM-HL00071 St. Lucie Habitat for Humanity	$ 194,000.00	$ -	Residential Wind Mitigation
DEM-HL00072 City of Lauderdale Lakes	$ 194,000.00	$ 163,005.94	Residential Wind Mitigation
DEM-HL00073 Miami Shores Village	$ 194,000.00	$ -	Public Building Wind Mitigation
DEM-HL00074 Banyan Community Health Center, Inc.	$ 194,000.00	$ -	Commercial Wind Mitigation
DEM-HL00075 City of North Lauderdale	$ 194,000.00	$ 3,476.36	Residential Wind Mitigation
DEM-HL00076 Pasco County Board of County Commissioners	$ 194,000.00	$ -	Public Building Wind Mitigation
DEM-HL00077 Calhoun County	$ 150,000.00	$ -	Residential Wind Mitigation
Total	**$ 2,866,000.00**	**$ 789,080.13**	

Figure 1.1

DIVISION HEADQUARTERS
2555 Shumard Oak Boulevard
Tallahassee, FL 32399-2100

Telephone: 850-815-4000
www.FloridaDisaster.org

STATE LOGISTICS RESPONSE CENTER
2702 Directors Row
Orlando, FL 32809-5631

Benefit-Cost Analysis

Figure 1.2 shows the Benefit-Cost Analysis on FY 2023 projects.

Recipient	BCA Generated Benefits	Cost	Return on Investment
DEM-HL00063 City of Fellsmere	$ 225,088.00	$ 169,600.00	32.72%
DEM-HL00064 Lake Support and Emergency Recovery, Inc.	$ 118,600.00	$ 117,010.00	1.36%
DEM-HL00065 Eckerd College	$ 216,076.00	$ 197,000.00	9.68%
DEM-HL00066 Miami Dade County - Community Action and Human Services Department	$ 337,421.00	$ 241,763.00	39.57%
DEM-HL00067 Florida Keys Aqueduct Authority	$ 548,095.00	$ 180,857.00	203.05%
DEM-HL00068 Centro Campesino Farmworker Center	$ 266,065.00	$ 193,850.00	37.25%
DEM-HL00069 Emerald Coast Regional Council	$ 101,622.00	$ 100,800.00	0.82%
DEM-HL00070 Jefferson County (Withdrawn)	$ -	$ -	0.00%
DEM-HL00071 St. Lucie Habitat for Humanity	$ 381,105.00	$ 182,880.00	108.39%
DEM-HL00072 City of Lauderdale Lakes	$ 135,810.00	$ 125,999.00	7.79%
DEM-HL00073 Miami Shores Village	$ 418,017.00	$ 180,285.00	131.86%
DEM-HL00074 Banyan Community Health Center, Inc. (Withdrawn)	$ -	$ -	0.00%
DEM-HL00075 City of North Lauderdale	$ 183,038.00	$ 166,940.00	9.64%
DEM-HL00076 Pasco County Board of County Commissioners (Withdrawn)	$ -	$ -	0.00%
DEM-HL00077 Calhoun County Board of County Commissioners	$ 197,706.00	$ 181,013.00	9.22%
TOTAL	**$ 3,128,643.00**	**$ 2,037,997.00**	**53.52%**

Figure 1.2

Closed Projects

Figure 1.3 shows all completed projects during FY 2023, which had over $1.3 million spent retrofitting residential and public properties.

Closed Project	Award Amount	Amount Spent	Project Type
DEM-HL00044 Calhoun County Board of County Commissioners	$ 194,000.00	$ 176,761.23	Residential Wind Mitigation
DEM-HL00047 Gulf County Emergency Management	$ 194,000.00	$ 193,556.83	Residential Wind Mitigation
DEM-HL00048 Franklin County	$ 194,000.00	$ 185,349.41	Residential Wind Mitigation
DEM-HL00049 Desoto County Board of County Commissioners	$ 194,000.00	$ 194,000.00	Public Building Wind Mitigation
DEM-HL00052 City of Bristol	$ 194,000.00	$ 172,273.15	Residential Wind Mitigation
DEM-HL00058 City of Panama City	$ 194,000.00	$ 194,000.00	Public Building Wind Mitigation
DEM-HL00067 Florida Keys Aqueduct Authority	$ 194,000.00	$ 194,000.00	Public Building Wind Mitigation
DEM-HL00070 Jefferson County	$ 194,000.00	$ -	Public Building Wind Mitigation
DEM-HL00074 Banyan Community Health Center, Inc.	$ 194,000.00	$ -	Commercial Wind Mitigation
DEM-HL00076 Pasco County Board of County Commissioners	$ 194,000.00	$ -	Public Building Wind Mitigation
TOTAL	**$ 1,940,000.00**	**$ 1,309,940.62**	

Figure 1.3

DIVISION HEADQUARTERS
2555 Shumard Oak Boulevard
Tallahassee, FL 32399-2100

Telephone: 850-815-4000
www.FloridaDisaster.org

STATE LOGISTICS RESPONSE CENTER
2702 Directors Row
Orlando, FL 32809-5631

FY 2024 New Projects

Figure 1.4 shows all the approved HLMP projects for FY 2024, which have a balanced set of residential and non-residential wind mitigation projects.

Newly Awarded Recipient	Award Amount	Project Type
DEM-HL00080 City of Fellsmere	$ 194,000.00	Public Building Wind Mitigation
DEM-HL00081 Miami Dade - Community Action and Human Services	$ 194,000.00	Residential Wind Mitigation
DEM-HL00082 Florida Keys Aqueduct Authority	$ 194,000.00	Public Building Wind Mitigation
DEM-HL00083 City of Arcadia	$ 100,000.00	Public Building Wind Mitigation
DEM-HL00084 City of Homestead	$ 194,000.00	Public Building Wind Mitigation
DEM-HL00085 City of Lauderdale Lakes	$ 194,000.00	Residential Wind Mitigation
DEM-HL00086 Flagler County Board of County Commissioners	$ 194,000.00	Residential Wind Mitigation
DEM-HL00087 City of Atlantic Beach	$ 194,000.00	Public Building Wind Mitigation
DEM-HL00088 Vizcaya Museum and Gardens Trust, Inc.	$ 194,000.00	Public Building Wind Mitigation
DEM-HL00089 St. Lucie County Board of County Commissioners	$ 194,000.00	Residential Wind Mitigation
DEM-HL00090 City of Bradenton	$ 194,000.00	Residential Wind Mitigation
DEM-HL00091 Hernando County Fire and Emergency Services	$ 194,000.00	Public Building Wind Mitigation
DEM-HL00092 City of Carrabelle	$ 194,000.00	Residential Wind Mitigation
DEM-HL00093 DeSoto County Board of County Commissioners	$ 194,000.00	Public Building Wind Mitigation
DEM-HL00094 Centro Campesino Farmworker Center	$ 194,000.00	Residential Wind Mitigation

Figure 1.4

DIVISION HEADQUARTERS
2555 Shumard Oak Boulevard
Tallahassee, FL 32399-2100

Telephone: 850-815-4000
www.FloridaDisaster.org

STATE LOGISTICS RESPONSE CENTER
2702 Directors Row
Orlando, FL 32809-5631

HURRICANE LOSS MITIGATION PROGRAM

PROGRAM GOALS AND RECOMMENDATIONS

The Division is committed to developing programs to educate the public on ways to reduce the impact of a disaster. The Division must continue to work with Florida homeowners, local governments, non-profit organizations, and state agencies to reduce the risk of hurricane losses. Research must continue to develop stronger wind mitigation measures to protect the residents of Florida and increase structural survivability for residences. Additionally, more communities will have an opportunity to participate in the grant program through a comprehensive outreach program.

The Division has the following goals for the Hurricane Loss Mitigation Program:

- Continue refining grant management activities in the Salesforce platform for better reporting and process improvement
- Where possible, leverage HLMP funds with other funds from federal, state, local government, or private sources
- Partner with Recovery and Mitigation Regional Coordinators to enhance HLMP outreach efforts.

Observations and Recommendations:

Observation – Grant recipients and contractors are continually under a confined time constraint for awarding and expending the appropriated funds within one fiscal year. Project solicitation, awarding, contracting, sub-contracting, construction, and project closeout must be completed by the end of each fiscal year. This condensed time frame does not allow the Division or its participants sufficient time to take full advantage of the funding provided.

Recommendation – Extend the funding and budget authority for the annual appropriation for up to two years. This would allow the Division's contracts to start upon full execution and have a period of performance that would expire at the end of the second fiscal year.

DIVISION HEADQUARTERS
2555 Shumard Oak Boulevard
Tallahassee, FL 32399-2100

Telephone: 850-815-4000
www.FloridaDisaster.org

STATE LOGISTICS RESPONSE CENTER
2702 Directors Row
Orlando, FL 32809-5631

SHELTER DEVELOPMENT PROGRAM

PROGRAM ACTIVITIES

Shelter Development Funding

In 2017, the Hurricane Loss Mitigation Program began managing the grant and contracting responsibilities of the Shelter Survey and Retrofit Program. In 2022, the program changed to the Shelter Development Program to encompass both the retrofitting of existing structures and the construction of new structures to be used as shelters. HLMP applies proven grant management processes to existing and new projects under the Shelter Development Program. With its resources available, the Mitigation Bureau's Finance Unit has been able to streamline processes for tracking shelter payments, contracting, and reporting.

The Hurricane Loss Mitigation Program also works with the Mitigation Bureau's Technical Unit to verify the work completed under the Shelter Development Program. Modernized scopes of work have been finalized with the collaboration of the Shelter Development Program, Technical Unit, and Hurricane Loss Mitigation Program. New review processes and detailed requirements within the scope of work will strengthen regulation and monitoring while providing the recipient with a clearer understanding of their goals and objectives.

DIVISION HEADQUARTERS
2555 Shumard Oak Boulevard
Tallahassee, FL 32399-2100

Telephone: 850-815-4000
www.FloridaDisaster.org

STATE LOGISTICS RESPONSE CENTER
2702 Directors Row
Orlando, FL 32809-5631

SHELTER DEVEOPMENT PROGRAM

PROGRAM ANALYSIS

Executed Projects

Figure 2.1 displays the shelter development agreements executed in FY 2023, totaling $1,186,950.00.

Recipient	Award Amount
DEM-SR00037 Gadsden County Community Hospital	$ 483,000.00
DEM-SR00038 Jefferson County School District	$ 126,000.00
DEM-SR00039 School District of Indian River County	$ 577,950.00
TOTAL	**$ 1,186,950.00**

Figure 2.1

Closed Projects

Figure 2.2 below summarizes the two projects closed during FY 2023, totaling $0. All projects closed during FY 2023 were projects that had been withdrawn from the program.

Recipient	Amount Spent
DEM-SR00025 Walton County Board of County Commissioners (Withdrawn)	$ -
DEM-SR00035 School Board of Clay County (Withdrawn)	$ -
TOTAL	**$0.00**

Figure 2.2

DIVISION HEADQUARTERS
2555 Shumard Oak Boulevard
Tallahassee, FL 32399-2100

Telephone: 850-815-4000
www.FloridaDisaster.org

STATE LOGISTICS RESPONSE CENTER
2702 Directors Row
Orlando, FL 32809-5631

Active Projects

Figure 2.3 shows all fifteen projects active at the end year of FY 2023. The projects divide into three major categories, including Engineering Study, Genset, and Retrofit. An Engineering Study determines the viability of a building for retrofitting. A Genset project installs the necessary electrical components to connect a generator to a building. Retrofit projects focus on hardening the envelope of a building.

2023 FY Shelter Retrofit Active Projects			
Recipient	**Projects**	**Project Type**	**# of Locations**
HLMPSR17-020 A Multi Clay County BOCC	Orange Park High School	Engineering Study	**5**
	Asbury Lake Jr High School	Gen Set	
	Oakleaf High School	Retrofit	
	Fleming Island High School	Retrofit	
	Keystone Heights High School	Retrofit	
DEM-SR00001 Seminole County BOCC	Winter Springs High School	Retrofit	**4**
	Teague Middle School	Gen Set	
	Teague Middle School	Retrofit	
	Lawton Chiles Middle School	Gen Set	
	Lawton Chiles Middle School	Retrofit	
	Lyman High School	Gen Set	
	Lyman High School	Retrofit	
DEM-SR00005 Orange County BOCC	South Econ Rec Gym	Retrofit	**5**
	West Orange Rec Gym	Retrofit	
	Silver Star Rec Gym	Retrofit	
	Meadow Woods Rec Gym	Retrofit	
	Goldenrod Rec Gym	Retrofit	
DEM-SR00010 Walton County BOCC	Freeport High School	Gen Set	**1**
DEM-SR00018 Sarasota School Board	Taylor Ranch Elementary	Retrofit	**3**
	Gulf Gate Elementary	Retrofit	
	North Port High School	Retrofit	
DEM-SR00020 Lake School Board	East Ridge High School	Retrofit	**17**
	Carver Middle School	Retrofit	
	Eustis Middle School	Retrofit	
	Mt. Dora High School	Retrofit	
	Leesburg High School	Retrofit	
	Tavares High School	Retrofit	
	Umatilla High School	Engineering Study	
	Umatilla High School	Retrofit	
	Eustis Middle School	Retrofit	
	Astatula Elementary School	Retrofit	
	Astatula Elementary School	Gen Set	
	Villages Elementary School	Gen Set	
	Villages Elementary School	Retrofit	
	Lost Lake Elementary School	Retrofit	
	Lost Lake Elementary School	Gen Set	
	Leesburg Elementary School	Gen Set	
	Umatilla Elementary School	Gen Set	
	Spring Creek Elementary Schools	Gen Set	
	Round Lake Elementary School	Gen Set	
	East Ridge Middle School	Gen Set	
	Tavares Middle School	Retrofit	
DEM-SR00021 DeSoto School District	West Elementary School	Retrofit	**3**
	Nocatee Elementary School	Retrofit	
	DeSoto High School	Retrofit	

DIVISION HEADQUARTERS
2555 Shumard Oak Boulevard
Tallahassee, FL 32399-2100

Telephone: 850-815-4000
www.FloridaDisaster.org

STATE LOGISTICS RESPONSE CENTER
2702 Directors Row
Orlando, FL 32809-5631

DEM-SR00027 Marion County - Retrofit	Belleview High School	Retrofit	**6**
	Belleview Middle School	Retrofit	
	Legacy Elementary School	Retrofit	
	Saddlewood Elementary School	Retrofit	
	South Ocala Elementary School	Retrofit	
	West Port High School	Retrofit	
DEM-SR00030 The School Board of Polk County	Ben Hill Griffin JR Elementary School	Retrofit	**5**
	Frostproof Middle Senior School	Retrofit	
	Ft Meade/SR High	Retrofit	
	Ridge Community High School	Gen Set	
	Berkley Charter Elementary School	Retrofit	
DEM-SR00032 Alachua County BOCC	Freedom Center	Retrofit	**1**
	Freedom Center	Gen Set	
DEM-SR00033 Bay County BOCC	Bay County Public Library	Retrofit	**1**
	Bay County Public Library	Gen Set	
DEM-SR00034 City of Gainesville	Grace Marketplace	Retrofit	**1**
DEM-SR00037 Gadsden Board of County Commissioners	Gadsden County Community Hospital	Retrofit	**1**
	Gadsden County Community Hospital	Gen Set	
DEM-SR00038 Jefferson County School District	Jefferson County K-12 School	Retrofit	**1**
DEM-SR00039 School District of Indian River County	Treasure Coast Elementary School	Retrofit	**1**

Engineering Study	2
Retrofit	46
Gen Set	17
Total	**65**

Figure 2.3

DIVISION HEADQUARTERS
2555 Shumard Oak Boulevard
Tallahassee, FL 32399-2100

Telephone: 850-815-4000
www.FloridaDisaster.org

STATE LOGISTICS RESPONSE CENTER
2702 Directors Row
Orlando, FL 32809-5631

SHELTER DEVELOPMENT PROGRAM

PROGRAM GOALS AND RECOMMENDATIONS

Under the guidance of the Hurricane Loss Mitigation Program, the Shelter Development Program has grown in scope and efficiency. By collaborating with the Division's Infrastructure Section, the Program continues to eradicate shelter deficits throughout the state. From better reporting to improved funding accountability, the Program looks forward to providing greater resiliency and preparedness for future disasters throughout the state.

The Division has the following goals to accomplish in the next Fiscal Year:

- Meet the Legislature's goal to eliminate the deficit of safe public hurricane evacuation shelter space in all regions of the state
- Develop standards of cost-effectiveness towards new construction
- Continue refining grant management activities in the Salesforce platform for better reporting and process improvement
- Maintain a strong relationship between the Division's Infrastructure staff and Mitigation staff
- Coordinate with the Mitigation Technical Unit to increase integration within the Program.

DIVISION HEADQUARTERS
2555 Shumard Oak Boulevard
Tallahassee, FL 32399-2100

Telephone: 850-815-4000
www.FloridaDisaster.org

STATE LOGISTICS RESPONSE CENTER
2702 Directors Row
Orlando, FL 32809-5631

Appendix A

2022-2023 ANNUAL REPORT
GULF COAST STATE COLLEGE
MOBILE HOME TIE-DOWN PROGRAM

Florida Statute (F.S.) 215.559 which governs the Hurricane Loss Mitigation Program and the Mobile Home Tie-down Program funding, awarded the project oversight to Gulf Coast State College (GCSC) effective July 1, 2022. In addition to the annual two million eight-hundred thousand ($2,800,000) award funding, the legislative budget committee also awarded an additional seven million ($7,000,000) in general appropriations, for a combined total award of nine million eight-hundred thousand ($9,800,000). Though the program shifted to GCSC and Florida suffered several debilitating storms, the program remained successful, serving several parks retained from the Tallahassee Community College (TCC) MHTDP waiting list as well as several new parks that were previously not eligible due to skirting type.

Program Highlights:

- TCC shared all contracts and RFP files, and archived program data including current waiting list, parks served, and park databases. This allowed GCSC to pick up where TCC left off, and easily review and report on previously served parks as requested.
- GCSC recruited Jennifer Shaw who had prior knowledge of the MHTDP program requirements as the new Program Manager. Mrs. Shaw had an established relationship with the FL Division of Emergency Management, Hurricane Loss Prevention Program (DEM), as well as the MHTDP Advisory Council, and prior vendors, ensuring a successful transition between colleges.
- GCSC maintained the pre-established MHTDP Advisory Council which includes DEM, Florida Highway Safety and Motor Vehicles, Manufactured Housing Division (FHSMV), Federation of Manufactured Home Owners of Florida (FMO), and Florida Manufactured Housing Association (FMHA).
- The 2022-23 Request for Proposals for vendor installation contracts was published July 11th, 2022; Proposals were due August 25th, and RFP Award Recommendation to Storm Ready Services was posted September 2nd, 2022.
- Additional support contracts for tie-down installations (Florida Homes Direct, Region 1), and post-installation quality assurance inspections (Beryl Project Engineering and Structure's Engineering and Inspection) were also issued.
- Gulf Coast State College elected to include homes with non-removable skirting. This requires installing anchoring from beneath the home when skirting is not easily removable. The process is more expensive and requires additional materials and man-hours. However, this program addition has proved successful and has allowed many previously denied parks access to the program services.
- The use of Quality Assurance Inspectors continued for the Individual component (FHSMV post-inspects parks).

- FHSMV completed a random inspection of a minimum of 10% of the homes for the Parks component. This inspection verifies the items as invoiced installed by the vendor according to 15C-1 and the manufacturer's specifications.

Impact of Program Shift and 2022 Hurricanes:

The shift from TCC to GCSC impact was fairly minimal. The DEM award was executed August 11th, 2022. RFP vendor contract for installations was executed September 6th, 2022. At this point parks were assigned for evaluations, previously approved parks remaining from the TCC program were assigned, and Storm Ready Services was cleared to start park meetings and installations.

However, Hurricane Ian affected travel, meetings, and installation services in Southwest Florida September 2022. All counties in Hurricane Ian's path suffered widespread destruction due to wind, storm surge, and flooding. Several counties on the MHTDP waiting list had to be put on hold until damage could be assessed and parks reevaluated post-storm cleanup. Flooding from additional 2022 storms also affected installation efforts in Central Florida. Thanks to archived record retention, GCSC was able to report to DEM and FHSMV the list of parks in affected counties that received prior retrofit tie-down installations under TCC's MHTDP.

The 2022 Hurricane Ian Storm Damage Assessment report published by the Florida Highway Safety and Motor Vehicles, Manufactured Housing Division noted several parks in affected counties which previously had retro-fitting completed under the TCC Mobile Home Tie-Down Program faired better than homes that did not have adequate tie-down installations. This supports the continued need for tie-down improvements across the state. https://www.flhsmv.gov/motor-vehicles-tags-titles/dealers-installers-manufacturers-distributors-importers/mobile-home-installer/mobile-home-damage-reports/

Final Numbers:

Twenty-five (25) total park site visits were completed throughout the year. The following deliverables were completed during this process:

- Community Information sessions explaining program and answering homeowner questions.
- Intake training for the homeowners' association representatives.
- Visual inspections of all homes within the community.
- Collection of homeowner authorization forms.

During the 2022-2023 program year seventeen (17) initial resident meetings were conducted by

the Program Contractors, and six (6) follow-up meetings were conducted. These meetings were conducted with homeowner's association board members, park managers, FMO volunteers and residents of each community. In several parks, all homes were owned by the property management firm and did not require community information meetings.

Gulf Coast State College installation vendors completed a total of one thousand eighty-three (1,083) homes between parks and individual homes. The program was successfully completed in twenty-three (23) manufactured home communities, with two (2) partial parks to be completed in 2023-24. In addition, ninety-four (94) individual homes were served in various counties. Twenty-five (25) counties received installation services in either parks or individual homes. In total, two million six hundred ninety-two thousand six-hundred ninety-one dollars and eighty-two cents ($2,692,691.82) was utilized of the FY2022 DEM-HL00061 grant, or 27.5% grant utilization.

Parks Completed	**Address**	**City**	**County**	**# Homes Served**
Commerce Park Sun Estates 1	6800 NW Gainesville Rd	Ocala	Marion	39
Commerce Park Sun Estates 2	4023 NW Gainesville Rd	Ocala	Marion	12
Forest, The (The Forest Club)	400 N. Forest Blvd	Lake Mary	Seminole	152
Gulfstream Harbor Part 1	4505 S Goldenrod Road	Orlando	Orange	207
High Point Part 1	8008 Baltic St	Brooksville	Hernando	127
Lake Mary MHP	1651 Spring Hammock Way	Longwood	Seminole	41
Maitland Sun Estates	9165 US Hwy 17/92	Maitland	Orange	24
Mark Park	3200 13th Street	St. Cloud	Osceola	53
North Orlando Sun Estates 1	950 S Woodland Blvd	Deland	Volusia	19
North Orlando Sun Estates 2	481 Sunshine Court / Lee St	Deland	Volusia	27
Pelican 1	11123 N Nebraska Ave	Tampa	Hillsborough	14
Pelican 2	10921 N Nebraska Ave	Tampa	Hillsborough	18
Pete's Place MHP	32702 Random Ln	Dade City	Pasco	9
St. Petersburg Sun Estates 1	2600 58th Ave N	St Petersburg	Pinellas	19
St. Petersburg Sun Estates 2	5000 28th St N	St Petersburg	Pinellas	20
Sunshine MHP Cocoa	1633 Lake Drive	Cocoa	Brevard	18
Tampa Sun Estates 1	10101 N Florida Ave	Tampa	Hillsborough	34
Tampa Sun Estates 2	10803 N Annette Ave	Tampa	Hillsborough	18
Tampa Sun Estates 3	10603 N Nebraska Ave	Tampa	Hillsborough	28
Tampa Sun Estates 4	14011 N Nebraska Ave	Tampa	Hillsborough	29
Tampa Sun Estates 5	221 21st St SE	Ruskin	Hillsborough	15
Tampa Sun Estates 6	17123 Jo Rich Circle	Lutz	Hillsborough	24
University Sun Estates 1	16268 E Colonial Drive	Orlando	Orange	21
University Sun Estates 2	514 Glenn Rd	Orlando	Orange	4
Villages Sun Estates	32321 Haven Court	Leesburg	Lake	17
Individuals (addresses vary), 24 Counties Served				94

Moving Forward:

- Nearing the end of FY2022-23, GCSC requested a No Cost Extension to utilize the remaining DEM-HL00061 funding. This was approved July 2023, and will extend DEM-HL00061 grant funding use through June 30th, 2024.
- Due to Cost of Business inflation and the additional cost of installing on non-removable skirting, SRS did not wish to renew contract at 2022-23 bid pricing. A new RFP was published April 3rd, 2023 and Award Recommendation posted June 29th, 2023 for the 2023-24 grant year.
- Four (4) vendors submitted bid proposals. Storm Ready Services won the RFP bid, and will continue to serve Regions 3-5. Additional vendors (Bosarge & Sons Construction and Top Notch Mobile Home Services) will also be issued small support contracts to complete installations. HAS Inspections, Beryl Project Engineering, and Top Notch will be contracted for post-installation quality assurance inspections for individual homes.
- Fifty-two (52) parks have been evaluated and are awaiting installation services. Sixty-eight (68) parks have completed park application and are awaiting program eligibility evaluations. An additional thirty-nine (39) parks have shown resident interest and are pending completed application from park representatives.

Please refer any questions relating to this report or the Program in general to:

Jennifer Shaw
Program Manager, MHTDP
Gulf Coast State College
jshaw6@gulfcoast.edu
488-201-6882

A Resource for the State of Florida

HURRICANE LOSS REDUCTION FOR HOUSING IN FLORIDA

FINAL REPORT
For the Period November 21, 2022 to June 30, 2023

A Research Project Funded by:
The State of Florida Division of Emergency Management
Through Contract #DEM-HL00062

Prepared by
The International Hurricane Research Center (IHRC)
Florida International University (FIU)

July 31, 2023

Final Report

Table of Contents

Section 1
Executive Summary

Three major research efforts were identified by the International Hurricane Research Center (IHRC) for the Hurricane Loss Mitigation Program (HLMP) Fiscal Year 2022-23. Funding was dedicated to areas of Manufactured housing structural mitigation analysis, economic loss analysis, and education and outreach. In keeping with the comprehensive agenda of the research topics for this project, the IHRC organized a multidisciplinary team of researchers, students and support staff to complete the stated objectives. The following is a summary of research findings:

Research Area 1: Understanding Hurricane Effects on Manufactured Homes (Chowdhury, Zisis, Elawady, Sutley, Dao)

Manufactured Housing (MH) units are one of the most vulnerable residential structures to windstorms, including hurricanes. The overall goal of this research is to provide the fundamental knowledge needed to reduce the physical vulnerability of manufactured homes to wind events. While extensive research has been conducted on more traditional residential construction methods (e.g. light-frame wood construction - LFWC) little research exists on MHs. Of particular importance is the performance of anchorage systems of MHs, with limited research that does not capture many observed failure modes, including roof and wall cladding loss. Also, previous research doesn't capture the critical role of aerodynamic effects of the crawlspace beneath the units. In addition, there is no available knowledge regarding the interference effects caused by interactions between multiple units in a mobile home park. With an estimated 2.7 million MH units located within mobile home parks in the U.S., we strongly believe that there is an important gap in understanding hurricane effects on manufactured homes.

Three universities including Florida International University (FIU), Kansas University (KU) and University of Alabama (UA), will collaborate in this research which will address the significant gaps through a series of research tasks to be carried out over three years (total period envisioned to complete all research tasks discussed). The research that was carried out has the potential to provide transformative impacts to new and existing mobile home parks, and to manufactured housing units through critical fundamental and practical knowledge that can change code provisions, policies, and manufacturing processes. The findings can inform new ASCE 7 provisions and lead to significantly improved HUD design standards for MH units. The findings can also be shared with MH builders and park owners and residents, as well as FEMA to inform new site development for post-disaster temporary housing that uses manufactured homes. Findings are applicable beyond MH units used as permanent housing including post-disaster temporary shelters and housing used in the U.S. and internationally. The research is important for Florida and Floridians (and the entire U.S.) in terms of understanding and reducing the vulnerability of MH units. The research activities helped in training students in three universities with expertise in hurricane damage mitigation.

Part A: Large-scale Wind Tunnel Testing of Manufactured Home Communities (Florida International University)

Earlier research has identified three primary areas where critical damage occurs in manufactured homes. Firstly, damage is commonly observed in the trailer structure itself, often caused by building envelope damage, inadequate roof-to-truss, or roof-to-wall connections. Secondly, the foundation of the home is susceptible to issues such as the trailer sliding off the foundation or experiencing overturning failure. Finally, attached structures, which are often poorly connected, can suffer damage themselves and create vulnerabilities within the trailer, potentially leading to a cascade of failures. This research aims to investigate the aerodynamics of MHs using large-scale wind tunnel experiments at the National Science Foundation (NSF)-designated Wall of Wind (WOW) Experimental Facility (EF) at FIU. The main objectives of the study were to investigate wind loads on a large-scale MH model by considering typical connections used in actual construction practice. This research validated the development of a finite element model of the MH. This entailed conducting aerodynamic experiments in simulated open terrain boundary layer flows at the WOW EF. Statistics of pressure, force, and moment coefficients obtained from the collected pressure time histories were used to assess wind effects on MHs. Based on these results, the following conclusion were made:

• The spatial pressure distribution on isolated MHs is similar to that of typical low-rise buildings. Critical peak roof suctions of up to -5.0 were recorded near the corners and leading edges.
• Critical peak suctions of up to -2.0 and peak positive pressures of 1.4 were recorded on the walls.
• Critical peak suctions of up to -1.1 and peak positive pressures of 0.8 were recorded at the floor.
• Laser displacement and load cell data were collected mainly for the purpose of calibration of the developed finite element model

The data obtained from this study will be used to inform building component testing and numerical simulations (using finite element modeling) of the behavior of MHs during extreme wind events. Most importantly, the findings of this study may also be used to help improve the provisions in building design codes and standards as well as to inform risk assessment models.

The planned workshop in collaboration with UA and KU was postponed until FY 23-24.

Part B: Understanding Hurricane Effects of Manufactured Homes (Kansas University)

A significant portion of Florida households live in MH units (approximately 7%). While the performance of MHs continues to be a problem after hurricanes and other major windstorms, the structural design level of MHs is not well understood. The overall goal of this research is to provide the fundamental and practical knowledge needed to significantly reduce the physical vulnerability of manufactured homes to wind events through a quantitative capture of structural design levels for Wind Zone II and Wind Zone III MHs. Extensive research has been conducted on site-built light-frame wood construction, whereas little research exists on MHs. Of the limited research that

exists on MHs, the focus is on anchorage systems, and there is a dearth in coverage on many observed failure modes, including roof and wall cladding loss and system failure. Research documented in this report aims to advance code provisions, policies, and manufacturing processes, to better protect manufactured home residents. This report presents the research from Phase II of the project carried out at the University of Kansas, which included (a) stakeholder engagement; (b) experimental testing of full-scale connections; and (c) a numerical benchmark study.

Stakeholder Engagement

Phase II stakeholder engagement was initiated through phone calls, emails and social media (LinkedIn and Facebook) communications that led to scheduled discussions with members of the Manufactured Housing Institute, HUD's Manufactured Housing Consensus Committee, the Lincoln Institute, the Federal Emergency Management Agency, and Institute for Business and Home Safety to discuss the state of design and construction practice, gaps in current code provisions and the code change process, and/or goals of the FLDEM study, including exploring the possibility of testing a full-scale manufactured home in the FIU Wall of Wind. The team failed to reach any manufacturers of manufactured home despite continued efforts.

Manufactured home manufacturers continue to be challenging to connect with. Through conversations with federal and non-governmental agencies, there is significant interest in this research to quantify and improve the wind performance of manufactured homes, and in full-scale wind tunnel testing of a manufactured housing unit.

Components and Connection Testing Study

Fastener component monotonic testing informed cyclic testing protocols. Subsequent cyclic testing of various sheathing fastener configurations provided data that will be used in detailed finite element models of manufactured homes. As shown in the results of this report, the mean capacities for the nail connections in SYP lumber are substantially (2.5 to 3 times) less than the mean capacities for screw connections in SPF. Similarly, the COV was always 2.5 times higher for the nail connections in SYP compared with the screw connections in SPF. Given that nail connections are the more common connection used in the actual construction of Wind Zone II manufactured homes which have roof failure as the most common observed failure mode in the field, switching fasteners from nails to screws is expected to provide significantly higher performance. The study completed on common wall to floor connections shows that the expected capacity is often achieved for these connections. However, the pattern of the fasteners can make a critical difference, where the pattern was not specified in the documentation from HUD or the drawings our team received from a manufacturer. As observed in the field, stagger, row, random patterns are all common in practice. The stagger pattern is recommended as it distributes the load more evenly across a larger area of the wood member. More research is needed to understand this relationship for edge fasteners, as well as for the roof-to-wall connection. Additionally, more research is needed to understand the material and labor cost difference that is associated with (a) using screws instead

of nails at the roof sheathing to rafter connection, and (b) staggering fasteners connecting the strap at the wall to floor connection.

Numerical Benchmark Study

The numerical benchmark study was performed to evaluate the differences in HUD Code wind loads with the wind loads specified in ASCE/SEI 7-22. As presented in Tables 9 through 12, there were significant differences between the pressures calculated using the two provisions. ASCE/SEI 7-22 has gone through major revision over the past 35 years, continuously incorporating new findings, updated statistics, and the best science, whereas the HUD Code has remained stagnant. Based on the findings in the benchmark study, it may be the case that HUD Code wind pressures are conservative for MWFRS and unconservative for C&C. The significance in the difference in the C&C loads could be a source for the disparate failures of manufactured homes observed after major wind events.

Part C: Numerical Analysis of Manufactured Homes Under Hurricane Effects (University of Alabama)

Hurricanes and windstorms pose a serious threat to MH units MHU. This study's main objective is to offer the fundamental and useful knowledge required to drastically decrease the physical susceptibility of manufactured homes to wind events. Although LFWC has been the subject of much investigation, little is known about MHUs. Although there is little research on anchorage systems, it does not account for many documented failure types, such as loss of roof and wall cladding. Manufactured homes are designed following the U.S. Department of Housing and Urban Development's Manufactured Home Construction and Safety Standards, Part 3280, (hereafter referred to as HUD Code). Notably, this code hasn't been substantially updated since 1994, and its hazard maps use lower wind speeds than the current ASCE-7 standard, stemming from the 1988 ASCE Standard 7. These manufactured housing units are the most susceptible residential structures to wind-related disasters, including hurricanes and tornadoes. Although these units employ wood frame construction, their structure differs significantly from traditional site-built homes, necessitating a distinct analysis. The HUD Code's design provisions are rather ambiguous, giving manufacturers a broad scope for interpretation. Our post-calamity field surveys show considerable inconsistency in the construction of manufactured homes, which corresponds to their performance, both within and across Wind Zones. Currently, there is no public information about the construction process of manufactured homes. However, our research team has acquired structural details from HUD and a leading U.S. manufacturer of these homes. Significant variability is present even within these documents.

In this study, the team introduced a general hysteresis model that can capture the cumulative damage of wood connections within the MHU. This new hysteresis model can be used for different types of connections by condensing the connection data using scattered data points and backbone curve of which the information can be extracted within the testing data.

Research Area 2: Investigation and Incorporation of WOW testing outputs in the Florida Public Hurricane Loss Model (Gurley and Pinelli)

One of the key components of a better mitigated and therefore more disaster-resilient Florida involves recovery and reconstruction funding for homeowners, and a key element of that funding derives from insurance coverage, which is increasingly driven by cost considerations. The Florida Public Hurricane Loss Model (FPHLM), which has been supported by the State, provides a means of evaluating hazard insurance rate requests independently of the proprietary models used by private insurers. The model is continually refined to both satisfy the standards issued by the Florida Commission on Hurricane Loss Projection Methodology, and incorporate the current state-of-knowledge in the methodologies employed by the meteorological, engineering, actuarial, statistical, and computer science teams.

An experimental study at the FIU WOW EF identified significant differences in roof overhanging sheathing when compared with ASCE 7 guidance. FIU published a paper (Mostafa et al. 2023) that included recommended changes to the roof overhand load coefficients. The FPHLM explicitly accounts for overhanging sheathing wind loads, and thus offered an opportunity to investigate the influence of the FIU study on the outputs of a hurricane wind loss projection model. It was determined that, while the changes in loading resulted in larger mean losses to overhang roof sheathing over a range of strength models, the influence this had on overall building loss projections was negligible. However, since it reflects more accurately the actual wind-structure interaction than current ASCE 7 provisions, and given that it might be included in future ASCE provisions, formal inclusion of the WOW results in the FPHLM Unified Model, currently being validated, is warranted.

Research Area 3: Education and Outreach Programs to Convey the Benefits of Various Hurricane Loss Mitigation Devises and Techniques (PI: Erik Salna)

The IHRC developed and coordinated education and outreach activities to build on the foundation of previous work under this grant and showcased the hurricane-loss mitigation objectives of the HLMP.

For the 2022-23 performance period, the below mentioned educational partnerships, community events, and outreach programs were developed:

Wall of Wind Mitigation Challenge (WOW! Challenge): Wednesday, March 15th, 2023
The International Hurricane Research Center (IHRC), located on the campus of Florida International University (FIU), has developed the Wall of Wind Mitigation Challenge (WOW! Challenge), a judged competition for South Florida high school students. As the next generation of engineers to address natural hazards and extreme weather, this STEM education event features a competition between high school teams to develop innovative wind mitigation concepts and real-life human safety and property protection solutions. The mitigation concepts are tested live at the FIU NSF-NHERI Wall of Wind (WOW) Experimental Facility (EF), located on FIU's Engineering Campus.

- The objective for the 2023 Wall of Wind (WOW) Mitigation Challenge was to reduce the wind-induced uplift force on a building's roof, by optimizing its overall shape. Solutions demonstrated a sound comprehension of aerodynamic principles.
- The high school teams prepared three components for the competition: a physical test, an oral presentation, and a written technical paper.
- The competition involved teams from eight South Florida high schools, including about 100 students and eight teachers.
- *First Place* was awarded to TERRA Environmental Research Institute.
  Second Place was awarded to Booker T. Washington Senior High School.
  Third Place was awarded to G. Holmes Braddock Senior High School.
- A complete scoring summary can be found on the following link: https://www.ihrc.fiu.edu/wp-content/uploads/2023/04/2023_WOW_CHALLENGE_RESULTS_SUMMARY.pdf

Media exposure resulted in great positive visibility for the IHRC, FIU and FDEM's message of mitigation:

- FOX Weather Network: https://www.youtube.com/watch?v=cXKl1cgiBp0
- WOW Challenge Highlights Video: https://youtu.be/W2pInso5IXk
- FIU News: https://news.fiu.edu/2023/wall-of-wind-challenge-is-launching-pad-for-high-school-students

Eye of the Storm (Science, Mitigation & Preparedness) In-Person Event: May 20th, 2023
The Museum of Discovery & Science (MODS), located in Fort Lauderdale, FL, assisted the IHRC in planning, coordinating, and facilitating this free admission public education event that showcased special hands-on, interactive activities and demonstrations teaching hurricane science, mitigation and preparedness. There was also the opportunity for visitors to support recovery efforts for the April flooding event in Fort Lauderdale through volunteering or monetary donations.

- A record 4,900 visitors attended Eye of the Storm, showcasing special interactive activities and demonstrations teaching hurricane science, mitigation and preparedness.
- A Participant Post Survey showed 80.2% of respondents increased their knowledge about wind engineering and mitigating hurricane damage and 81.4% will be taking steps to mitigate hurricane damage.
- Media Release and Flyer: 2023 Eye of the Storm – Hurricane (Science, Mitigation & Preparedness) Free Museum Event, Saturday, May 20th, 10am to 5pm | IHRC Website (fiu.edu)

Special Guest:

- Grant Goodwin, HLMP Program Manager, Florida Division of Emergency Management

Media exposure resulted in great positive visibility in the community for the IHRC, FIU and FDEM's message of mitigation.

- Museum of Discovery and Science 'Eye of the Storm' Event – NBC 6 South Florida (nbcmiami.com)

NOAA Hurricane Awareness Tour: IHRC did not participate because the stop in Marathon, Florida was cancelled due to aircraft mechanical problems.

Get Ready, America! The National Hurricane Survival Initiative: Cancelled due to lack of sponsorships.

SECTION 2 PART A:

Large-scale Wind Tunnel Testing of Manufactured Home Communities

FINAL REPORT

(Period: 2023)

A Research Project Funded by:

The State of Florida Department of Emergency Management

Prepared by

Dr. Arindam Gan Chowdhury

Dr. Ioannis Zisis

Dr. Amal Elawady

Graduate Student

Omar Metwally

1. Introduction

Manufactured homes (MHs), also known as mobile homes or trailers, are used by more than 20 million people in the US as they offer affordable housing options for many individuals and families (Sutley et al., 2020). However, when it comes to facing the wrath of natural disasters like hurricanes, these homes are particularly vulnerable. Their construction and mobility characteristics make them more susceptible to damage and destruction in the face of strong winds, heavy rain, and storm surges. This vulnerability poses significant risks for the residents living in these structures during hurricane events and in the past, the consequences were significantly obvious after hurricanes. The responsibility for ensuring standardized construction quality of manufactured homes was given to the US Department of Housing and Urban Development (HUD) in 1976. In 1992, Hurricane Andrew resulted in the destruction or damage of more than 10,000 manufactured homes (Sutley et al., 2020). These devastating outcomes served as a catalyst for utilizing existing research, promoting new studies, and enhancing design standards for manufactured homes. In 1994, HUD provisions were amended to incorporate updated standards. Post-hurricanes studies reported damage to manufactured homes. Following the devastating hurricanes Charley (2004), Katrina (2005), and Rita (2005), extensive field investigations were conducted to assess the impact on manufactured homes. Surprisingly, even though the wind speeds during Hurricane Charley reached only 50% to 75% of the design loads specified for post-1994 manufactured homes, approximately 40% of the observed structures still suffered damage (IBTS 2005). In the aftermath of Hurricanes Katrina and Rita, (Hebert & Levitan, 2009) conducted a comprehensive analysis of a sample of 251 units. Their findings revealed that 62% of post-1994 manufactured homes and 61% of pre-1994 manufactured homes in the sample were damaged. In the aftermath of Hurricanes Irma (2017) and Michael (2018) in Florida, (Sutley et al., 2020) undertook a detailed analysis of post-hurricane imagery and damage assessment specifically focusing on manufactured homes (MHs). Out of the 279 homes examined in the aftermath of these two storms, it was found that 11% remained undamaged, while 20% were destroyed. Additionally, 59% of the surveyed homes suffered nonstructural damage, and 30% endured structural damage. Examples of reported damage are shown in Fig. 1. Their research shed light on the inherent physical vulnerabilities of MHs and emphasized the urgent requirement for additional studies aimed at improving their resistance to high winds. Earlier research has identified three primary areas where critical damage occurs in manufactured homes (Sutley et al., 2020). Firstly, damage is commonly observed in the trailer structure itself, often caused by building envelope damage, inadequate roof-to-truss, or roof-to-wall connections. Secondly, the foundation of the home is susceptible to issues such as the trailer sliding off the foundation or experiencing overturning failure. Finally, attached structures, which are often poorly connected, can

suffer damage themselves and create vulnerabilities within the trailer, potentially leading to a cascade of failures.

Due to the lack of information regarding the wind actions on MHs and their observed vulnerabilities during strong windstorms, this research aims to investigate the aerodynamics of MHs using large-scale wind tunnel experiments at the National Science Foundation (NSF)-designated Wall of Wind (WOW) Experimental Facility (EF) at Florida International University (FIU). The model construction details are presented in Section 2 along with the test protocol. Pressure, force, and moment coefficients obtained from this study are then discussed in Section 3. Finally, concluding remarks and recommendations for future work are presented in Section 4. The data obtained from this study will be used to inform building component testing and numerical simulations (using finite element modeling) of the behavior of MHs during extreme wind events. Most importantly, the findings of this study may also be used to help improve the provisions in building design codes and standards as well as to inform risk assessment models.

Figure 1. Examples of reported damage (Sutley et al. 2020)

2. Methodology

2.1. Model construction

In this study, a 1:4 scale MH was tested using actual member sizes based on the survey conducted by (Sutley et al., 2020). The model was a gable roof structure with plan dimensions of 82” x 144” (corresponding to 27’-4” x 48’ in full scale) with roof height of approximately 38” (corresponding to 12’-8” in full scale). The schematic of a typical framing section is shown in Fig. 2. The assembly of the trusses was performed in-house at the WOW EF with Simpson strong tie 4”x2” and 3”x6” mending plates (Strong-Tie, 2021), as shown in Fig. 3.

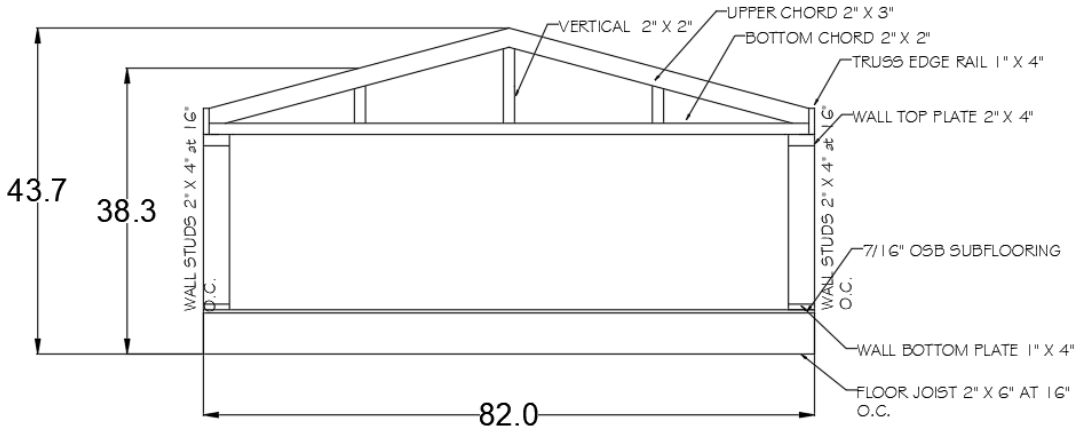

Figure 2 Schematic of typical framing

Figure 3 Truss assembly

The details of the roof-to-wall and floor-to-wall connections utilized a 26-gauge metal strap with six 0.131”x3” nails at each end. The details of the wall-to-roof connections are shown in Fig. 4. Similarly, the details of the floor-to-wall connection are shown in Fig. 5. Oriented Strand Board (OSB) sheathing was attached to framing members using 0.131”x2-3/8” nails with 6” edge spacing and 12” field spacing as

shown if Fig. 6. The completed model placed on the WOW turntable is shown in Fig. 7. The model was elevated and placed on six degree-of-freedom (6DOF) load cells at the four corners, as shown in Fig. 8

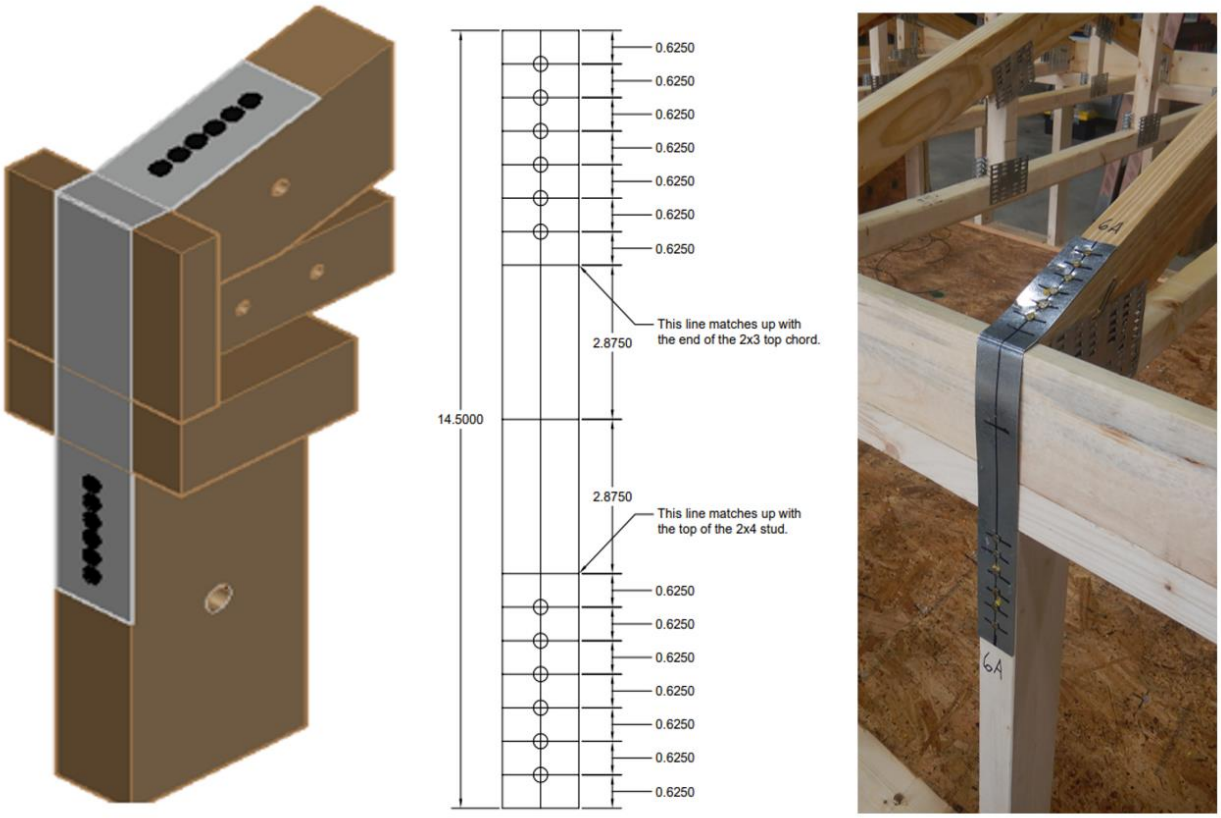

Figure 4 Roof-to-wall connection detail

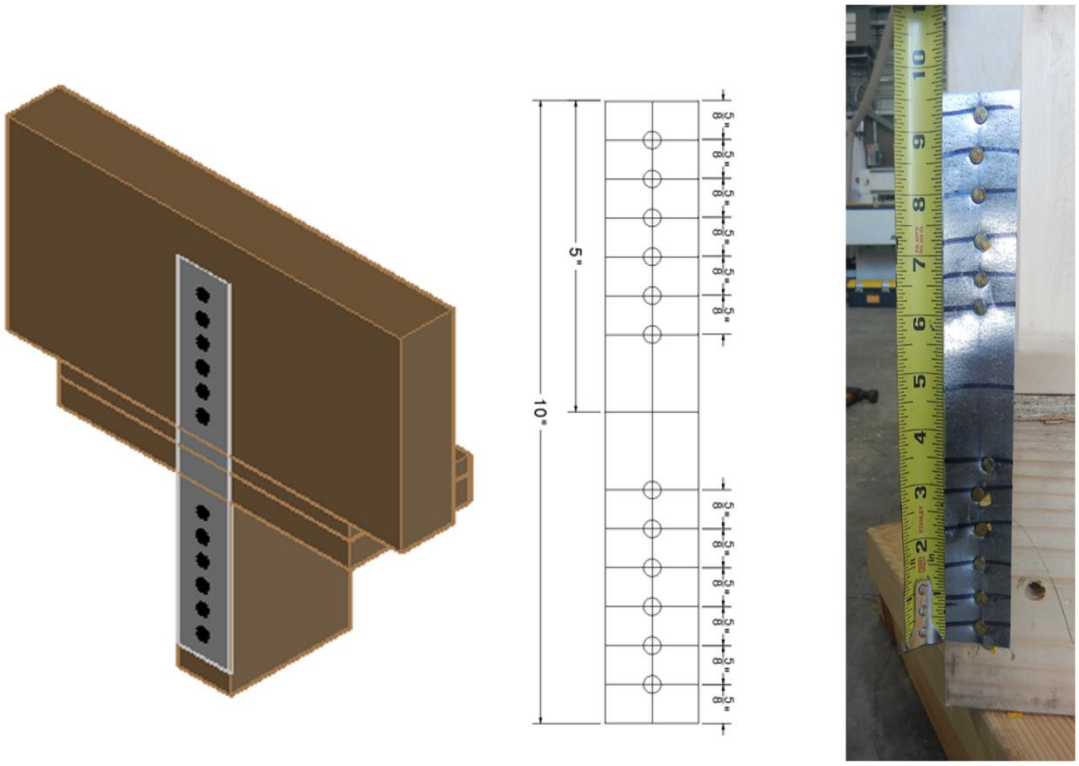

Figure 5 Wall-to-floor connection detail

Figure 6 Edge and field spacing of sheathing nails

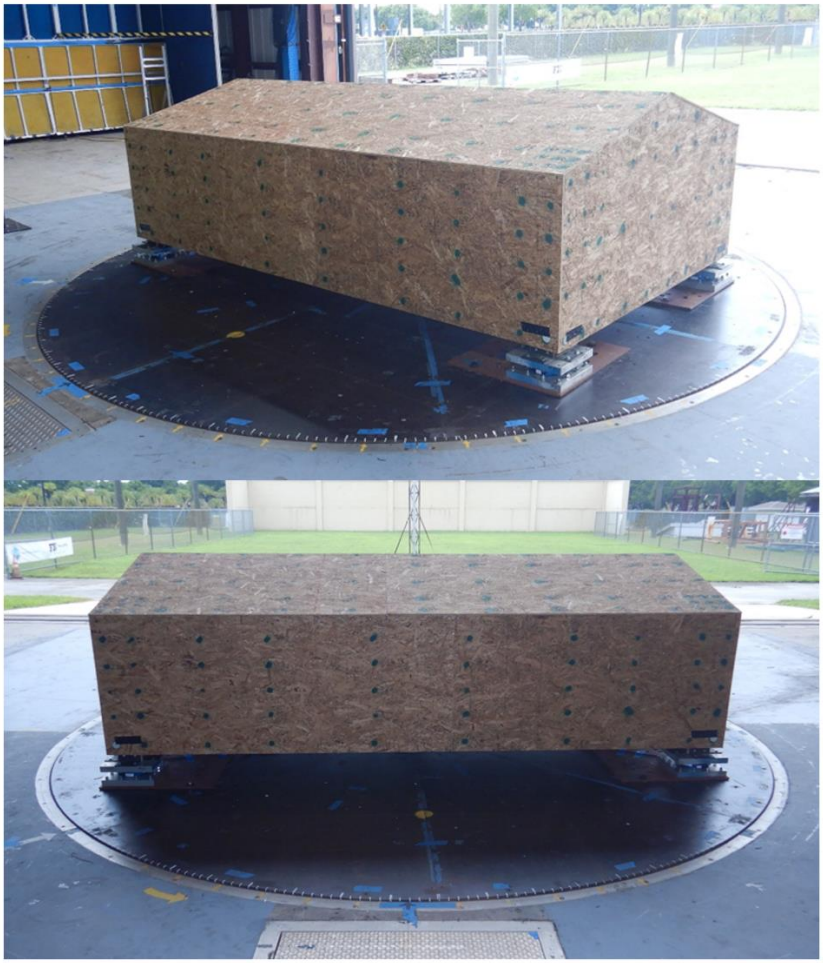

Figure 7 Final model on WOW turntable

Figure 8 Typical 6DOF load cell installation

2.2. Instrumentation

To inform the finite element modeling (FEM), the 1:4 experimental model was equipped with 376 external and four internal pressure taps as shown in Fig. 9, marked by the green paint. Specifically, 46 taps were installed on each gable wall ("East" and "West" walls), 50 taps were installed on each side wall ("North" and "South" walls), 150 taps were installed on the roof, and 34 taps were installed on the floor. The pressure taps were connected to a ZOC33/DSM4000 Scanivalve data acquisition system, which sampled pressures at a rate of 625 Hz. A tubing transfer function was used to correct the recorded pressure data for distortion effects introduced by the tubing length (Irwin et al., 1979)(Irwin et al., 1979)(Irwin et al., 1979)(Irwin et al., 1979)(Irwin et al., 1979)(Irwin et al., 1979)(Irwin et al., 1979)(Irwin et al., 1979)(Irwin et al., 1979)(Irwin et al., 1979)(Irwin et al., 1979)(Irwin et al., 1979). The pressure tap layout is shown in Fig. 10. The model was also outfitted with 12 Banner L-GAGE model LE550 laser gauging sensors to measure different connection displacements within the model, such as the wall-to-floor connection, roof-to wall connection and roof sheathing displacement. The measurement sensitivity of these sensors was < 0.02 in (< 0.5mm). A schematic diagram of the location of the laser sensors is shown in Fig. 11. The model was secured to the WOW EF turntable via 6DOF load cells to measure the overall forces imposed on the model by the wind. Figure 12a shows the instrumentation inside the model and Fig. 12b shows the installed laser displacement sensors.

2.3. Test Protocol

The model was tested at different wind speeds and wind directions ranging from 60 mph to 140 mph measured at mean roof height. At each wind speed the model was tested at 15 degrees wind direction increments ranging from 0 degrees to 345 degrees, yielding a total of 24 wind directions per wind speed.

Figure 9 Examples of pressure tap location.

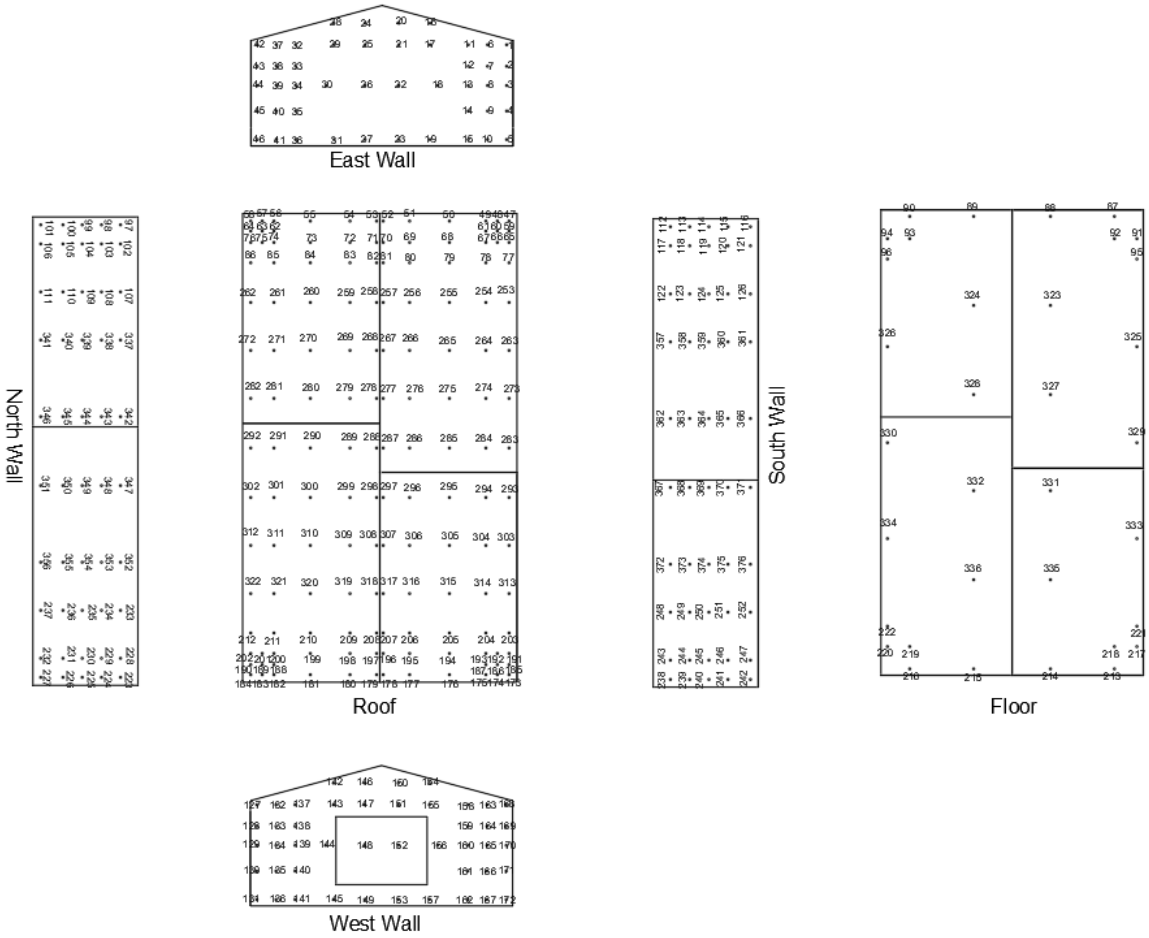

Figure 10 Pressure taps layout.

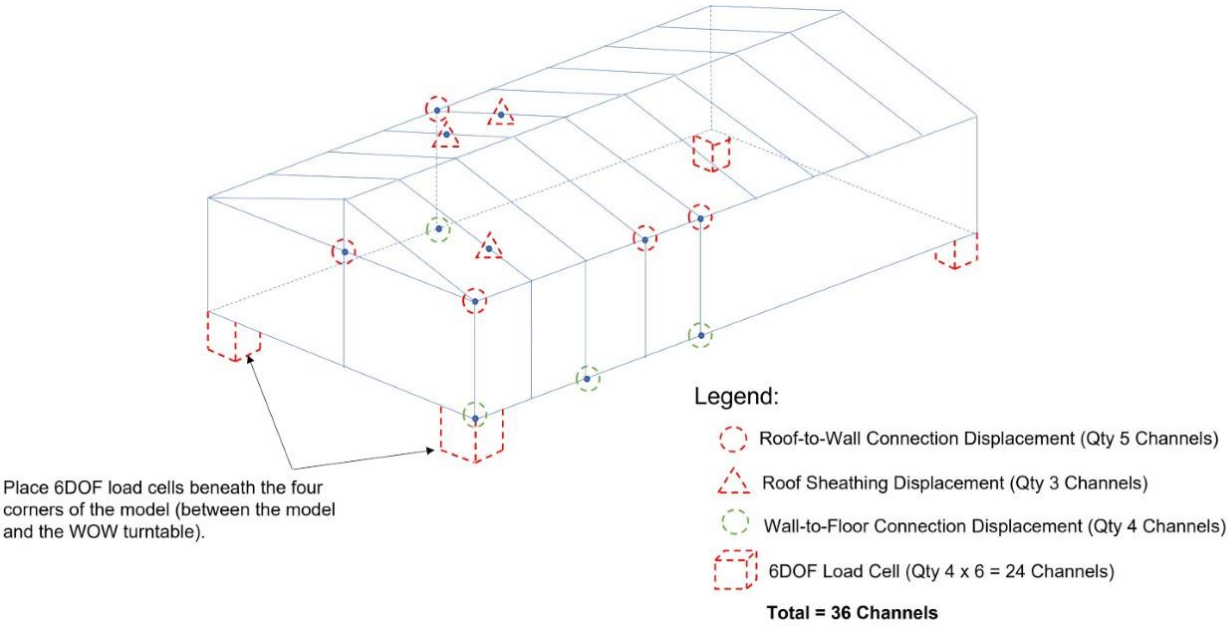

Figure 11 Schematic of the location of the laser sensors

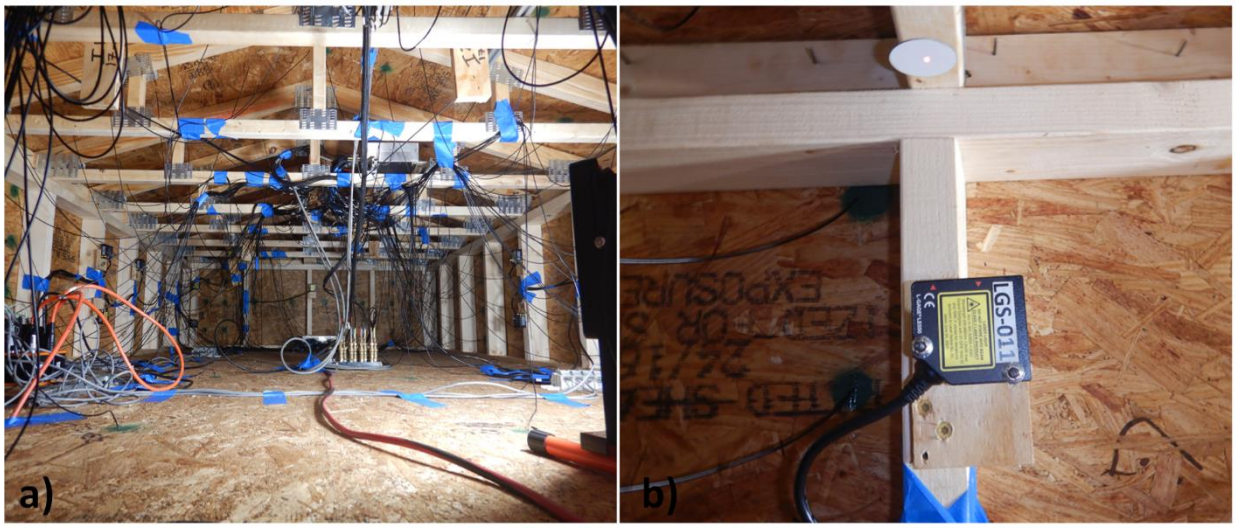

Figure 12 a) Instrumentation inside the model, b) Installed laser sensor with target (typical)

2.4. Flow simulation

The 12-fan WOW EF, depicted in Fig. 13a, is a unique testing facility designed for large-scale experiments. It has the capability to generate wind speeds of up to 70 m/s (157 mph) and turbulence characteristics comparable to those observed in Category 5 hurricanes according to the Saffir-Simpson scale (Chowdhury

et al., 2018; Gan Chowdhury et al., 2017). To simulate wind flows in the Atmospheric Boundary Layer (ABL) across different terrains, the WOW is equipped with spires and floor roughness elements as shown in Fig. 13 (b). Wind speed probes (Turbulent Flow Instrumentation Cobra Probes) were used to measure free-stream wind speeds at model heights of 6.9 in, 27.5 in, 45.8 in, 92 in, 114.5in.

Figure 13 a) 12-fan WOW EF; b) Spires and floor roughness elements

The mean wind velocity and turbulence intensity profiles are presented in Figure 14a. Figure 14b shows the power spectral density (PSD) of the WOW longitudinal velocity fluctuations at the mean roof height along with the full-scale Von-Karman PSD based on ESDU item 85020 (ESDU, 2001) for a roughness length Z_0 = 0.08m.

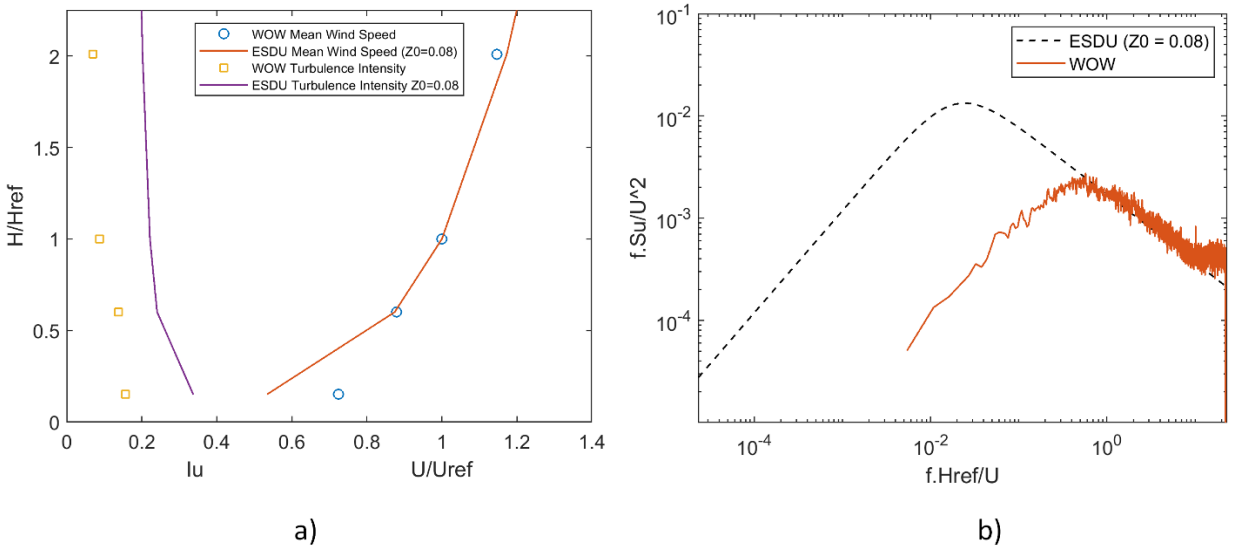

Figure 14 a) Mean wind speed and turbulence intensity profiles; b) PSD of the longitudinal wind velocity fluctuations.

As shown in the simulation of the power spectral density, due to the large-scale of the model, the low frequency turbulence fluctuations are not adequately simulated at the WOW due to the limited cross-section of the wind tunnel. This can be corrected by analytically correcting the data by applying the Partial Turbulence Simulation (PTS) technique to account for the missing low frequency (Asghari Mooneghi et al., 2016). However, for this study such correction is not deemed necessary as the main purpose is to calibrate a FEM technique that will use the physical model responses (e.g., displacements) for validation. A follow up study should consider applying the PTS method to account for the missing low frequency turbulence.

2.5. Data Analysis

External pressure time histories were collected for the first two experimental wind speeds, i.e., 60mph and 80mph. Pressure coefficient time histories $C_p(\theta,t)$ were calculated using Equation (1), where $P(\theta,t)$ is the pressure time series in Pa (psf), P_0 is the static reference pressure in Pa (psf), ρ is the air density in kg/m^3 (slugs/ft^3), θ is the wind azimuth, and $\overline{U}$ is the mean wind speed in m/s (mph) at the mean roof height.

$$C_p(\theta,t) = \frac{P(\theta,t) - P_0}{\frac{1}{2}\rho\overline{U}^2} \quad (1)$$

Net force $C_F(\theta,t)$ and moment $C_M(\theta,t)$ coefficient time series were computed for the x, y, and z directions. These coefficients represent the drag, lift, and overturning moment coefficients depending on the wind azimuth θ, as described in Equations (2) to (6), where d_i in m (ft) refers to the moment arm measured from the pressure tap location to the height where the model is anchored to the load cells, H in m (ft) refers to the mean roof height, and A_i refers to the tributary area of each pressure tap.

$$C_{F_x}(\theta,t) = \frac{\sum_i \left(C_{P_{East,i}}(\theta,t) - C_{P_{West,i}}(\theta,t)\right).A_i}{\sum_i A_i} \quad (2)$$

$$C_{F_y}(\theta,t) = \frac{\sum_i \left(C_{P_{South,i}}(\theta,t) - C_{P_{North,i}}(\theta,t)\right).A_i}{\sum_i A_i} \quad (3)$$

$$C_{F_z}(\theta,t) = \frac{\sum_i \left(C_{P_{Roof,i}}(\theta,t) - C_{P_{Floor,i}}(\theta,t)\right).A_i}{\sum_i A_i} \quad (4)$$

$$C_{M_x}(\theta,t) = \frac{\sum_i C_{F_{y,i}}(\theta,t).d_i}{H} \quad (5)$$

$$C_{M_y}(\theta, t) = \frac{\sum_i C_{F_{x,i}}(\theta, t).\, d_i}{H} \quad (5)$$

Peak pressure, force, and moment coefficients, referenced by the 3-sec full-scale gust wind speed $\overline{U}_{3s} = \overline{U}_{1hr}(1 + 3.4I_{u,p})$, were estimated for a 1-hr storm duration using Extreme Value Analysis with 100 subintervals. Specifically, the peaks were fitted into a Fisher Tippet Type-I distribution based on a non-exceedance probability of 0.78 (Lieblein, 1974).

3. Results and Discussion

Results of the large-scale aerodynamic experiments on MHs are presented in this section for a range of wind speeds and directions. The mean and peak pressure, force, and moment coefficients on the isolated MH model are discussed in Section 3.1

3.1. Aerodynamics of an isolated MH

3.1.1. Spatial distribution of pressure coefficients

The aerodynamics of an MH followed those of a typical bluff body under the action of wind flows. The distribution of mean pressure coefficients $\bar{C}_p$on the roof and walls of the isolated MH model are presented for wind directions 0°, 45°, and 90° in Figures 15, 16, and 17, respectively. For perpendicular wind directions, the highest roof suctions are observed at the leading edges under the separation bubble. The suctions are larger along the roof's length than those along its width [e.g., $\bar{C}_p$ (0°) = - 1.4 and $\bar{C}_p$ (90°) = -0.8]. This is due to the flow separation being more significant on the leading edge parallel to the ridge. As the distance from the leading-edge increases, $\bar{C}_p$ tend to decrease in magnitude from -1.4 to -0.2 for 90° due to flow reattachment. For cornering winds, high suctions were observed at the upwind corner and leading edges due to the formation of conical vortices [e.g., $\bar{C}_p$ (45°) of -1.8]. The windward wall was subjected to positive $\bar{C}_p$ of around 0.5 to 0.9, while suctions around -0.4 to -0.6 were observed on the leeward and side walls.

In addition to $\bar{C}_p$, critical peak pressure coefficients $\hat{C}_P$ (maximum and minimum) from all wind directions are presented in Figures 18 & 19, respectively. For minimum results, $\hat{C}_P$ distribution ranging from around -1.5 to -5.0 was observed on the roof; values ranging from -0.8 to -2.0 were observed on the walls; and values ranging from -0.8 to -1.1 were observed on the floor. For maximum results, $\hat{C}_P$ distribution ranging from around 0.2 to 0.5 was observed on the roof; values ranging from 1.0 to 1.4 were observed on the walls; and values ranging from 0.4 to 0.8 were observed on the floor.

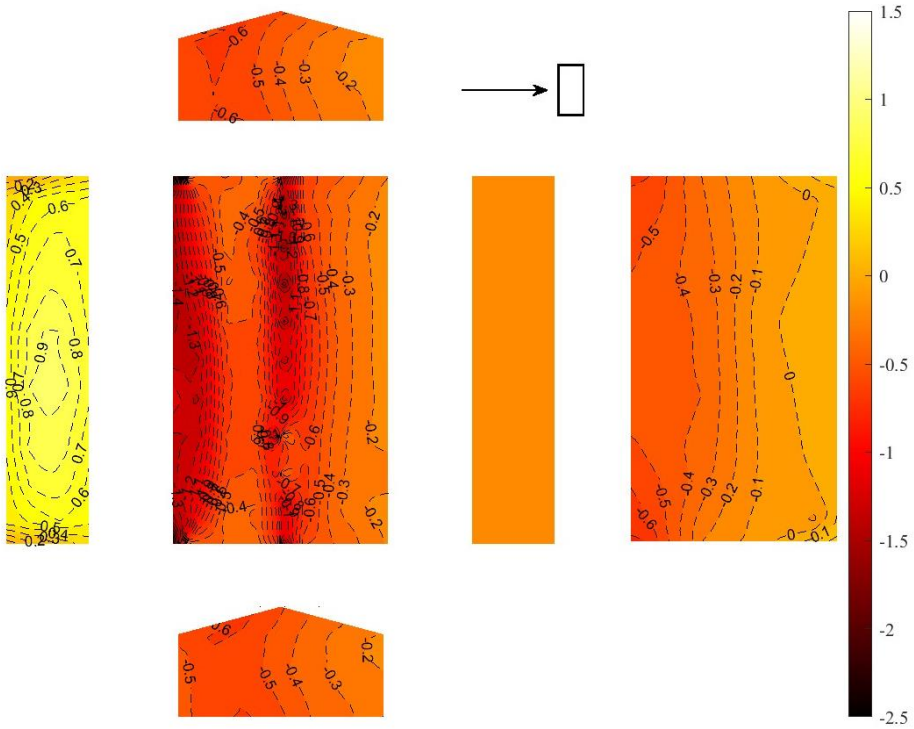

Figure 15 $\bar{C}_p$ for 0° wind direction

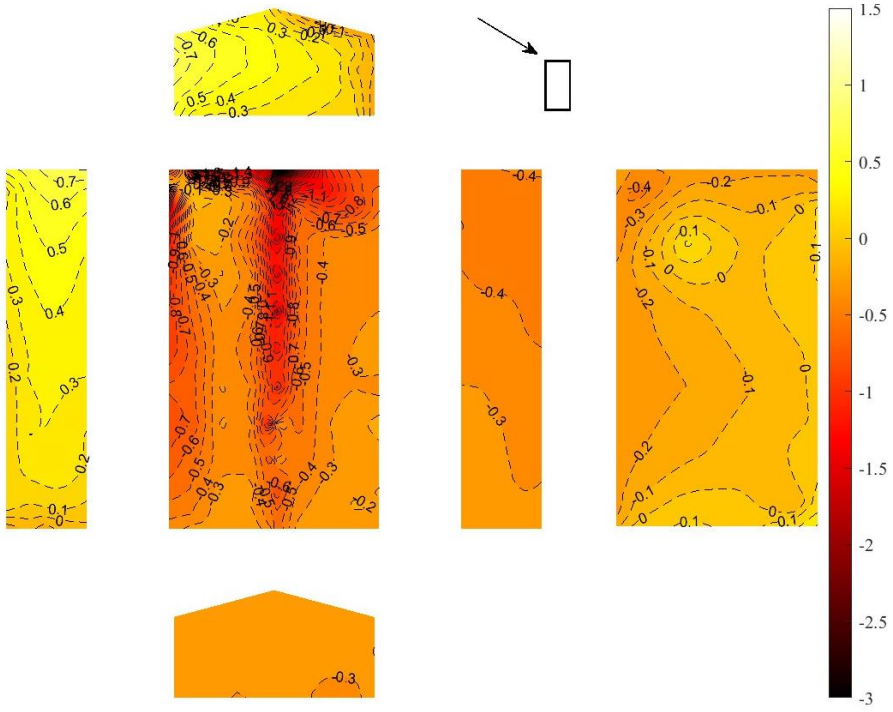

Figure 16 $\bar{C}_p$ for 45° wind direction

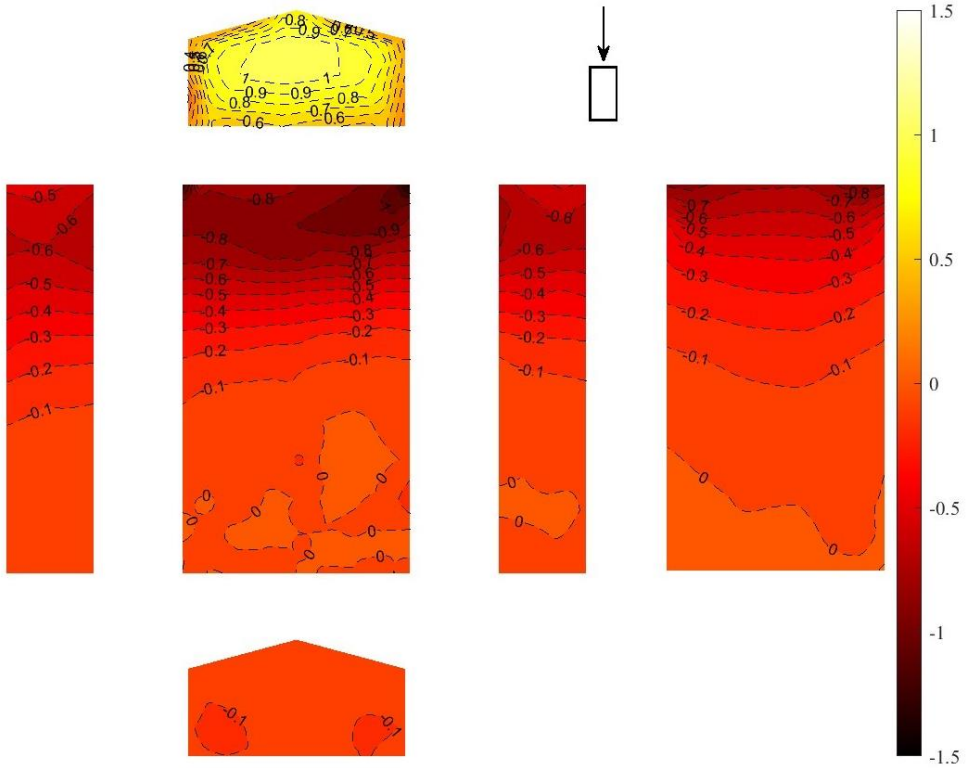

Figure 17 $\bar{C}_p$ for 90° wind direction

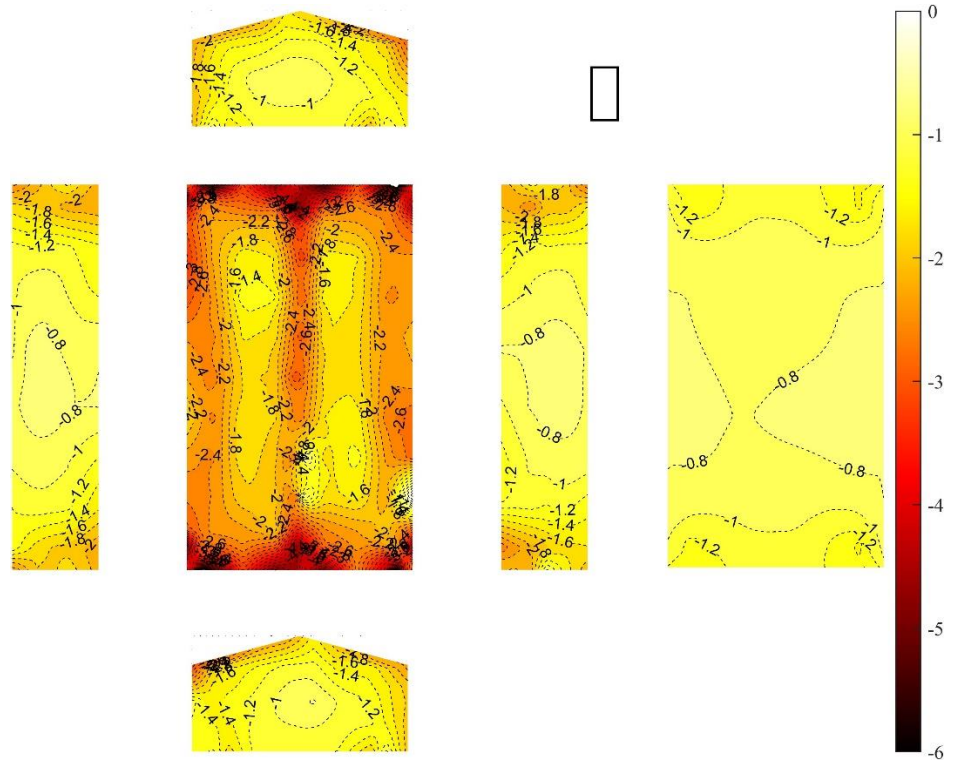

Figure 18 Critical minimum $\hat{C}_P$

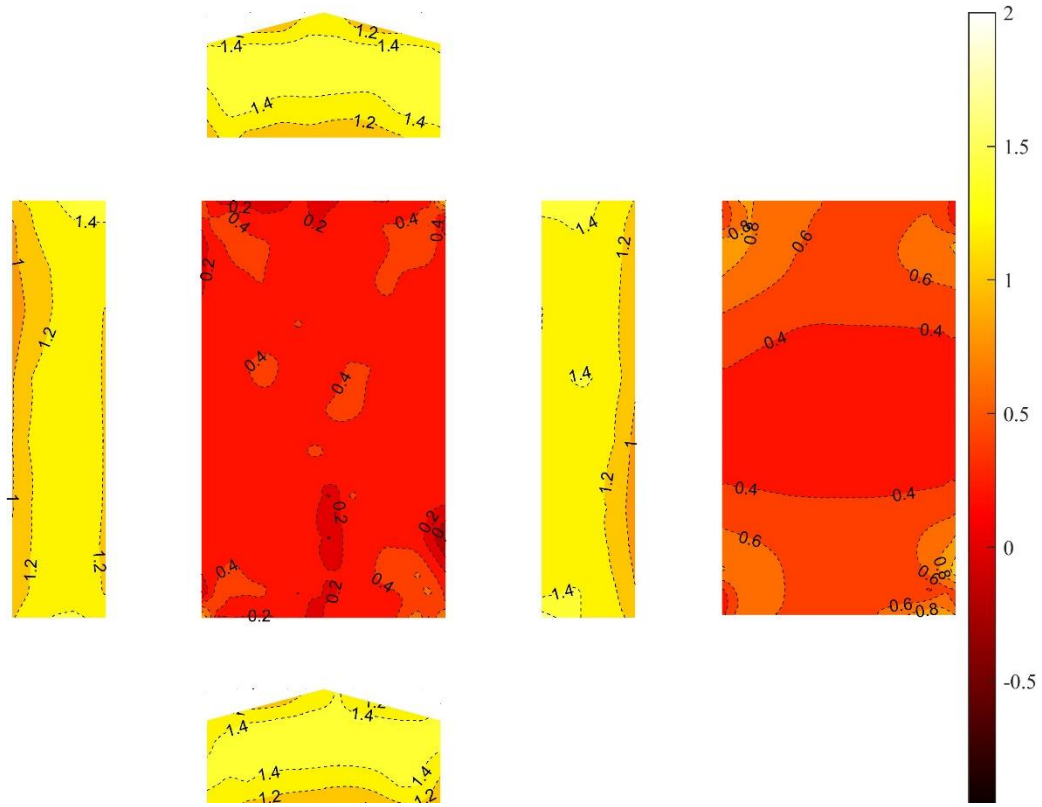

Figure 19 Critical maximum $\hat{C}_P$

3.1.2. Force and moment coefficients

From a design perspective, force and moment coefficients can be used to calculate the base shear and base overturning moments— important loads in the wind design of the foundation system. The largest $\bar{C}_{Fx}$ of +/-0.8 and $\hat{C}_{Fx}$ of +/-1.1 acting normal to the East and West walls (Gable walls) were observed for wind directions of 90° and 270°. On the other hand, $\bar{C}_{Fy}$and $\hat{C}_{Fy}$ acting normal to the side walls are the largest for 0° and 180° wind directions ($\bar{C}_{Fy}$ of +/-0.8 and $\hat{C}_{Fy}$ of +/-1.1). In addition, it was observed that the magnitude of $\bar{C}_{Fx}$ and $\hat{C}_{Fx}$ increased as $\bar{C}_{Fy}$ and $\hat{C}_{Fy}$ decreased, and vice versa. This indicates that the drag coefficients C_{Fx} and C_{Fy} are the most critical when they are parallel to the wind direction. Similar observations were made for the moment coefficients: the largest $\bar{C}_{Mx}$ of +/-0.35 and $\hat{C}_{Mx}$ of +/-0.45 were detected for 0° and 180°, while the largest $\bar{C}_{My}$ of +/-0.48 and $\hat{C}_{My}$ of +/-0.6 were observed for 90° and 270°, which are in line with the critical directions of C_{Fx} and C_{Fy} respectively. These results are shown in Fig. 20.

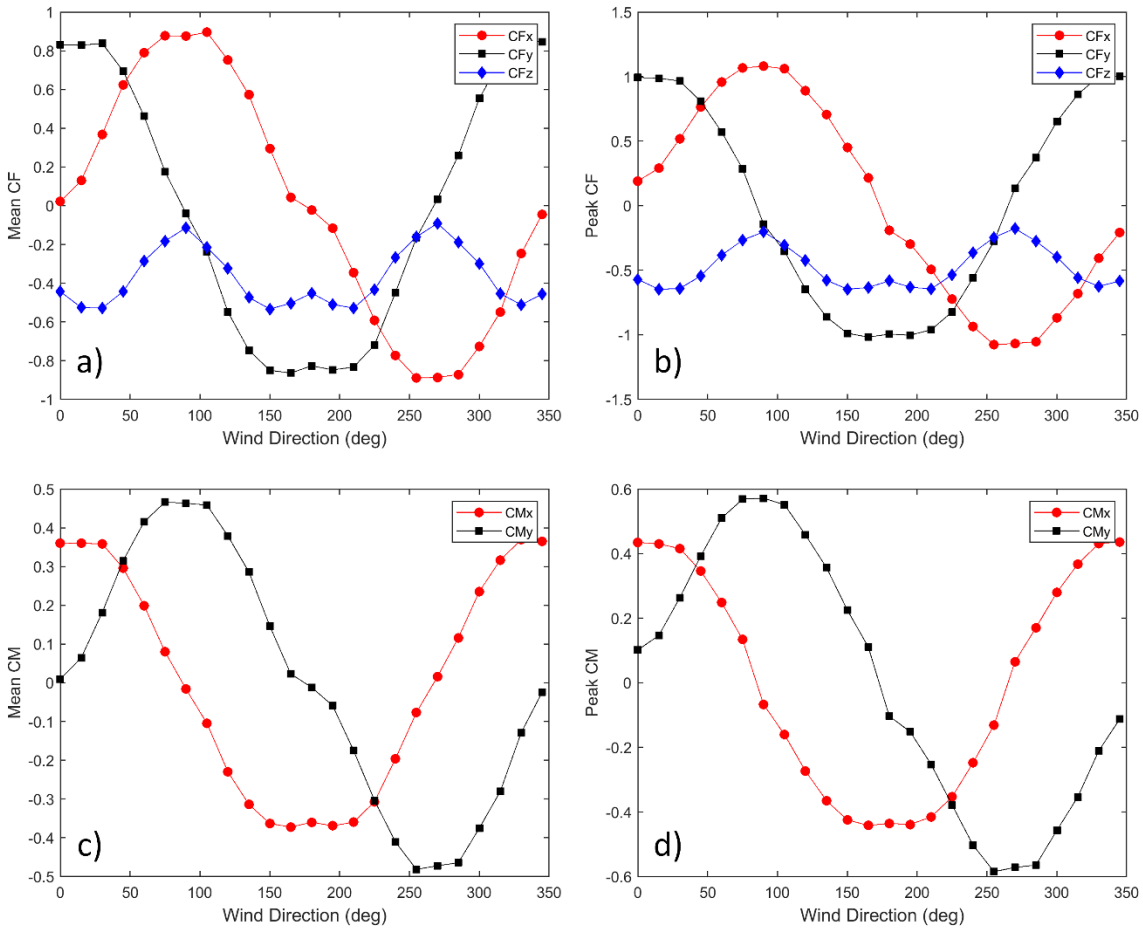

Figure 20 a) $\bar{C}_F$ b) $\hat{C}_F$ c) $\bar{C}_M$ d) $\hat{C}_M$

3.1.3. Laser Displacement Data

Laser displacement data were mainly collected to provide a way of calibration to the finite element model. Therefore, only basic analysis of this data was conducted. In Fig. 21, the absolute value of the instantaneous peak displacement of all wind directions is plotted for each sensor at all wind speeds. For 11 of the 12 laser displacement sensors, the maximum deflections were less than 0.04 in (1.0 mm) for all wind speeds. The exception was LGS1, which measured the wall-to-floor connection displacement at one of the building model's corner joints. This sensor measured maximum instantaneous displacements consistently greater than all other sensors, with an overall maximum displacement of 0.098 in (2.5 mm) during the 140 mph test case. This indicates a potential vulnerability at this connection point. However, the connection's displacement was not noticeable to the naked eye before or after the experiments, and no failure of the connection was observed during the experimental campaign.

3.1.4. Load Cells Data

Similar to laser displacement data, load cell data are mainly collected for finite element modeling calibration purposes. Therefore, only basic analysis of this data was conducted. In Fig. 22, the mean value of the forces and moments are plotted for all wind directions at wind speed of 120 mph.

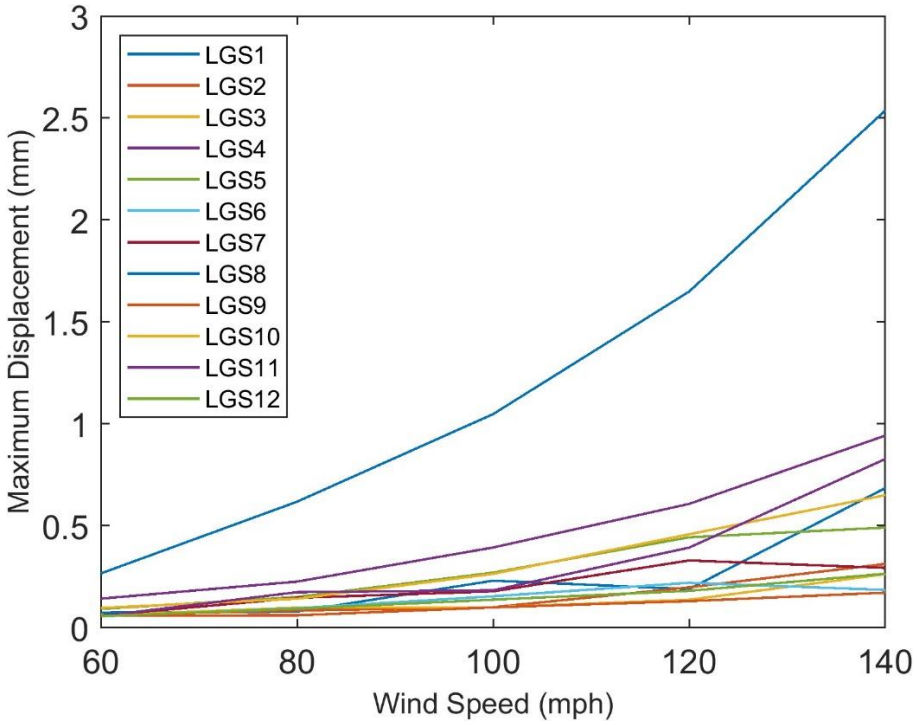

Figure 21 Absolute instantaneous peak of each laser sensor at all wind speeds

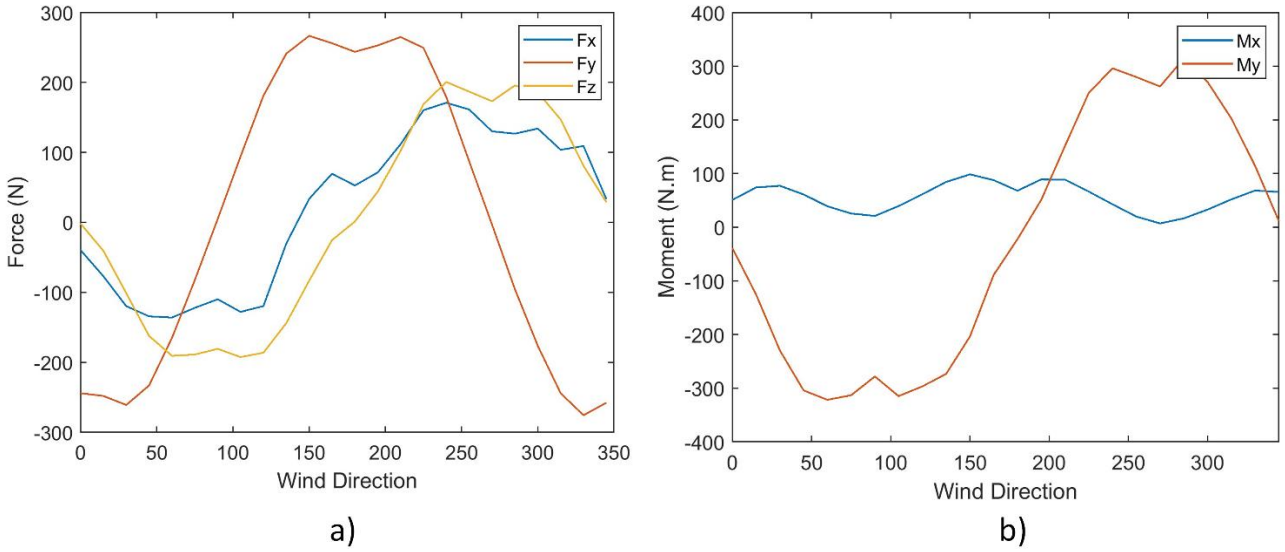

Figure 22 a) Mean Forces b) Mean Moments

4. Conclusions

This study evaluated wind loads on manufactured homes (MHs) using a large-scale experimental facility. The main objectives of the study were to investigate wind loads on a large-scale MH model by considering typical connections used in actual construction practice. This will serve the final target of the project: to validate the development of a finite element model of the MH. This entailed conducting aerodynamic experiments in simulated open terrain boundary layer flows at the WOW EF. Statistics of pressure, force, and moment coefficients obtained from the collected pressure time histories were used to assess wind effects on MHs. Based on these results, the following concluding remarks are provided:

• The spatial pressure distribution on isolated MHs is similar to that of typical low-rise buildings. Critical peak roof suctions of up to -5.0 were recorded near the corners and leading edges.

• Critical peak suctions of up to -2.0 and peak positive pressures of 1.4 were recorded on the walls.

• Critical peak suctions of up to -1.1 and peak positive pressures of 0.8 were recorded at the floor.

• Laser displacement and load cell data were collected mainly for the purpose of calibration of the developed finite element model

The findings of this study can be used to help improve the MH design provisions in current building design codes and standards as well as risk assessment models.

Benefits to the State of Florida

The research that was carried out has the potential to provide transformative impacts to new and existing mobile home parks, and to manufactured housing units through critical fundamental and practical knowledge that can change code provisions, policies, and manufacturing processes. The findings can inform new ASCE 7 provisions and lead to significantly improved HUD design standards for MH units. The findings can also be shared with MH builders and park owners and residents, as well as FEMA to inform new site development for post-disaster temporary housing that uses manufactured homes. Findings are applicable beyond MH units used as permanent housing including post-disaster temporary shelters and housing used in the U.S. and internationally. The research is important for Florida and Floridians (and the entire U.S.) in terms of understanding and reducing the vulnerability of MH units. The research activities helped in training students in three universities with expertise in hurricane damage mitigation.

Acknowledgment

The authors would like to acknowledge the financial support from the State of Florida Division of Emergency Management (FDEM). The experiments at the NSF NHERI WOW EF were greatly facilitated by the collaborative work of WOW staff members Dr. Steven Diaz, Walter Conklin, Dr. Dejiang Chen, James Erwin, and Manuel Matus. The authors also would like to acknowledge the help provided in model construction by PhD students: Haitham Ibrahim, Houssam Al Sayegh and Mohamed Eissa. The opinions, findings, conclusions, or recommendations expressed in this article are solely those of the authors and do not represent the opinions of the funding agencies.

References

Asghari Mooneghi, M., Irwin, P., & Gan Chowdhury, A. (2016). Partial turbulence simulation method for predicting peak wind loads on small structures and building appurtenances. *Journal of Wind Engineering and Industrial Aerodynamics*, *157*, 47–62. https://doi.org/10.1016/j.jweia.2016.08.003

Chowdhury, A. G., Vutukuru, K. S., & Moravej, M. (2018). Full-and large-scale experimentation using the wall of wind to mitigate wind loading and rain impacts on buildings and infrastructure systems. *Proceedings of the 11th Structural Engineering Convention (SEC18)*.

ESDU, I. H. S. (2001). Characteristics of Atmospheric Turbulence Near the Ground—Part II: Single Point Data for Strong Winds (Neutral Atmosphere). *Engineering Sciences Data Unit, IHS Inc., London, UK, Report No. ESDU*, *85020*.

Gan Chowdhury, A., Zisis, I., Irwin, P., Bitsuamlak, G., Pinelli, J.-P., Hajra, B., & Moravej, M. (2017). Large-scale experimentation using the 12-fan wall of wind to assess and mitigate hurricane wind and rain impacts on buildings and infrastructure systems. *Journal of Structural Engineering*, *143*(7), 04017053.

IBTS. (2005). Assessment of Damage to Manufactured Homes Caused by Hurricane Charley.

Hebert, K., & Levitan, M. (2009). Performance of manufactured housing in Louisiana during Hurricanes Katrina and Rita. *Proc., 11th American Conf. on Wind Engineering. San Juan, PR: American Association of Wind Engineering, Polytechnic Institute of Puerto Rico*.

Irwin, H., Cooper, K. R., & Girard, R. (1979). Correction of distortion effects caused by tubing systems in measurements of fluctuating pressures. *Journal of Wind Engineering and Industrial Aerodynamics*, *5*(1–2), 93–107.

Lieblein, J. (1974). Efficient Lillethods of Extreme-Value Methodology. *No. October*.

Strong-Tie, S. (2021). *Catalog: Wood Construction Connectors 2021-2023 (C-C-2021)*.

Sutley, E. J., Asce, A. M., Vazquez, K., Asce, S. M., Kim, J. H., Dao, T., Johnston, ; Blythe, & Hunt, J. (2020). *Performance of Manufactured Housing during Hurricanes Irma and Michael*. https://doi.org/10.1061/(ASCE)CF.1943

SECTION 2 PART B:
UNDERSTANDING HURRICANE EFFECTS ON MANUFACTURED HOMES

FINAL REPORT
(Period: 2023)

A Research Project Funded by:
The State of Florida Department of Emergency Management

Prepared by
Kansas University

Dr. Elaina J. Sutley
Dr. William Collins

Graduate Students
Jon Hankins
Afeez Badmus

Introduction

A significant portion of Florida households live in manufactured housing units (MHUs) (approximately 7%). While the performance of MHUs continues to be a problem after hurricanes and other major windstorms, the structural design level of MHUs is not well understood. The overall goal of this research is to provide the fundamental and practical knowledge needed to significantly reduce the physical vulnerability of manufactured homes to wind events through a quantitative capture of structural design levels for Wind Zone II and Wind Zone III MHUs. Extensive research has been conducted on site-built light-frame wood construction, whereas little research exists on MHUs. Of the limited research that exists on MHUs, the focus is on anchorage systems, and there is a dearth in coverage on many observed failure modes, including roof and wall cladding loss and system failure. Research documented in this report aims to advance code provisions, policies, and manufacturing processes, to better protect manufactured home residents. This report presents the research from Phase II of the project carried out at the University of Kansas, which included (a) stakeholder engagement; (b) experimental testing of full-scale connections; and (c) a numerical benchmark study. The report is organized with a brief background to provide context to the study, which is followed by the methodology, results, and conclusions for each task.

Background

The design of manufactured homes is governed by the U.S. Department of Housing and Urban Development standard *Manufactured Home Construction and Safety Standards, Part 3280*, (termed HUD Code herein) which has not seen significant updates since 1994, and in which the wind hazard maps are developed from and reference use of the 1988 version of ASCE/SEI 7 *Minimum Design Loads and Associated Criteria for Buildings and Other Structures*. While site-built housing, and all other built structures have benefited from 35 years of technical and statistical advancements in wind engineering, provisions for manufactured homes have remained stagnant. Past events have demonstrated manufactured housing units to be the most vulnerable residential structure to windstorms, including hurricanes and tornadoes. Manufactured housing uses wood frame construction that is constructed fundamentally differently from site-built housing necessitating the need for MHUs to be studied specifically. Design provisions in the HUD Code are vague and leave a fair amount of interpretation for manufacturers. Our post-disaster field reconnaissance demonstrates high variability in manufactured home construction, within and across Wind Zones, which correlates to performance. There is no publicly available information on how manufactured homes are constructed. However, our team has obtained structural details from HUD and a major U.S. manufacturer of manufactured homes. Within those documents, there is significant variability. The true structural design level(s) of manufactured homes are unknown; quantifying such is a critical first step in being able to improve their wind performance.

Methodology

Stakeholder Engagement

During Phase I, the stakeholder engagement task had an intentional structure which involved hosting meetings with an advisory board to gain feedback on important decisions early in the project, to build new connections for the project team with relevant experts, and to stimulate interest and momentum in the study of manufactured housing. Phase II continued building on many of the decisions made during Phase I, and leveraged new relationships gained during Phase I to facilitate focused conversations instead of large advisory group discussions.

Phase II stakeholder engagement was initiated through phone calls, emails and social media (LinkedIn and Facebook) communications that led to scheduled discussions with members of the Manufactured Housing Institute, HUD's Manufactured Housing Consensus Committee, the Lincoln Institute, the Federal Emergency Management Agency, and Institute for Business and Home Safety to discuss the state of design and construction practice, gaps in current code provisions and the code change process, and/or goals of the FLDEM study, including exploring the possibility of testing a full-scale manufactured home in the FIU Wall of Wind. The team failed to reach any manufacturers of manufactured home despite continued efforts.

Components and Connection Testing

The primary goal of the experimental component and connection testing of this project is to provide a quantitative measurement of the performance of key connection(s) needed for advancing the finite element model being developed at the University of Alabama (UA). In Phase I, the roof sheathing to rafter (S2R) connection was identified as the most important, and thus was the sole focus of Phase I. Phase II continued the RSR connection tests, and also initiated tests for wall to floor (W2F) connections, a site of common failures observed in practice. Using structural details provided by HUD and a major U.S. manufacturer, typical connection details for Wind Zone II and Wind Zone III MHUs homes were tested to quantify behavior and thereby wind performance. For each of the three connections, the testing adopted a two-step quasi-static cyclic testing protocol that started with monotonic testing to inform the second step of cyclic testing. This section reports the test configuration, nomenclature, setup, and load protocol.

Test Configuration

The HUD Code does not specify connection design or fastener schedules beyond the requirement that connections be engineered to resist the specified loads. For the S2R connection, a 150-mm (6-in.) fastener spacing was adopted per International Building Code (2006) for hurricane-prone regions. Table 1a provides the fastener diameter, length, and thread patterns, and geometric properties for the wood materials used in the S2R connections per National Design Specification (2018). Table 1b provides the fastener diameter, length, and thread patterns, and geometric properties for the wood materials used in the W2F connections per National Design Specification (2018).

Table 1a. Geometric Properties of Roof Sheathing to Rafter (S2R) Connection

Component	Description	Geometric Properties		
Rafter	Spruce-Pine-Fir (SPF)	38.1-mm x 88.9-mm (1.5-in. x 3.5-in.)		
	Southern Yellow Pine (SYP)	38.1-mm x 88.9-mm (1.5-in. x 3.5-in.)		
Sheathing	Oriented Strand Board (OSB)	11.1-mm (7/16-in.) thick		
	3-Ply Plywood	12.7-mm (0.5-in.) thick		
Fastener	**Type**	**Length mm (in.)**	**Shank Diameter mm (in.)**	**Head Diameter mm (in.)**	**Thread Length mm (in.)**
Smooth Shank Nail	8d common	60.33 (2.38)	2 3/8 (0.11)	7.15 (9/32)	n/a
Screw	#8	50.8 (2.0)	2.819 (0.11)	10.82 (0.43)	33 (1.3)

Table 1b. Geometric Properties of Wall to Floor (W2F) Connection

Component	Description	Geometric Properties		
Stud	Spruce-Pine-Fir (SPF)	38.1-mm x 88.9-mm (1.5-in. x 3.5-in.)		
Bottom Plate	Spruce-Pine-Fir (SPF)	19.1-mm x 88.9-mm (0.75-in. x 3.5-in.)		
Sheathing	Oriented Strand Board (OSB)	11.1-mm (7/16-in.) thick		
Floor Joist	Spruce-Pine-Fir (SPF)	38.1-mm x 139.7-mm (1.5-in. x 5.5-in)		
Fastener	**Type**	**Length mm (in.)**	**Shank Diameter mm (in.)**	**Head Diameter mm (in.)**	**Crown Length mm (in.)**
Staple	15 Gauge	63.5 (2.5)	1.83 (0.072)	N/A	11.1 (7/16)
	16 Gauge	31.75 (1.25)	1.59 (0.0625)	N/A	11.1 (7/16)

Smooth Shank Nail	Clipped Head	76.2 (3)	3.3 (0.131)	7.3 (0.286)	N/A
		50.8 (2)	2.9 (0.113)	6.9 (0.272)	N/A
		50.8 (2)	2.5 (0.099)	6.1 (0.242)	N/A

The drawings and documentation from HUD specified multiple design options for each of the connections tested here. Table 2a summarizes the component details and number of tests for the S2R connection specimens. Three S2R configurations were fabricated. The first consisted of a single field fastener on 203-mm x 203-mm (8-in. x 8-in.) sheathing. The second configuration consisted of two field fasteners spaced 150-mm (6-in.) center-to-center on 203-mm x 203-mm (8-in. x 8-in.) sheathing. For the first and second configurations, 40 specimens of each nailed and screw connection type were tested. The third configuration consisted of two field fasteners with 150-mm (6-in.) center-to-center spacing on 203-mm x 330-mm (8-in. x 13-in.) sheathing, where 24 specimens of each nailed and screw configuration were tested.

Similarly, Table 2b summarizes the component details for the W2F connections. Using the drawings and documentation from HUD, the capacity of each connection was calculated in accordance with NDS or manufacturer data for any specific product. The connection designs tested here represent the lowest and highest capacity connections for each wall section of the MHU. The strap for the wall-to-floor connection remained a constant 254-mm (10-in.) length based on the feedback from HUD. To keep fastener patterns similar, a common length of 16-mm (5/8-in.) was selected for the fasteners located at the top and bottom ends of the strap connecting to the stud and floor joist or roof rafter. The floor sheathing and bottom plate required a gap of 30-mm (1 3/16-in.), so the remaining 160-mm (6 5/16-in.) was evenly divided between the wall stud and floor joist. Each quantity of fasteners has its own spacing based on equally dividing the 80-mm (3 5/32-in.) of strap overlaying the wood members.

The four wall sections, namely, endwall, endwall with openings, sidewall, and shearwall, result in eight total fastener configurations. The division of connections by wall section is a differentiation made by the manufacturer. Fastener patterns were not specified in the drawings or documentation from HUD; photographs taken of damaged manufactured homes after Hurricane Michael (Sutley et al. 2021) show variations of stagger, row, and somewhat random patterns of fasteners on the strap connections. Thus, for each fastener type, a stagger and row pattern were considered. All combinations considered, there are 16 unique configurations for the W2F connections tested here. For each of these, three specimens were constructed and tested for both a set of monotonic tests and a set of cyclic tests.

Table 2a. Roof Sheathing to Rafter (S2R) Test Matrix

			Single fastener		Two fasteners			
			Monotonic test	Cyclic test	Monotonic test	Cyclic test	Monotonic test	Cyclic test
Sheathing type	Rafter type	Fastener	203 mm x 203 mm (8 in. x 8 in.) sheathing		203 mm x 203 mm (8 in. x 8 in.) sheathing		203 mm x 330 mm (8 in. x 13 in.) sheathing	
OSB	SPF	#8 screw	5	5	5	5	3	3
		Nail	5	5	5	5	3	3
	SYP	#8 screw	5	5	5	5	3	3
		Nail	5	5	5	5	3	3
Plywood (3-ply)	SPF	#8 screw	5	5	5	5	3	3
		Nail	5	5	5	5	3	3
	SYP	#8 screw	5	5	5	5	3	3
		Nail	5	5	5	5	3	3

Table 2b. Wall to Floor (W2F) Test Matrix

Fastener	Species	Monotonic Tests		Cyclic Tests		Wall Section
		Row	Stagger	Row	Stagger	
(2) 15- Gauge Staple	SPF	4	3	0	0	Endwall
(4) 2.5-mm (0.099 in.) Nails	SPF	3	3	0	0	Endwall
(4) 15 Gauge Staples	SPF	3	3	0	0	Endwall Opening
(8) 2.5-mm (0.099 in.) Nails	SPF	3	3	0	0	Endwall Opening
(6) 3.3-mm (0.131 in.) Nails	SPF	3	4	7	0	Sidewall
(13) 16-Gauge Staples	SPF	1	0	0	0	Sidewall
(8) 16-Gauge Staples	SPF	3	4	0	0	Shearwall
(7) 2.9-mm (0.113 in.) Nails	SPF	3	3	0	0	Shearwall

All lumber and sheathing used in this study were purchased at a local lumber store. S2R specimens were comprised of a rafter, sheathing, and fastener. Rafters were nominal 2x4 with dimensions of 38.1 mm x 88.9 mm (1.5 in. x 3.5 in.) southern yellow pine (SYP) or spruce-pine-fir (SPF) lumber, sheathing was oriented strand board (OSB) or 3-ply plywood, and fasteners were 8d common smooth shank nails or #8 screws. All lumber was graded No. 2 or better. Nails were installed using a pneumatic nail gun; screws were installed using a cordless drill driver. Screw holes were not pre-drilled to mimic the condition of how these structures are built in practice. Of note, in typical Wind Zone II manufactured homes, nails are the more common fastener used for roof sheathing-to-rafter connections. Based on HUD Code and field observation of manufactured homes after hurricane events, screws are rarely, if ever, used, but were tested here to investigate the potential increase in capacity with the upgrade of fastener. All specimens were tested under monotonic and quasi-static cyclic loading. Representative photographs of the S2R specimens are shown in Figure 1.

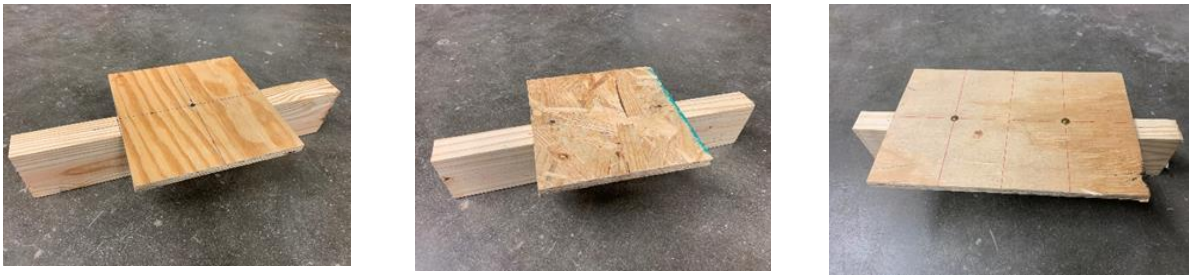

a) b) c)

Figure 1. S2R specimens: (a) single field fastener on 203-mm x 203-mm (8-in. x 8-in.) sheathing; (b) two field fasteners spaced 72-mm (6-in.) center-to center on 203-mm x 203-mm (8-in. x 8-in.) sheathing; (c) two field fasteners with 72-mm (6-in.) center-to-center spacing on 203-mm x 330-mm (8-in. x 13-in.) sheathing

The W2F specimens consisted of a wall stud, bottom plate, floor sheathing, floor joist, strap, and multiple fasteners. The wall studs were nominal 2x4 spruce-pine-fir (SPF) stud grade lumber with dimensions of 38.1 mm x 88.9 mm x 177.8 mm (1.5 in. x 3.5 in. x 7 in). The bottom plates were nominal 1x4 spruce-pine-fir (SPF) No. 3 grade lumber with dimensions of 19.1 mm x 88.9 mm x 215.9 mm (0.75 in. x 3.5 in. x 8.5 in.). The floor sheathing was 11.1 mm (7/16 in.) thick oriented strand board (OSB) with dimensions to match the nominal 1x4 bottom plate. The bottom plate was fastened to the wall stud using a single smooth shank nail with a diameter of 3.3 mm (0.131 in.) and a length of 76.4 mm (3 in) in the center of the stud. The bottom plate and stud assembly were fastened to the floor joist through the floor sheathing using two of the same smooth shank nails; these two nails were centered widthwise of the floor joist and located 44.4 mm (1.75 in.) from each end of the bottom plate. Finally, the strap was secured by maximizing the spacing possible on either end based on the number of specified fasteners for the given connection design (as described previously). An example image of each of these steps is provided in Figure 2.

a) b) c)

Figure 2 W2F specimen construction phases: (a) single nail joining the bottom plate and the wall stud; (b) two nails connecting the bottom plate and sheathing to the floor joist; (c) a sample of the strap fastened to the specimen using six nails with a diameter of 3.3 mm (0.131 in.)

The quantity of fasteners placed into the strap varied for each of the wall sections, but the fastener types remained the same. Of the five fastener types investigated, three were smooth shank nails with shank diameter of 3.3 mm (0.131 in.), 2.9 mm (0.113 in.), and 2.5 mm (0.099 in.). The other two fastener types were 7.9 mm (5/16 in) crown staples in both 15- and 16- gauge. All fasteners were placed using pneumatic tools that fit the specified fastener. Each connection design consisted of different quantities of fasteners per the drawings and HUD guidance. The endwall W2F connection designs consisted of (i) two 15-gauge staples for the lower end strength and (ii) four 2.5 mm (0.099 in.) diameter nails for the higher end capacity. The connections that represented the lower and upper bound capacity of endwall openings included (i) four 15-gauge staples and (ii) eight 2.5 mm (0.099 in.) diameter nails, respectively. The sidewall W2F connection lower limit used six 3.3 mm (0.131 in.) diameter nails, and the upper limit used thirteen 16-gauge staples. For the shearwall, the lower limit used eight 16-gauge staples, and the upper limit used seven 2.9 mm (0.113 in.) diameter nails.

Test Name Nomenclature

The test name nomenclature for the S2R connection corresponds to the test type, sheathing materials, rafter lumber species, fastener type, and fastener location. Monotonic tests are represented by an M; quasi-static cyclic tests are represented by a C. Sheathing material is denoted as O for OSB or P for plywood. Rafter lumber species is spelled out using the entire acronym for the species, either SPF or SYP. Fastener type is denoted as S for screw or N for nail; fastener location is denoted as F1 or F2 for one or two field fasteners, or E for edge. Finally, the last number in the name designates the test number in the series of similar tests. For example, M-O-S-SPF-F1-1 corresponds to the first monotonic test on OSB sheathing connected via screw to a SPF rafter with one field fastener.

The W2F connections adopt a similar nomenclature which indicates the test type, the fastener type and quantity, floor joist lumber species, and test number. Monotonic and quasi-static cyclic testing are represented by an M and C, respectively, and the floor joist species is spelled out using the acronym for the species (either SPF or SYP). A combination of a number, representing the quantity, and a letter, representing the type of fastener, were used to identify the fasteners securing the strap. For each fastener type, there are two letters. The letter that comes first in the alphabet indicates a row pattern (A, D, G, or M), and the letter that follows in alphabetical order indicates the stagger pattern (B, E, H, or N). Between each letter set a letter is left out to ensure a clean break between sets of letters (e.g., the first grouping is A-B and the second grouping is D-E, where C is skipped to provide distinction between connection details). The letters A and B designate the row and stagger pattern respectively for the nail with a 3.3 mm (0.131 in.) diameter shank. For the nail with a 2.9 mm (0.113 in.) diameter shank, the row and stagger pattern use the letters M and N, respectively. The letters representing the 2.5 mm (0.099 in.) diameter nails were G and H. The letters for the 15-gauge staple are J and K, and the letters that represent the 16-gauge staple are D and E. Lastly, the last set of numbers indicates the test number in the set of tests. Therefore, if a specimen uses a spruce-pine-fir floor joist, a fastener pattern of six nails with a diameter of 3.3 mm (0.131 in.) in a row, and is the first specimen of the set, the label for the specimen is M-6A-SPF-001.

Test Fixture

For each of the connection types, a steel fixture was designed and fabricated to be compatible with a 266 kN (60 kip) capacity Baldwin screw-drive test frame. Each fixture utilizes a 57.2-mm (2.25 in.) wide plate with a thickness of 25.4-mm (1 in.) and a length necessary to pass through the grips of the Baldwin and onto the associated grips. The fixtures allow for monotonic and cyclic force to be transferred to the connections.

The test fixture for the S2R connection is shown in Figure 3. The test fixture consists of a bottom sheathing grip made from A36 steel plate with dimension 76.2-mm x 457.2-mm x 25.4-mm (3-in. x 18-in. x 1-in.), top sheathing grip is a hollow square section (HSS) with dimension 254-mm x 101.6-mm x 12.7-mm (10-in. x 4-in. 0.5-in.). A 101.6-mm (4-in.) opening along one side of the 254-mm (10-in.) length of the HSS was made to create allowance for holding the sheathing While the bottom holds the rafter fixed in place, the top fixture grip transfers force through the sheathing into the fasteners, mimicking wind uplift on roof sheathing by attempting to extract the fasteners vertically from the rafter. To enable fully reversed displacement during cyclic loading, clamps were used to attach the sheathing to the top grip as shown in Figure 3b.

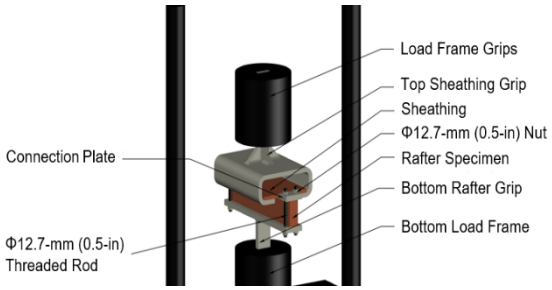

a)

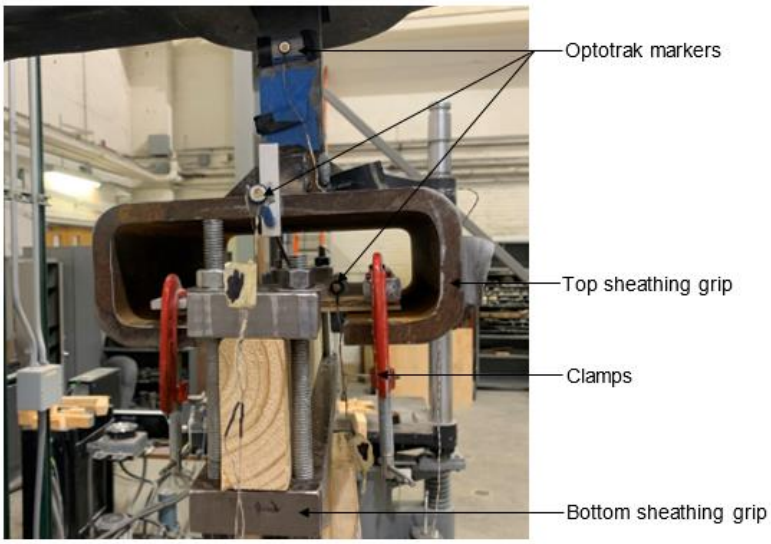

b)

Figure 3. Roof Sheathing to Rafter (S2R) Test Fixture: (a) Schematic; (b) Photograph in lab

The W2F connection has a similar steel frame. The frame consists of a set of grips which grip onto the floor joist and the wall stud separately, shown in Figure 4. The fixture is designed using welded A36 steel plates. For the bottom grip, two 12.7-mm (0.5 in.) bolts hold the stud in place by running through the stud and a set of 127-mm x 120.7-mm x 25.4-mm (5 in. x 4.75 in. x 1 in.) plates. These plates are welded to the base piece of steel which measures 127-mm x 158.8-mm x 25.4-mm (5 in. x 6.25 in. x 1 in.). This base piece is connected to the plates that run through the grips of the Baldwin. The floor joist is held in place by tightening a 50.8-mm x 152.4-mm x 25.4-mm (2 in. x 6 in. x 1 in.) connection plate onto each side of the floor joist using 12.7-mm (0.5 in.) threaded rods. These connection plates hold the floor joist firmly against the top piece of steel with dimensions of 330.2-mm x 152.4-mm x 25.4-mm (13 in. x 6 in. x 1 in.). This top piece is also connected to a plate that goes through the grips of the Baldwin. Each grip allows the specimen to remain tightly fit, meaning no additional changes are needed to run the cyclic tests.

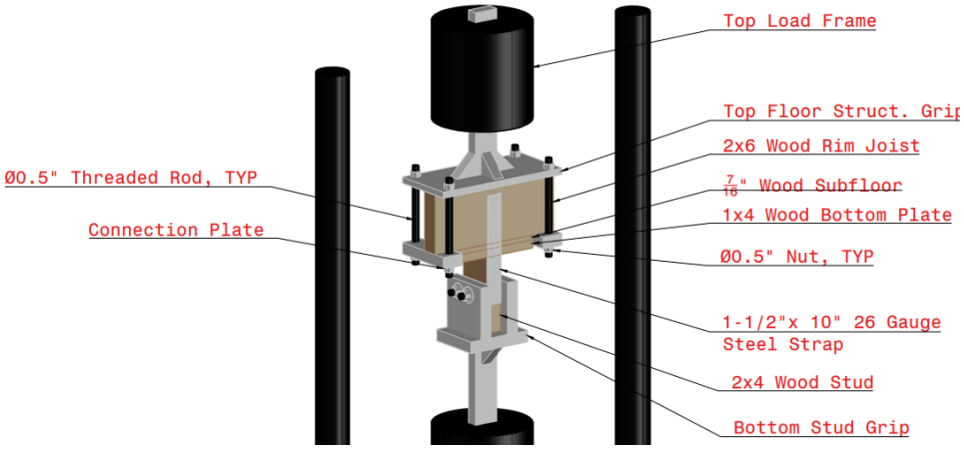

a)

b)

Figure 4. Wall to Floor (W2F) Test Fixture: (a) Schematic; (b) Photograph in lab

Load Protocol

The two-part loading protocol involved monotonic testing and a two-step quasi-static cyclic protocol based on FEMA 461 procedures (2007). The monotonic test was performed at a constant displacement rate of 2.54 mm/min (0.1 in./min) in accordance with ASTM D 1761 (2020). The results obtained from the monotonic test were used to determine the appropriate displacement amplitude for the cyclic tests. FEMA 461 protocols require the identification of a displacement corresponding to initial damage, Δ_0. The procedure then requires a minimum of six displacement cycles prior to reaching this initial damage state, with an additional ten cycles prior to reaching Δ_m, the displacement corresponding to maximum load. Due to the nature of sheathing connection failures, the procedure was modified for the current study. Based on the least ductile monotonic test result, the initial displacement for cyclic loading, defined herein as Δ_i was taken to be 5% of Δ_m. Subsequent displacement amplitudes were continuously increased by a factor of 1.4 until the load-carrying capacity of the connection was exceeded. At each displacement amplitude, two cycles were applied to the test specimen. An idealized loading history for a monotonic test is presented in Figure 5a, while a schematic loading protocol for quasi-static cyclic testing is shown in Figure 5b, with key displacement amplitudes labeled in each.

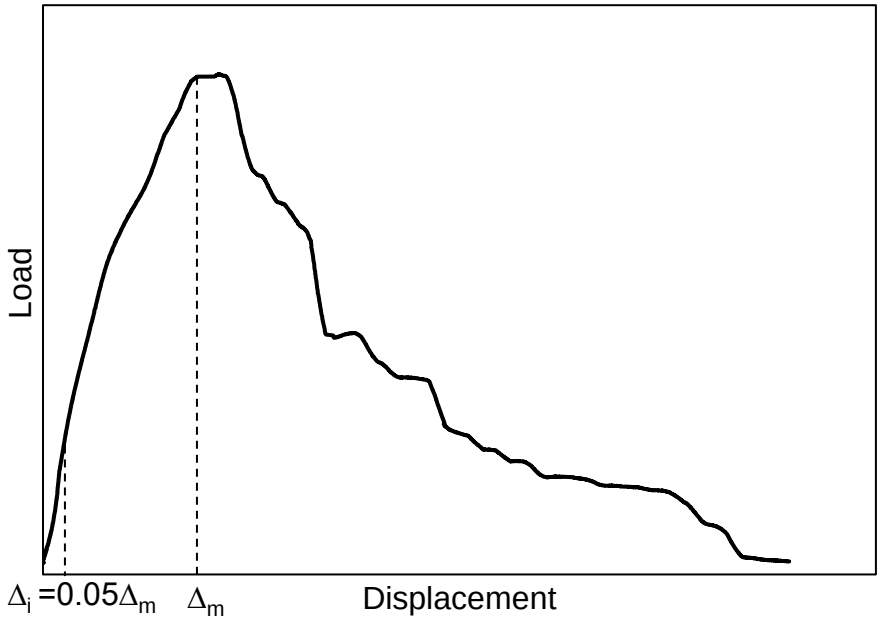

a)

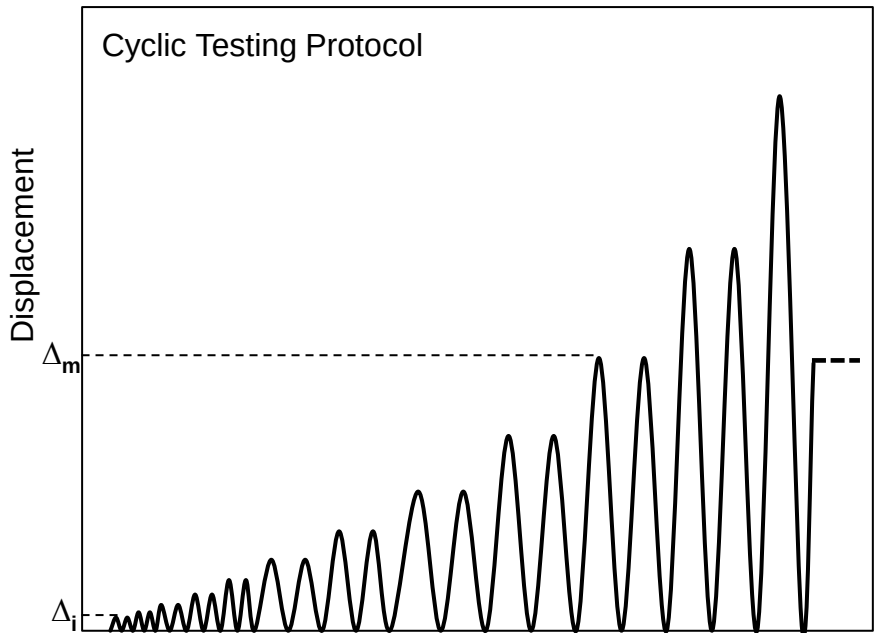

b)

Figure 5. Schematic representation of the load protocol with key displacement parameters identified for the: (a) Monotonic test; (b) Cyclic test

The load response was recorded using the load frame's built-in force transducer at a rate of 10 Hz. Three Optotrak markers, shown in Figure 3b for the S2R tests and Figure 4b for the W2F tests, were utilized to measure vertical displacement at various locations. For the S2R tests, a marker was attached to the top sheathing grip to measure crosshead displacement, the sheathing centerline to allow for the removal of sheathing bending included in crosshead displacement, and the fastener head to allow for determination of any relative displacement between the fastener and sheathing. For the W2F connection, a maker was attached to the floor joist grip to measure crosshead displacement, the left and right side of the floor joist to accurately measure the displacement of the connection, and the stud to measure relative displacement between the two previously mentioned locations.

Numerical Benchmark Study

Based on feedback from the stakeholder engagement in Phase I, a benchmark study was performed to evaluate the differences in HUD Code wind loads with the wind loads specified in ASCE/SEI 7-22. As mentioned previously, the HUD Code uses wind maps derived from the 1988 version of ASCE/SEI 7, which does not incorporate the past 35 years of technical advancements in wind engineering. The HUD Code provides two options for wind loads, the first is provided through

tabulated values in the HUD Code. The second option references the use of ASCE/SEI 7-88 with specific parameters specified. For the comparison here, the tabulated wind load requirements in the HUD Code are compared to load calculations using ASCE/SEI 7-22.

The HUD Code defines three wind regions in the U.S., where Wind Zones II and III require specific design requirements for wind and can generally be considered the high wind regions for manufactured homes. The HUD Code wind zones are assigned at the county-level, where all Florida counties are either Wind Zones II or III. Wind Zone II specifies a design wind speed of 44.7 m/s (100mph), whereas Wind Zone III specified a design wind speed of 49.2 m/s (110 mph). Tabulated values in the HUD Code include wind pressures for the main wind force resisting system (MWFRS), components and cladding (C&C), and anchorage for lateral and vertical stability, where only MWFRS and C&C wind pressures are compared here.

The provisions of Chapter 27, the Directional Procedure, were followed for MWFRS, and the provisions of Chapter 30, Part I, were followed for C&C. An excel spreadsheet was developed for the calculations, where different tabs were used for calculating MWFRS and C&C. The development and use of a spreadsheet allowed for the quick manipulation of different variables that impact the calculation for wind pressures. These variables include location, dimensions of the manufactured housing unit (MHU), exposure factor, and other pertinent information to the specific calculations. Despite the dimensions of the structure being easy to manipulate, consistent measurements are required to make a comparison, so representative values must be selected. The model MHU used for the comparison here is a single-wide MHU with a width of 4.3 m (14 ft.), length of 12.2 m (40 ft.), and a gable roof with a shallow roof slope of 15 degrees and no overhangs. These parameters were selected based on geometries listed in the manufacturer drawings, and to represent a lower bound (size-wise) for MHUs.

In Chapter 27, the directional procedure for determining the loads breaks the process down into seven steps. Step 1 is to determine the Risk Category of buildings, and the recommended source is Table 1.5-1. Based on common practice for site-built homes, here we assume Risk Category II for manufactured homes. Step 2 is to determine the basic wind speed. For the comparison, first, two Florida counties were selected. The ASCE 7 Hazards Tool was used to determine accurate wind speeds for the county with the highest wind speed for each wind zone to establish a worst case. Then, a major city within each county was selected for the comparison.

Step 3 is to determine the wind parameters. The seven parameters that must be checked include the wind directionality factor, exposure category, topographic factor, ground elevation factor, gust effect factor, enclosure classification, and internal pressure coefficients. Several of these parameters require assumptions. The enclosure classification was assumed to be partially open due to the likely failure of windows during high wind events. The topographic factor is assumed to be 1.0 given that the assumed geometry results in a mean roof height less than 4.6 m (15 ft). Another

assumption is that the structure falls within the restrictions of ASCE 26.11, so that a gust effect factor of 0.85 can be assumed. Additionally, the exposure category is selected as C to match the assumptions made by HUD. Many of the remaining parametric values are tabulated in ASCE/SEI 7-22 or obtained using specified empirical formulas, including the wind directionality factor (K_d = 0.85 given by ASCE 7-22 Table 26.6-1 for both the calculation for MWFRS and C&C loads) and the internal pressure coefficient (GC_{pi} = ±0.18 given by ASCE 7-22 Table 26.13-1 for the assumed enclosure classification of partially open). The remaining factor is the elevation factor given by:

$$K_e = e^{-0.0000362 z_e} \quad \text{Eq. 1}$$

Where z_e is the ground elevation above sea level.

Step 4 is to determine the velocity pressure coefficients. For purposes of using a spreadsheet, the equation in note 1 was used. Because the assumed geometry results in a height below 4.6 m (15 ft) the velocity pressure coefficient is given by:

$$4.6 \text{ m (15 ft)} \leq z \leq z_g \qquad K_z = 2.41(z/z_g)^{2/\alpha} \quad \text{Eq. 2}$$

Where α = 9.8 for exposure category C, and z_g = 750 m (2,460 ft) for exposure category C per Table 26.11-1.

Step 5 is to calculate the velocity pressure, q_z or q_h, using Equation 26.10-1 which is given as:

$$q_z = 0.00256 K_z K_{zt} K_e V^2 \quad \text{Eq. 3}$$

Where V represents the basic wind speed, and the remaining variables were defined in step 3.

Step 6 is to determine the external pressure coefficients. The gable end roof coefficients and wall coefficients both come from Figure 27.3-1. Two important values required to select the most applicable coefficients are the dimension parallel to the wind direction (L = 12.2 m (40 ft) for wind blowing parallel to the long dimension and 3.7 m (14 ft) for wind blowing perpendicular to the long dimension), the dimension perpendicular to the wind direction (B = 3.7 m (14 ft) for wind blowing parallel to the long dimension and 12.2 m (40 ft) for wind blowing perpendicular to the long dimension), and the mean roof height (h = 3.3 m (10.9 ft) for all wind directions. Using these variables, the pressure coefficients can be determined. Because these coefficients are based on the geometry of the structure, which are fixed for all locations considered, these coefficients apply to all locations investigated here. The walls have three different zones, windward (C_p = 0.8 for both wind directions), leeward (C_p = -0.3 for wind parallel to the long dimension and –0.5 for wind perpendicular to the long dimension), and the sides (C_p = -0.7 for both wind directions). The walls are symmetric, so the zones have similar behavior regardless of the direction of the wind. In comparison, the roof is asymmetrical, so the zones act on the structure differently depending on

direction. This difference is represented through the pressure coefficients being divided by whether the wind acts parallel or perpendicular to the ridge of the roof. For wind that blows parallel to the ridge, or the long direction, there are up to four zones to consider depending on the length of the roof. These zones are from the front edge of the roof to a distance half of the mean roof height (C_p = -0.9 or –0.18), half of the mean roof height to the mean roof height (C_p = -0.9 or –0.18), the mean roof height to two times the mean roof height (C_p = -0.5 or –0.18), and anything past a distance two times the mean roof away from the front edge (C_p = -0.3 or -0.18). All zones are applicable for the structure being considered in this study because the long dimension is slightly shorter than four times the mean roof height. In contrast, wind that blows perpendicular to the ridge, or the long direction has two zones, a leeward (C_p = -0.91 or –0.18) and windward side (C_p = -0.57).

Step 7 is to calculate the pressures using Equation 27.3-1 which is given by:

$$p = qK_dGC_p - q_iK_d(GC_{pi}) \qquad \text{Eq. 4}$$

Where all of the variables have been defined in previous steps.

Of note, the calculations require additional manipulation to represent the wall sections presented by the HUD Code. The first of the manipulations is that the absolute value of the windward wall and the leeward wall will be added together to allow the total wind load in a single direction to be determined. This value will be compared to the combination of windward and leeward pressures from a wind perpendicular to the first and the side pressures. The maximum of the comparison will be used as the pressure for the shearwalls and diaphragms in the MWFRS. The next manipulation is that all roof pressures will be resolved into pure uplift and any side action as the pressure acts perpendicular to the surface of the roof. For the comparison, the only concern is the uplift generated on the roof because the pressures on the wall will drive any lateral design. Additionally, the roof pressures from the wind blowing perpendicular to the ridge is compared to the different zones of pressure generated when the wind blows parallel to the ridge, and the maximum of these two values is considered to control the uplift forces for the MWFRS. The lateral and uplift pressure were the only pressures required for this comparison.

The C&C calculations follow the procedures in Chapter 30 part I, which use any of the same variables as the directional procedure for the MWFRS. The only difference in the first five steps described above is that the variable G is not an independent variable, and it is tied to the pressure coefficients. With the first five steps complete, two steps remain for C&C. These steps are similar to the last two steps for MWFRS, where the difference is the introduction of GC_p instead of C_p.

For C&C, the external pressure coefficients are based on the effective wind area. The effective area is the greater of the actual effective area of the type of component or cladding being

investigated and the length multiplied by one-third the length. While the effective area for our representative structure can be accurately calculated using the geometry previously mentioned, an effective area of 0.9 m^2 (10 ft^2) was used for this research to represent a worst-case scenario. This assumption creates a 0.7% to 1.4% increase in wall pressures when compared to the exact calculations for the specific geometry used in this study, and it does not affect the roof pressures. Therefore, this assumption has negligible impact on this specific study. Then, the plots shown in the figure for each part of the structure can be used to select the appropriate value for GC_p. Many of the coefficients provide multiple values, where the one that resulted in the greatest absolute value was used for the comparison.

For the C&C calculations, the wall is divided into two different areas which can be seen in Figure 30.3-1 in ASCE/SEI 7-22. The first area, commonly labeled with a five, is the corner of the buildings a distance "a" away from the building (GC_p = -1.4 or 1). The remaining wall is the only other area on the wall, and it is labeled with a four (GC_p = -1.1 or 1). The value of "a" is minimum value of either ten percent of the least horizontal dimension or forty percent of the mean roof height, but neither of these values can be below 0.9 m (3 ft) (a = 1.4 m (4.7 ft) for the wall). These areas correspond with the load types described under the components and cladding section of the HUD Code as there are areas 0.9 m (3 ft) from edges of the building that receive a separate loading.

For C&C roof comparisons, the roof is divided into three zones based on the roof slope. One area of interest is the area a distance "a" from both the ridge and the gable ends which is often labeled with a two (GC_p = -2.7 or 6). The remaining two areas are the intersection of the ridge and gable end areas and the remaining area of the roof. These areas are labeled with a three (GC_p = -3.6 or 0.6) and one (GC_p = -2 or 0.6), respectively.

The last remaining step for C&C is to solve for the wind pressures using equation 30.3-1 from ASCE/SEI 7-22 which is given by:

$$p = q_h K_d[(GC_p) - (GC_{pi})] \quad \text{Eq. 5}$$

All variables have been defined previously. C&C pressures represent a specific area on the structure, so no additional manipulation is required to compare the final values.

Results

Stakeholder Engagement

While there are no tangible results to report for the stakeholder engagement, beyond that many conversations with federal and non-governmental agencies did take place, while conversations with manufacturers did not. All individuals engaged expressed interest in the research, and interest in full-scale wind tunnel testing. Additional professional connections were made, and the conversations are on-going.

Roof Sheathing to Rafter Connection Testing

This section presents the results for the S2R tests and makes a comparison to theoretical capacities. The theoretical capacities of these connections were calculated using the 2018 edition of the National Design Specification from the American Wood Council.

Determination of Theoretical Capacity Values for Roof Sheathing to Rafter Connections

Theoretical capacities for fasteners and connection details are presented in this section. The two failure modes observed in the S2R connection are pull-out and pull-through failure. Withdrawal capacity, also known as pull-out capacity, for both nails and screws, was calculated using empirical equations from the NDS. Similarly, pull-through capacity of screw connection was calculated; this failure mode was only observed in screw connections during the experimental testing. In the field, pull-out and pull-through capacities cannot be measured separately and are both referred to as uplift capacity of the connection.

NDS reduces the ultimate uplift capacity by a safety factor of 5 to determine allowable uplift values (Sutt et al. 2000), and the ultimate shear capacity is reduced by a safety of factor of 3.5, expressed as:

$$W_d = \frac{Ultimate\ Uplift\ Capacity}{5} \quad \text{Eq. 6}$$

$$Z_d = \frac{Ultimate\ Shear\ Capacity}{3.5} \quad \text{Eq. 7}$$

For nails, the ultimate withdrawal capacity is given by:

$$W_u = 6900\ G^{2.5} D \quad \text{Eq. 8}$$

where G is equal to the specific gravity of wood and D is the fastener shank diameter (D = 0.113 in.). The embedded length of the nail shank in the rafter member is 47.6-mm (1.9-in.). For SPF, G = 0.42 resulting in an ultimate withdrawal capacity of 167 lbf. For SYP, G = 0.55 and the resulting ultimate withdrawal strength equals 1460 N (328 lbf).

For wood screws, the ultimate withdrawal capacity is given by:

$$W_u = 14250\ G^2 D \quad \text{Eq. 9}$$

where G is equal to the specific gravity of wood and D is the diameter of screw shank (D = 0.11 in.). The embedded length of threaded portion in the rafter member is 33-mm (1.3-in.). For SPF, G = 0.42 resulting in an ultimate withdrawal capacity of 1,611 N (362 lbf). For SYP, G = 0.55 the resulting ultimate withdrawal strength equals 2,767 N (622 lbf).

The second common failure mode is fastener head pull-through, W_H, which is given by:

$$W_H = 690\ \pi\ D_H\ G^2\ t_{ns}$$ Eq. 10

where G is the specific gravity of the sheathing (G = 0.5 for OSB and plywood given by NDS (2018)), D_H is the fastener head diameter (D_H = 10-mm (0.4 in.)), and t_{ns} is the net side member thickness (t_{ns} = 11.1-mm (7/16 in.) for OSB and 12.7-mm (1/2 in.) for plywood), resulting in a value of W_H = 444 N (100 lbf) for OSB and 512 N (115 lbf) for plywood. As comparisons are being made with experimental data and capacity values are not being used for design, the implicit factor of safety of five that is empirically included in this calculation (Douglas et al 2018) was removed, resulting in an estimated pull-through capacity of 2,228 N (501 lbf) for OSB and 2,558 N (575 lbf) for plywood.

Monotonic Test for Single Field Fasteners for Roof Sheathing to Rafter Connections

Monotonic tests were conducted on the specimens using ASTM D1761, as described in the Methodology. A total of 40 rafter sheathing specimens with a single fastener were tested to investigate the uplift capacity behavior of fasteners described in Table 2a. The maximum load was recorded during the tests and regarded as the uplift capacity of the connection. Mean capacity and the coefficient of variation (COV) were evaluated for each sample group. All specimens were tested under the same conditions.

Table 3 shows the mean uplift capacity of sheathing-to-rafter connections constructed from combinations of sheathing type (OSB and plywood), rafter species (SYP and SPF), and fastener type (8d common nail and #8 screw), resulting in a total of eight unique joint configurations. COVs for nailed connections varied between 11% and 33%, and COVs of screwed connections varied between 7% and 30%.

Table 3. Mean uplift capacity of S2R connection for a single fastener

Sheathing type	Rafter species	8d Common nail			#8 Screw		
		# of tests	Mean capacity, N (lbf)	COV	# of tests	Mean capacity, N (lbf)	COV
OSB	SYP	5	928 (209)	0.12	5	1,854 (417)	0.07
	SPF	5	610 (137)	0.33	5	2,067 (465)	0.17
Plywood	SYP	5	1,071 (241)	0.14	5	2,698 (607)	0.23
	SPF	5	919 (207)	0.22	5	2,160 (486)	0.27

Figure 6 shows two failure modes observed during testing: pull-out and pull-through failure. In nail connections, only pull-out failure was observed. However, in screw connections, both pull-out and pull-through failures were observed, with pull-through being more common and often having a higher capacity than pull-out, contrary to empirical calculation results.

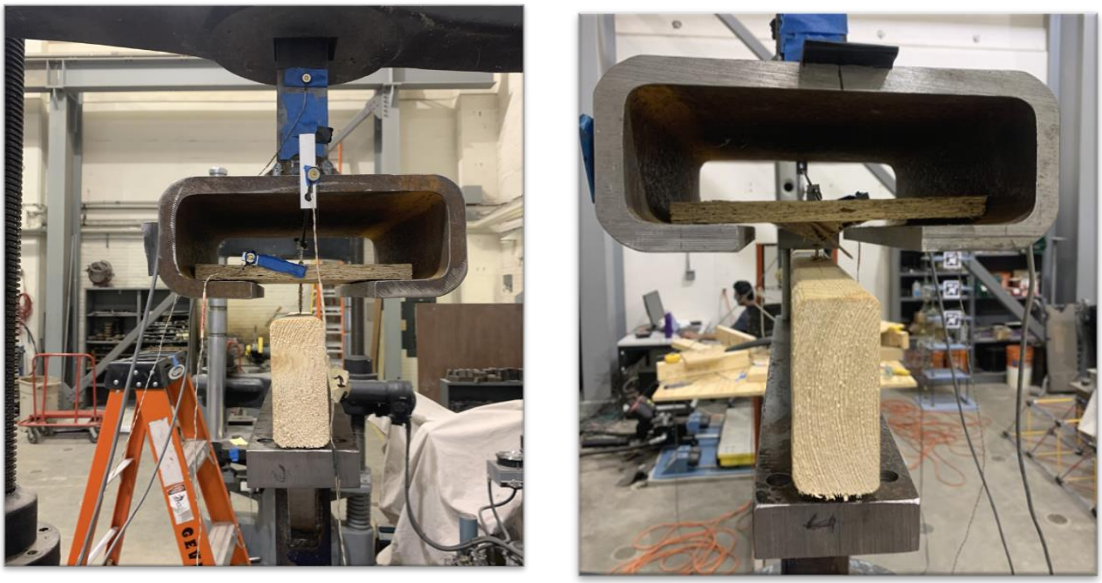

a) b)

Figure 6. S2R single fastener, screw test failure modes: (a) pull-through; (b) pull-out

Figures 7 and 8 show the withdrawal capacity for nails embedded in different rafter species through plywood and OSB, respectively. The dotted horizontal lines in Figures 7 and 4.3 are theoretical withdrawal capacities calculated previously. As shown in Figure 7, the mean withdrawal capacity measured for the SPF connection is 24% higher than the calculated theoretical value, whereas the mean withdrawal capacity measured for the SYP connection is 26% lower than the calculated theoretical value. In Figure 8, the mean withdrawal capacity measured for both rafter species are below the calculated theoretical values by 18% and 36% for the SPF and SYP connections, respectively.

Looking across Figures 7 and 8, differences can be observed based on rafter species and sheathing type. SYP rafter connections have 31% higher mean withdrawal capacity compared to SPF rafter connections, regardless of sheathing type, due to the higher specific gravity of SYP. For sheathing type, nails embedded through plywood have 29% higher mean withdrawal capacity compared to nails embedded through OSB.

For OSB sheathing, the COV for withdrawal capacity of nails embedded in SPF is 2.75 times greater than the COV for withdrawal capacity of nails in SYP. Similarly, for plywood sheathing, the COV for withdrawal capacity of nails embedded in SPF is 1.6 times greater than the COV for withdrawal capacity of nails in SYP. This illustrates the variability of nails when installed through different sheathing materials and driven into different rafter species.

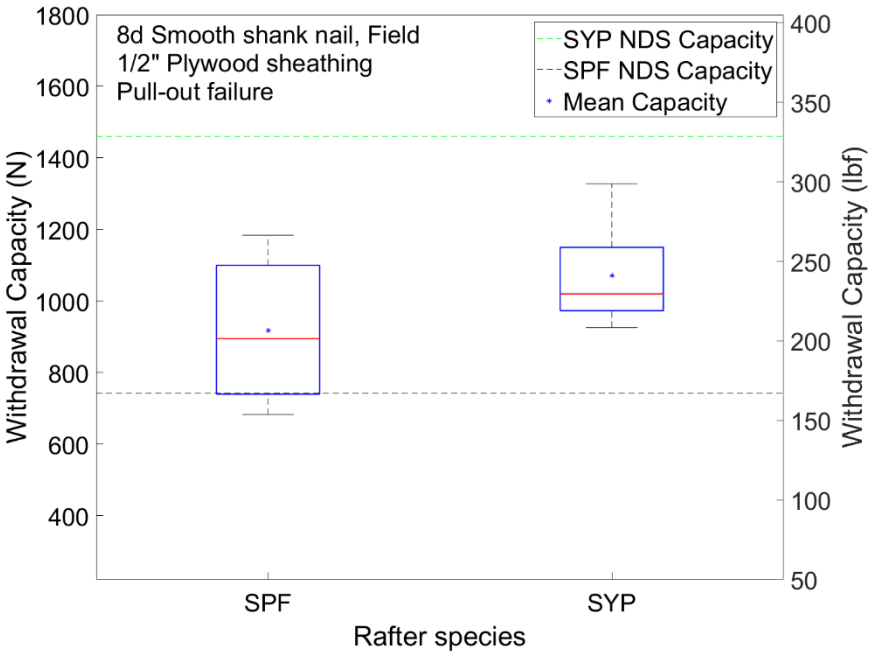

Figure 7. Comparison of S2R withdrawal capacity of SPF and SYP for nail embedded through plywood

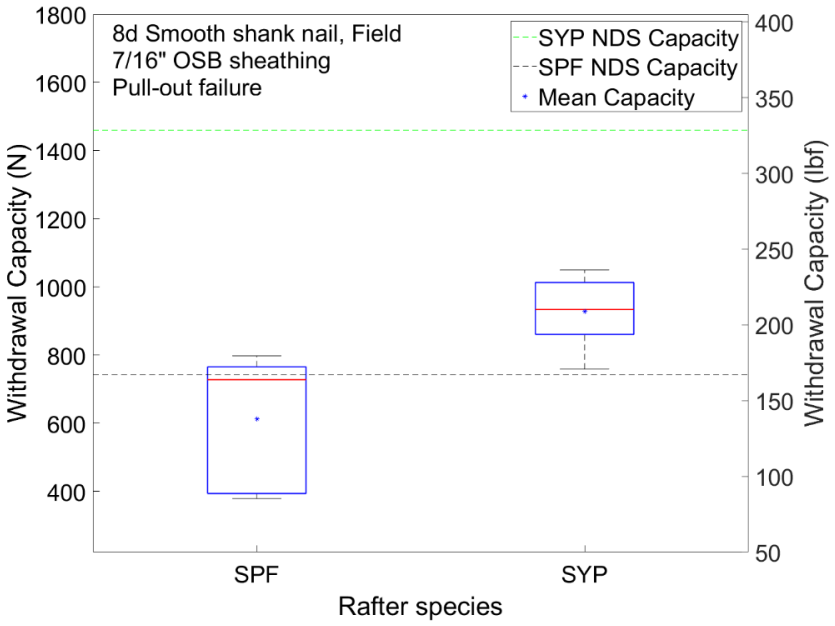

Figure 8. Comparison of S2R withdrawal capacity of SPF and SYP for nail embedded through OSB

As mentioned earlier, for screw connections pull-out and pull-through failure modes were both observed during the experimental testing. Hence, a force-deformation diagram is used to illustrate

the differences between the mean uplift capacities and failure modes. Figures 9 through 12 depict the force-displacement curves for the uplift capacity of #8 screws embedded in SPF and SYP through plywood and OSB and differentiate between pull-out and pull-through failure modes. The dotted horizontal lines in these figures represent the theoretical uplift capacities calculated previously.

In Figure 9, only one of the five tests failed via pull-out, with a withdrawal capacity 30% greater than the calculated theoretical value. The remaining four tests failed via pull-through, with the mean pull-through capacity being 8% lower than the calculated theoretical value. Similarly, in Figure 10, all five tests failed via pull-through, with the mean pull-through capacity being 17% lower than the calculated theoretical capacity. In Figure 11, only one of the five tests failed via pull-out, with a withdrawal capacity 18% lower than the calculated theoretical value. The remaining four tests failed via pull-through, with the mean pull-through capacity being 7% lower than the calculated theoretical value. In Figure 12, two of the five tests failed via pull-out, with a withdrawal capacity 32% lower than the calculated theoretical value. The remaining three tests failed via pull-through, with the mean pull-through capacity being 26% greater than the calculated theoretical value. For OSB sheathing, the COV for uplift capacity of screws embedded in SPF was 2.4 times greater than the COV for withdrawal capacity of nails in SYP. Similarly, for plywood sheathing, the COV for uplift capacity of screws embedded in SPF was 1.2 times greater than the COV for withdrawal capacity of nails in SYP. With reference to Figures 9 through 12, it can be observed that the pull-through failure mode was dominant and in cases where pull-out and pull-through failure mode occurred, pull-through capacity values were higher except for the specimen made with SPF rafter and OSB sheathing. Differences in failure modes can be attributed to the sheathing material. Plywood is comparatively stronger than OSB because of the material composition. Also, plywood has more fastener holding power. These attributes contribute to the failure modes and variability observed during testing.

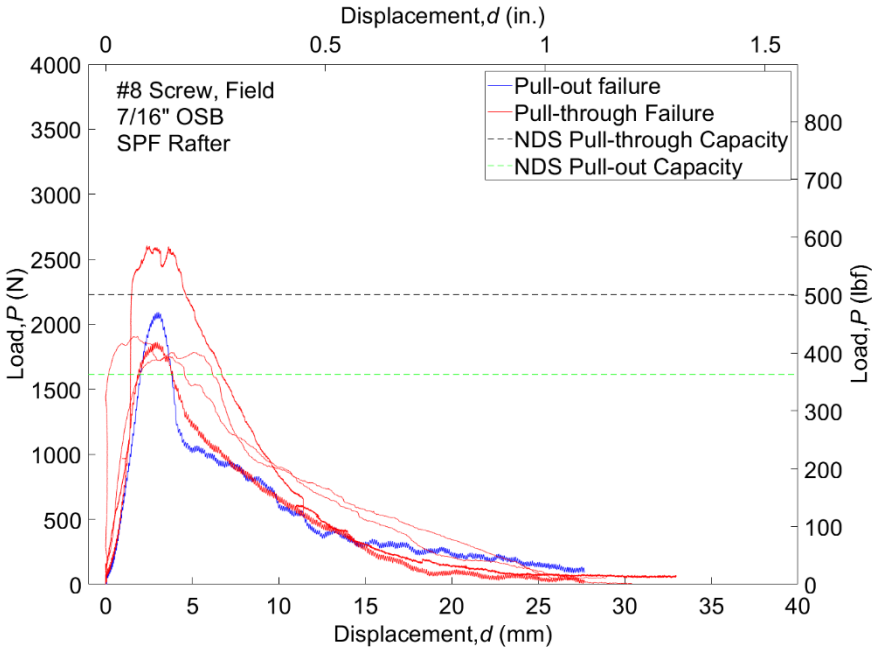

Figure 9. Monotonic load versus sheathing centerline displacement for single screw, OSB to SPF in S2R connection

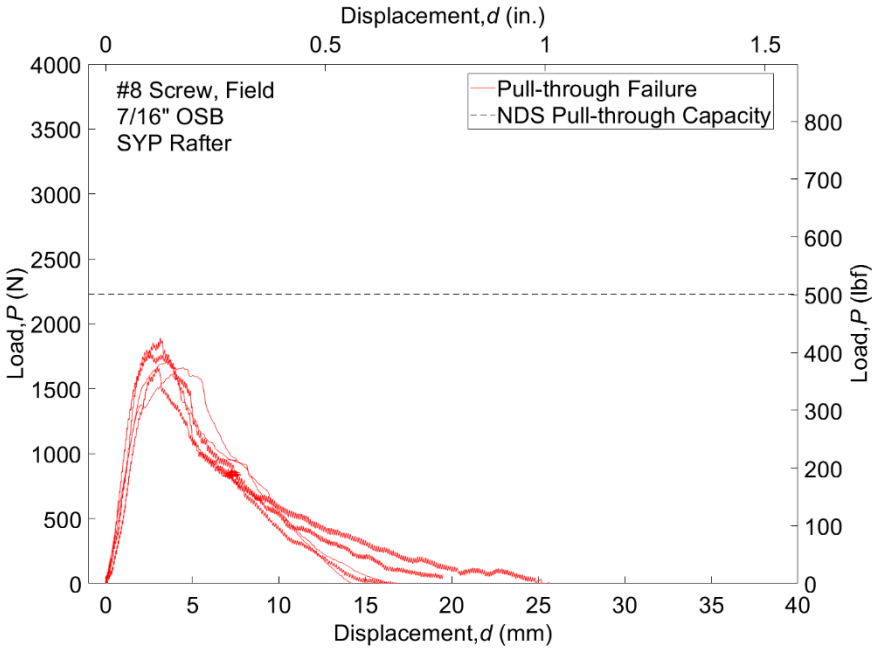

Figure 10. Monotonic load versus sheathing centerline displacement for single screw, OSB to SYP in S2R connection

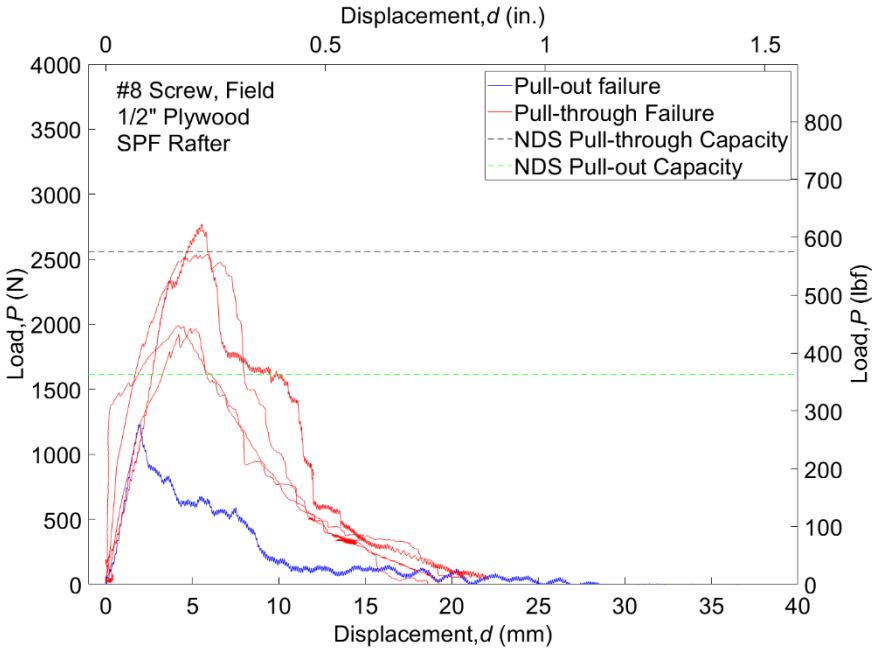

Figure 11. Monotonic load versus sheathing centerline displacement for single screw, plywood to SPF in S2R connection

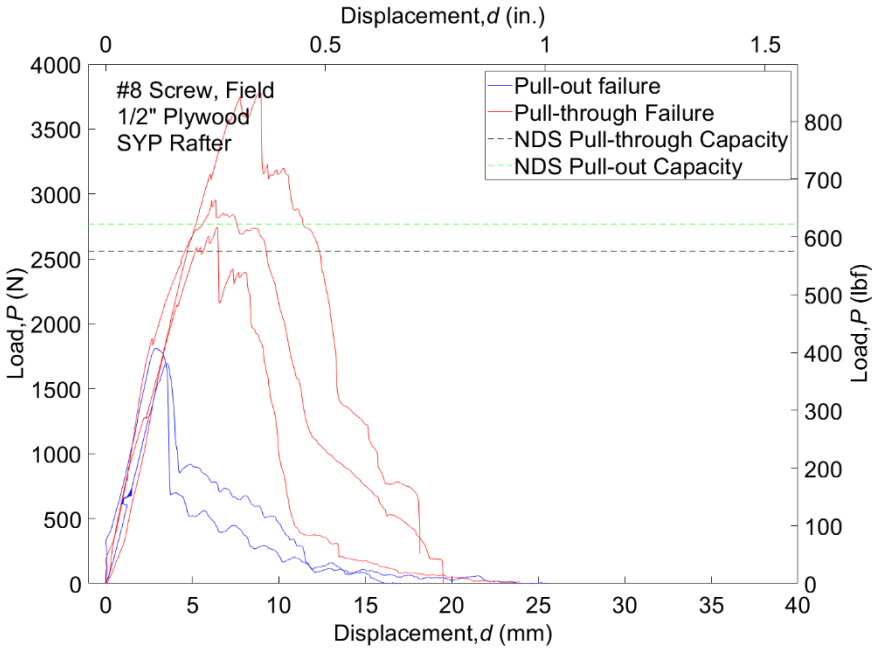

Figure 12 Monotonic load versus sheathing centerline displacement for single screw, plywood to SYP in S2R connection

Figures 13 and 14 compare the mean uplift capacity of screws and nails embedded in SYP and SPF rafters through plywood and OSB sheathing. In Figure 13, the mean uplift capacity of screws

was 2.5 times higher than nails for SYP connections, and 2.3 times higher for SPF connections. Additionally, screws embedded in SYP had a mean uplift capacity 25% greater than screws in SPF. In Figure 14, the mean uplift capacity of screws was 2 times higher than nails for SYP connections, and 3.4 times higher for SPF connections. Screws embedded in SYP had a mean uplift capacity 10% less than screws in SPF. Notably, Figures 13 and 14 reveal that the type of sheathing used can impact uplift capacity. Specifically, screws embedded in plywood had a 47% higher mean uplift capacity than those in OSB for SYP rafter species, and 5% higher for SPF rafter species. These figures also demonstrate the variability of uplift capacity for screws when installed through different sheathing materials and rafter species.

The results presented above for single nail connections suggest that the NDS value for the withdrawal capacity of nails may be too high, which indicates that the ultimate withdrawal capacity is less than what NDS predicts. As mentioned earlier, NDS applies a safety factor of 5 (Sutt et al. 2000), which results in a higher ultimate withdrawal capacity than the value obtained from experimental testing. The test results confirm the observation made by Kerr (2013) and Prevatt (2014) that the withdrawal capacity of nails decreases when driven through a layer of wood sheathing. This is an interesting finding that suggests that the uplift capacity of fasteners may not be as dependent on specific gravity of the rafter species as previously assumed. Similarly, the mean withdrawal capacity from the test yielded a value smaller than the calculated ultimate capacity from NDS for single screw connections. By comparing the mean withdrawal capacity from this study and the calculated withdrawal capacity values from NDS, the factor of safety for single fastener connections is estimated to be between 3 and 3.5.

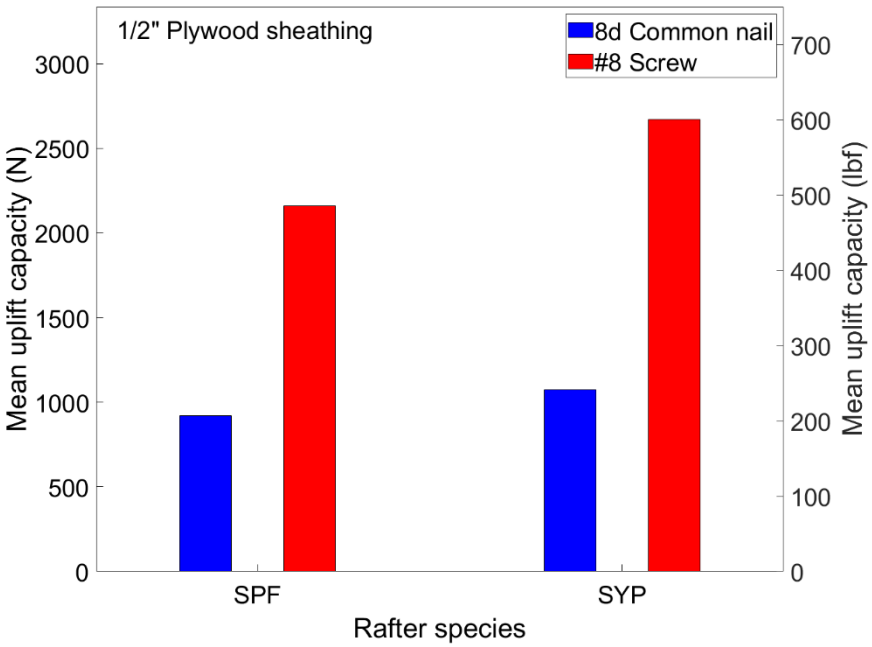

Figure 13. Comparison of uplift capacity of nail versus screw for plywood sheathing in S2R connections

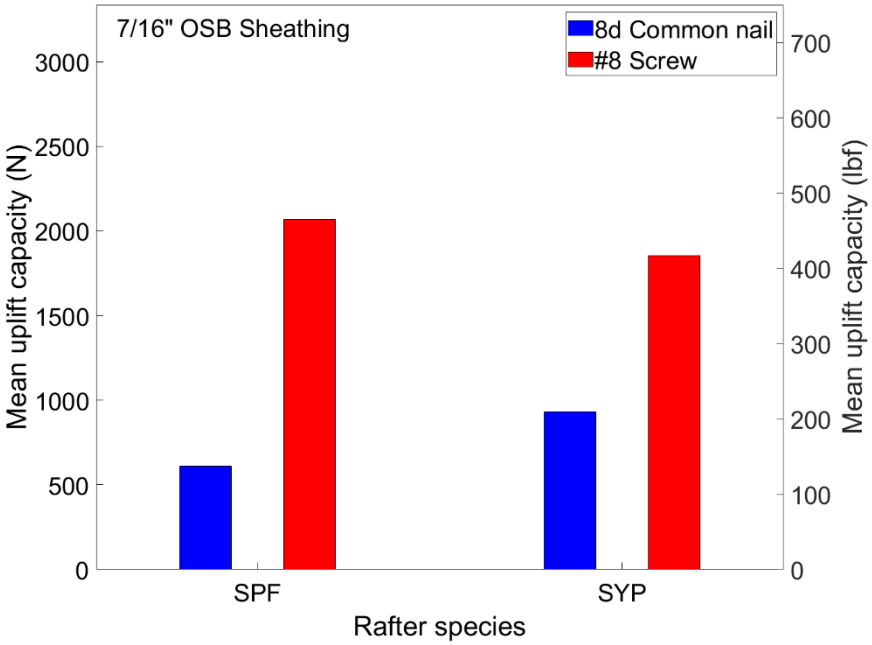

Figure 14. Comparison of uplift capacity of nail screw for OSB sheathing in S2R connections

Cyclic Test for Single Field Fasteners for Roof Sheathing to Rafter Connections

Cyclic testing was conducted on the specimens using the modified FEMA 461 loading protocol described in the Methodology. A total of 40 specimens were tested to investigate the cyclic behavior of S2R connections. A typical cyclic force-deformation curve based on results of the monotonic tests and the modified FEMA 461 loading protocol is provided in Figures 15 through 18. Additional cyclic tests results are provided in Appendix A. The same failure modes observed during the monotonic testing were observed during the cyclic test, namely pull-out and pull-through failure. Pull-out failure was observed in all nail connections. However, in screw connections, both pull-out and pull-through failures were observed. Pull-through failure was more common and, in most cases, corresponded with higher capacity than pull-out failure.

Figures 15 through 18. show the cyclic force-deformation curves for 8d common nails and #8 screws embedded in SPF and SYP through plywood and OSB and differentiate between the two observed failure modes, where applicable. Looking at Figure 15, the screw connection failed in pull-through, whereas the nailed connection failed via pull-out. Comparing the maximum peak force sustained during the test, it can be observed that the screw connection had a capacity that is about 3 times higher than that of the nailed connection. In addition, the screw connection was able to withstand higher displacement before failure occurred compared to the nailed connection. In relation to Figure 16, the screw and nail connections failed via pull-out. The screw connection had a capacity approximately two times higher than the nailed connection, as evidenced by the maximum peak force sustained. Additionally, the screw and nail connection endured similar displacements before failure.

In Figure 17, the screw connection failed via pull-through, while the nailed connection failed via pull-out. The screw connections sustained a maximum peak force at least two times higher than the nailed connection. Additionally, the screw connection withstood at least two times greater displacement before failure compared to the nailed connection. Similarly, as observed from Figure 18, the screw connection failed via pull-through, while the nailed connection failed via pull-out. However, the screw connection sustained a maximum peak force three times greater than the nailed connection. The area under the load-displacement curve represents energy dissipation. As evident in Figures 15 through 18, screw connections dissipated significantly more energy than nailed connections.

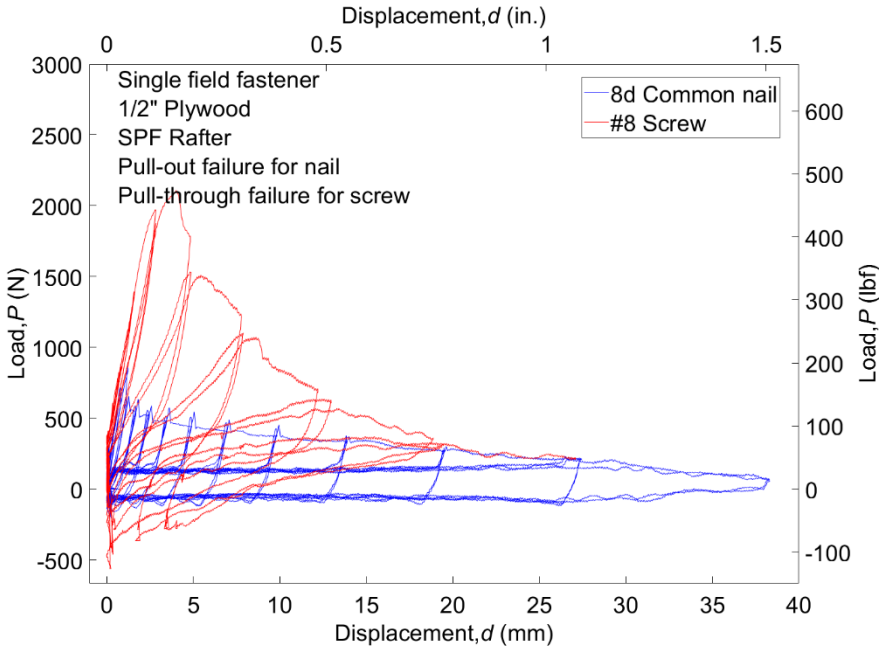

Figure 15. Cyclic force-deformation curve for single fastener, SPF rafter and plywood sheathing in S2R connections

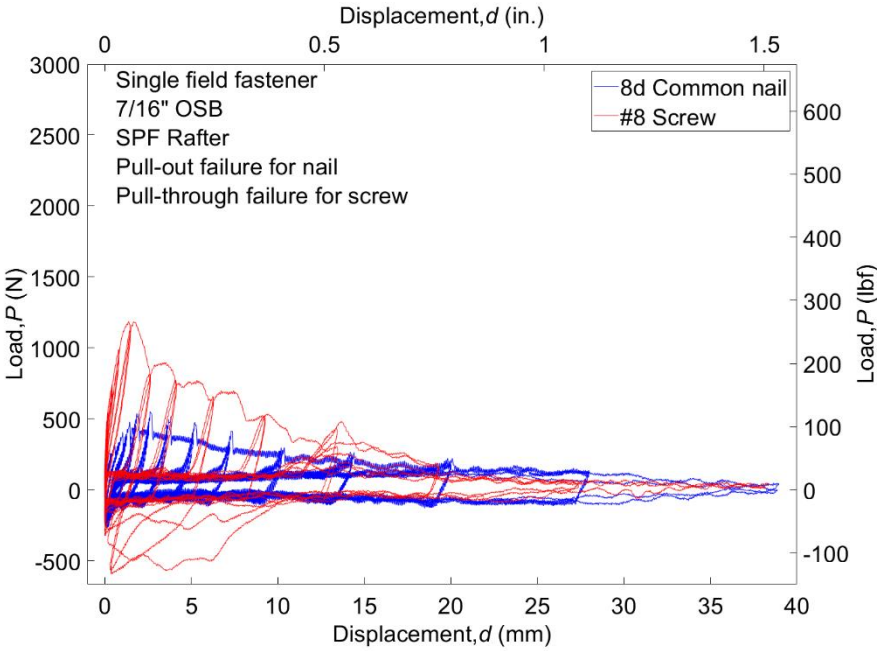

Figure 16. Cyclic force-deformation curve for single fastener, SPF rafter and OSB sheathing in S2R connections

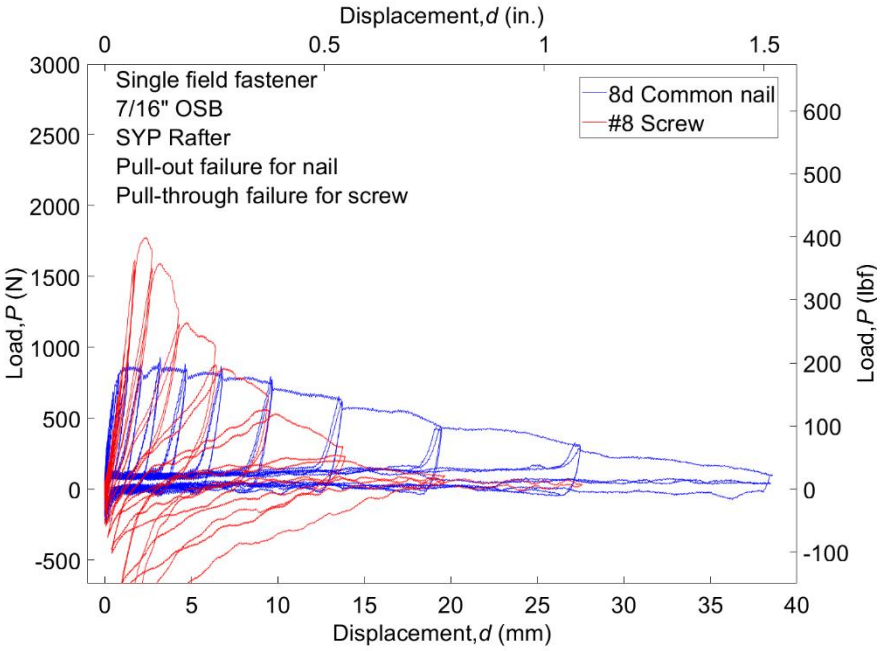

Figure 17. Cyclic force-deformation curve for single fastener, SYP rafter and OSB sheathing in S2R connections

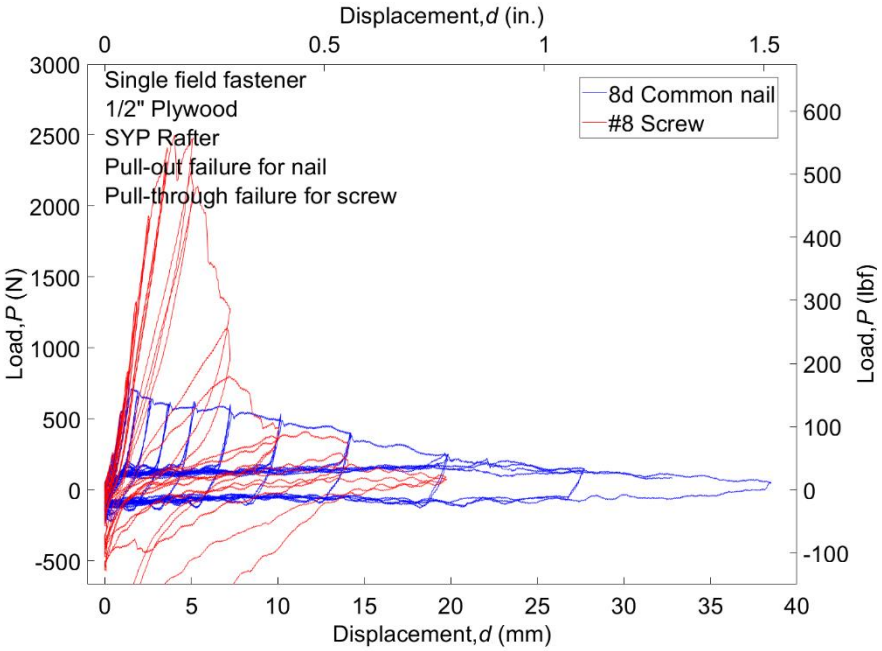

Figure 18. Cyclic force-deformation curve for single fastener, SYP rafter and plywood sheathing in S2R connections

Monotonic Test for Two Field Fasteners for Roof Sheathing to Rafter Connections

Monotonic testing was conducted on S2R connection specimens with two fasteners at 150-mm (6-in.) spacing center-to-center. A total of 64 specimens were tested to investigate the effect of grouping of fasteners on their uplift capacity. Out of the 64 specimens, 40 were constructed using a sheathing size of 203-mm x 203-mm (8-in. x 8-in.). The remaining 24 specimens were constructed using a sheathing size of 203-mm x 330-mm (8-in. x 13-in.). The maximum peak load was recorded during the test and was regarded as the uplift capacity of the connection. To understand the effect of grouping of fasteners, capacity per fastener was determined for each connection. Mean capacity values, capacity per fastener values, and COVs were evaluated for each sample group. Figure 19 illustrates the two failure modes observed during testing, pull-out and pull-through failure. Pull-out failure was observed in all nail connections. However, in screw connections, both pull-out and pull-through failures were observed. Pull-through failure was more common and, in most cases, had higher capacity than pull-out failure.

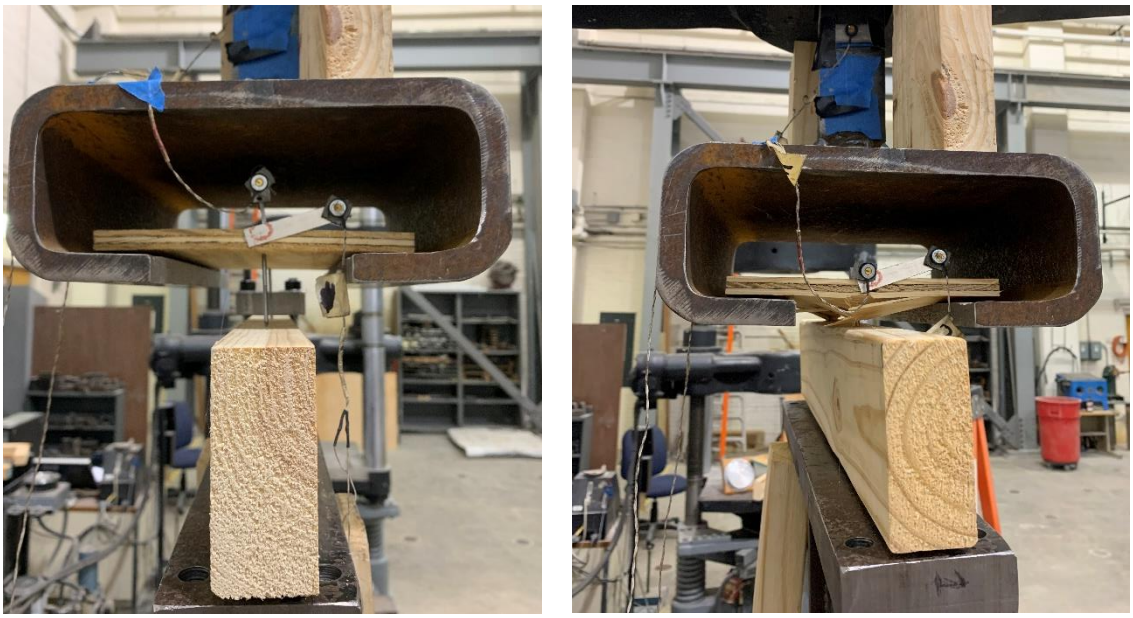

a) b)

Figure 19. S2R two fastener test failure modes: a) pull-out; b) pull-through

Table 4 presents the average uplift capacity of S2R connections using 203-mm x 203-mm (8-in. x 8-in.) sheathing made of OSB or plywood. The rafter species considered were SYP and SPF, and two types of fasteners were used: 8d common nails and #8 screws. This resulted in a total of eight different joint configurations. For the nailed connections, the coefficients of variation (COVs) ranged from 14% to 29%. The COVs for the screwed connections varied between 14% and 16%

Looking across Table 4, for nailed connections, differences can be observed based on rafter species and sheathing type. For rafter species, the SYP rafter connections had 37% greater mean withdrawal capacity per fastener compared to SPF rafter connections regardless of sheathing type, corresponding with higher specific gravity of SYP. For sheathing type, nails embedded through plywood had 5% higher mean withdrawal capacity per fastener compared to nail embedded through OSB. For OSB sheathing, the COV for withdrawal capacity of nails was 1.4 times greater for SYP connections compared to SPF connections. Conversely, for plywood sheathing, the COV for withdrawal capacity of nails was 1.7 times greater for SPF connections compared to SYP connections.

Similarly, for screwed connections, differences can be observed based on rafter species and sheathing type. For rafter species, the SYP rafter connections had 22% greater mean uplift capacity per fastener compared to SPF rafter connections regardless of sheathing type, corresponding with higher specific gravity of SYP. For sheathing type, screws embedded through plywood have 73% higher mean withdrawal capacity per fastener compared to nail embedded through OSB. For OSB sheathing, the COV for uplift capacity of screws embedded in SPF was about the same COV for

withdrawal capacity of nails in SYP. Similarly, for plywood sheathing, the COV for uplift capacity of screws embedded in SPF was the same as the COV for uplift capacity of nails in SYP.

Table 4. Mean uplift capacity of S2R connection for two-fasteners for 203-mm x 203-mm (8-in. x 8-in.) sheathing

Sheathing type	Rafter species	8d Common nail				#8 Screw			
		# of tests	Mean capacity, N (lbf)	Capacity per fastener, N (lbf)	COV	# of tests	Mean capacity, N (lbf)	Capacity per fastener, N (lbf)	COV
OSB	SYP	5	1399 (314)	699 (157)	0.2	5	2860 (643)	1430 (322)	0.14
	SPF	5	1038 (233)	519 (117)	0.14	5	3109 (699)	1555 (350)	0.16
Plywood	SYP	5	1493 (336)	746 (168)	0.17	5	6120 (1376)	3060 (688)	0.16
	SPF	5	1069 (240)	535 (120)	0.29	5	4241 (953)	2120 (477)	0.16

Table 5 shows the mean uplift capacity of S2R connection for two fasteners with additional sheathing on either side of the fasteners. COVs for nailed connection varied between 3% and 11% and COVs of screwed connection varied between 9% and 16%. Looking across Table 5, for nailed connections, differences can be observed based on rafter species and sheathing type. For rafter species, the SYP rafter connections had 17% higher mean withdrawal capacity per fastener compared to SPF rafter connections regardless of sheathing type, corresponding with the higher specific gravity of SYP. For sheathing type, nails embedded through plywood had 5% higher mean withdrawal capacity per fastener compared to nail embedded through OSB. For OSB sheathing, the COV for withdrawal capacity of nails embedded in SYP was 3.6 times greater than the COV for withdrawal capacity of nails in SPF. For plywood sheathing, the COV for withdrawal capacity of nails embedded in SPF was 1.4 times greater than the COV for withdrawal capacity of nails in SYP.

Table 5. Mean uplift capacity of S2R connection for two-fasteners for 203-mm x 330-mm (8-in. x 13-in.) sheathing

Sheathing type	Rafter species	8d Common nail				#8 Screw			
		# of tests	Mean capacity, N (Ib)	Capacity per fastener, N (lbf)	COV	# of tests	Mean capacity, N (Ib)	Capacity per fastener, N (lbf)	COV
OSB	SYP	3	1573 (354)	787 (177)	0.11	3	4718 (1061)	2359 (531)	0.16
	SPF	3	1565 (352)	782 (176)	0.03	3	4450 (1000)	2225 (500)	0.14
Plywood	SYP	3	1505 (338)	752 (169)	0.07	3	4545 (1022)	2273 (511)	0.12
	SPF	3	1070 (241)	535 (120)	0.1	3	4789 (1077)	2394 (538)	0.09

Table 6 provides information regarding the capacity per fastener across all tests. It is known that grouping of fasteners influence their individual capacity. There have been debates (see Dao and van de Lindt, 2008 and Hill, 2009) on whether fastener spacing affects the uplift capacity of a connection or not. The present study did not evaluate multiple fastener spacings; only fastener grouping effect is investigated. It can be observed that for nailed connection, the capacity per fastener is higher for a single fastener test when compared to two-fastener tests except for specimens made with 203-mm x 330-mm (8-in. x 13-in.) sheathing OSB and SPF as rafter. The two-fastener test with 203-mm x 330-mm (8-in. x 13-in.) OSB sheathing and SPF rafter has the highest uplift capacity per connection as it was 28% higher than its corresponding single fastener test. Similarly, for screw connection, it can be observed that for tests for specimen made from OSB sheathing, the capacity per fastener was greatest in tests with 203-mm x 330-mm (8-in. x 13-in.) sheathing. Where SYP rafter was used, the capacity per connection is 27% higher than its corresponding single fastener test, and where a SPF rafter was used, the capacity per connection was 7% higher than its corresponding single fastener test. For tests where plywood was used as sheathing, the capacity per fastener was greater from test with 203-mm x 203-mm (8-in. x 8-in.) sheathing. Where a SYP rafter was used, the capacity per connection was 13% higher than its corresponding single fastener test. However, where a SPF rafter was used, the capacity per connection is 11% greater than its corresponding single fastener test.

Considering grouping effects of fasteners, it can be observed that the capacity per fastener from the two-fastener connection was lower than the capacity obtained during a single fastener connection test. This indicates that the capacity of each fastener used to connect the roof sheathing to rafter is independent of each other. Use of grouped fasteners can be expected to reduce the factor of safety. However, the NDS does not specify how to determine the capacity per fastener for multiple fastener connections. Considering grouping effects of fasteners, it can be observed that the capacity per fastener from the two-fastener connection was lower than the capacity obtained during a single fastener connection test. This indicates that the capacity of each fastener used to connect the roof sheathing to rafter is independent of each other. Use of grouped fasteners can be expected to reduce the factor of safety. However, the NDS does not specify how to determine the capacity per fastener for multiple fastener connections. Furthermore, when comparing the grouped fastener capacity for screwed connections, the disparity in capacity per fastener was due to a mixture of failure modes across specimens. During testing, both screws could either pull-out or pull-through, or one screw could pull-out while the other screw pulled-through. These differing failure modes created significant differences in averaged capacities. The differing failure modes could have been caused by over-driving the screws and discontinuities in the sheathing, however neither of these causes were directly observed or evaluated.

Table 6. Grouping effect of fasteners across all S2R monotonic tests

Sheathing type	Rafter species	8d Common nail			#8 Screw		
		Capacity per fastener, N (lbf)			Capacity per fastener, N (lbf)		
		Single fastener	Two fasteners		Single fastener	Two fasteners	
		203 mm x 203 mm (8 in. x 8in.) sheathing	203 mm x 203 mm (8 in. x 8in.) sheathing	203 mm x 330 mm (8 in. x 13 in. sheathing)	203 mm x 203 mm (8 in. x 8in.) sheathing	203 mm x 203 mm (8 in. x 8in.) sheathing	203 mm x 330 mm (8 in. x 13 in. sheathing)
OSB	SYP	928 (209)	699 (157)	787 (176)	1,854 (417)	1,430 (322)	2,359 (531)
	SPF	610 (137)	519 (116)	782 (176)	2,067 (465)	1,554 (350)	2,225 (500)
Plywood	SYP	1,071 (241)	746 (167)	752 (169)	2,698 (607)	3,060 (688)	2,272 (511)
	SPF	919 (207)	534 (120)	535 (120)	2,160 (486)	2,120 (477)	2,394 (538)

Cyclic Test for Two Field Fasteners for Roof Sheathing to Rafter Connections

Cyclic testing was conducted on specimens with two fasteners at 150-mm (6-in.) spacing center-to-center. A total of 64 specimens were tested to investigate the cyclic behavior of S2R connection. A typical cyclic force-deformation curve from each sample group is provided in Figures 20 through 23. Additional cyclic test results are provided in Appendix A. The same failure modes observed during the monotonic testing were observed during the cyclic test, pull-out and pull-through failure. Pull-out failure was observed in all nail connections. However, in screw connections, both pull-out and pull-through failures were observed. Pull-through failure was more common and, in most cases, had higher capacity than pull-out failure.

Figures 20 through 23 show the cyclic force-deformation curves of two 8d common nail and #8 screw spaced at 150 mm (6 in.) center-to-center embedded in SPF and SYP through plywood and OSB sheathing, 203 mm x 203mm (8 in. x 8 in.). The figures also differentiate between the two observed failure modes. Looking at Figure 21, the screw connection failed via pull-through, whereas the nailed connection failed via pull-out. Comparing the maximum peak force sustained during the test, it can be observed that the screw connection had a capacity approximately 2.5 times greater than that of the nailed connection. In addition, the screw connection was able to withstand greater displacement before failure compared to the nailed connection. In relation to Figure 21, the screw and nail connections failed via pull-out. The screw connection had a capacity approximately two times higher than the nailed connection, as evidenced by the maximum peak force sustained. Additionally, the screw connection was able to withstand greater displacement before failure occurs compared to the nailed connection. In Figure 22, the screw connection failed via pull-through, while the nailed connection failed via pull-out. The screw connection sustained a maximum peak force at least three times greater than the nailed connection. Additionally, the screw connection was able to withstand more displacement before failure compared to the nailed connection. Similarly, as observed from Figure 23, the screw connection failed via pull-through, while the nailed connection failed via pull-out. However, the screw connection sustained a maximum peak force three times that of the nailed connection.

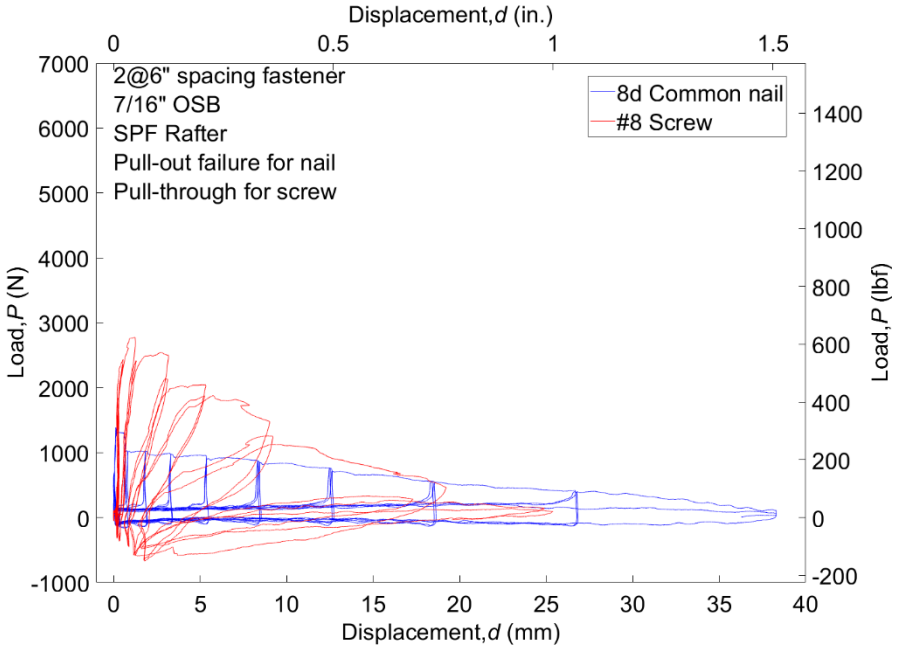

Figure 20. Cyclic force-deformation curve for two-fastener, SPF rafter and OSB sheathing

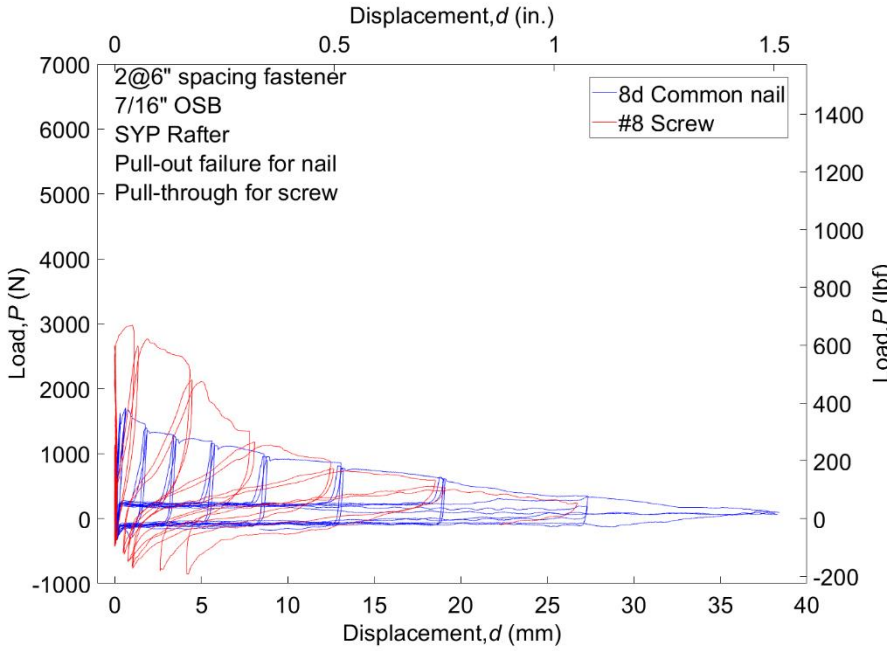

Figure 21. Cyclic force-deformation curve for two-fastener, SYP rafter and OSB sheathing

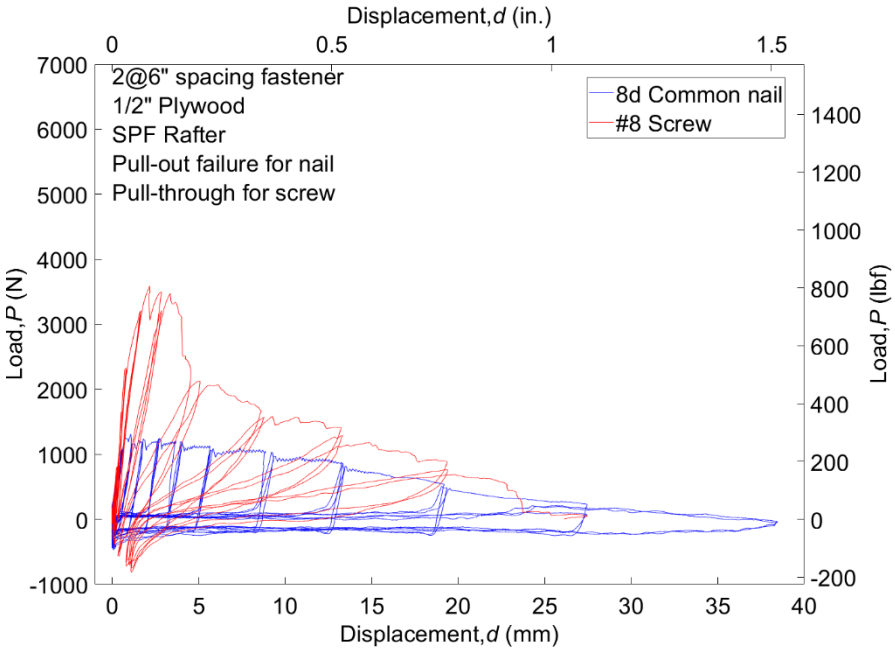

Figure 22. Cyclic force-deformation curve for two-fastener, SPF rafter and plywood sheathing

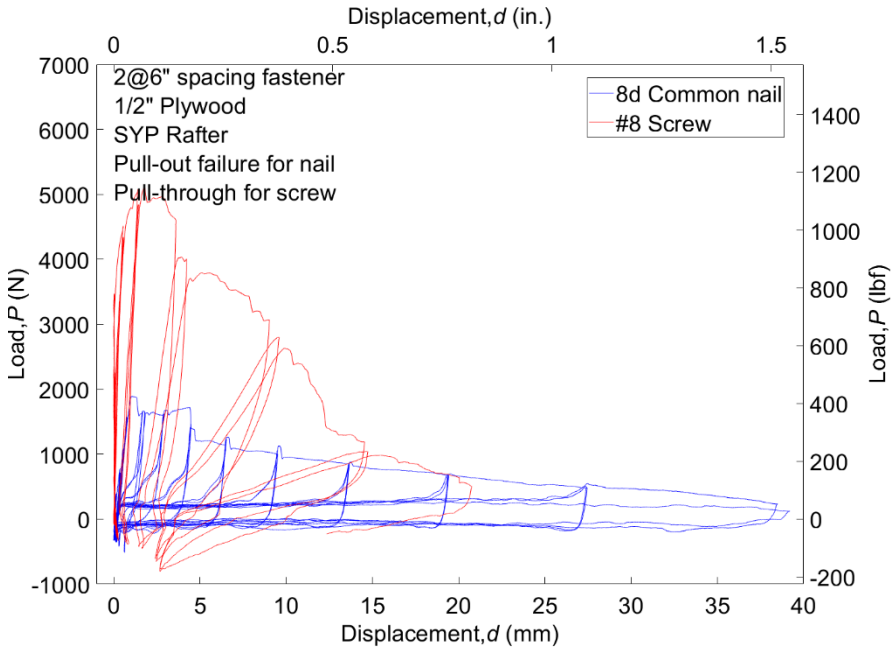

Figure 23. Cyclic force-deformation curve for two-fastener, SYP rafter and plywood sheathing

Wall to Floor Connection Testing

This section presents the results for the S2R tests and makes a comparison to theoretical capacities. The theoretical capacities of these connections were calculated using the 2018 edition of the National Design Specification from the American Wood Council.

Determination of Theoretical Capacity Values for Wall to Floor Connections

The W2F connections experience failure in shear. These fastener shear failures are divided into four main categories which articulate failure occurring in either a main member or side member. The main member is defined as the connection member that receives the fastener while the side member is the member that is fastened through. For the W2F connection, the main member is the wood stud or floor joist depending on the end of the strap, and the side member is the steel strap. The first shear failure category represents a bearing failure in the wood fibers of the main member (I_m) or the steel in the side member (I_s). While this first failure mode can occur in either the side or main member for a nail connection, this failure only occurs in the side member for stapled connections (I). The second failure mode occurs when the fastener pivots at the shear plane inducing local crushing of the wood (II). The third failure mode is characterized by bending of the fastener and either a bearing failure of the wood fibers of the main member (III_m) or the steel in the side member (III_s). Like the first mode of failure, a connection that uses nails can fail in either the side or the main member, but a connection that uses staples only fails in the main member (III). The fourth failure mode is defined by the fastener forming two plastic hinges with wood crushing near the shear plane (IV). Additionally, the members included in the shear connection could fail.

For nails, the shear capacity, Z, is the minimum value of the four previously mentioned failure modes which are given by:

I_m	$$Z = \frac{D\ l_m\ F_{em}}{R_d}$$	Eq. 11
I_s	$$Z = \frac{D\ l_s\ F_{es}}{R_d}$$	Eq. 12
II	$$Z = \frac{k_1\ D\ l_s\ F_{es}}{R_d}$$	Eq. 13
III_m	$$Z = \frac{k_2\ D\ l_m\ F_{em}}{(1 + 2R_e)R_d}$$	Eq. 14
III_s	$$Z = \frac{k_2\ D\ l_s\ F_{em}}{(2 + R_e)R_d}$$	Eq. 15
IV	$$Z = \frac{D^2}{R_d}\sqrt{\frac{2\ F_{em}\ F_{yb}}{3\ (1 + R_e)}}$$	Eq. 16

Where D is the diameter of the shank (D = 3.3-mm (0.131 in.), 2.9-mm (0.113 in.), or 2.5-mm (0.099 in.)), F_{yb} is the dowel bearing yield strength (F_{yb} = 689.5 MPa (100,000 psi) given by NDS (2018)), R_d is the reduction term (R_d = 2.2 for all nail diameters and failure modes given by NDS (2018) Table 12.3.1B), l is the dowel bearing length of either the main member (l_m = 76.2-mm (3 in.) for 3.3-mm diameter nail when placed in the stud, 50.4-mm (2 in.) for both the 2.9-mm and 2.5-mm diameter nail when placed in the stud, and 38.1-mm (1.5 in.) for all diameters of nails when placed in the floor joist) or the side member (l_s = 0.660-mm (0.026 in.) for all diameters of nails), F_e is the member dowel bearing strength of either the main member (F_{em} = 23.1 MPa (3,350 psi) given by NDS (2018) Table 12.3.3 based on the specific gravity of the wood species) or the side member (F_{es} = 426.4 MPa (61,850 psi) given by the NDS (2018) Table 12P), and R_e is calculated dividing the main member dowel bearing strength by the side member dowel bearing strength (R_e = 0.054). The remaining variables, k_1, k_2, and k_3, are calculated using the following equations:

$$k_1 = \frac{\sqrt{R_e + 2{R_e}^2\left(1 + R_t + {R_t}^2\right) + {R_t}^2{R_e}^3} - R_e(1 + R_t)}{(1 + R_e)} \quad \text{Eq. 17}$$

$$k_2 = -1 + \sqrt{2(1 + R_e) + \frac{2F_{yb}(1 + 2R_e)D^2}{3F_{em}{l_m}^2}} \quad \text{Eq. 18}$$

$$k_3 = -1 + \sqrt{\frac{2(1 + R_e)}{R_e} + \frac{2F_{yb}(2 + R_e)D^2}{3F_{em}{l_s}^2}} \quad \text{Eq. 19}$$

Where R_t is calculated by dividing the main member dowel bearing length by the side member dowel bearing length (R_t = 115.3 for the 3.3-mm diameter nail when placed in the stud, 76.9 for the 2.9-mm and 2.5-mm diameter nails when placed into the stud, and 57.7 for all nail diameters when placed in the floor joist). The remaining variables have been defined in the explanation of the shear equations. Therefore, the values of k_1, k_2, and k_3 can be determined as follows. k_1 equals 2.57 for the 3.3-mm diameter nail when placed in the stud, 1.71 for the 2.9-mm and 2.5-mm diameter nail when placed in the stud, and 1.28 when any diameter of nail is placed into the floor joist). k_2 equals 0.47 or 0.51 for the 3.3-mm diameter nail when placed in the stud or floor joist respectively, 0.48 or 0.49 for the 2.9 mm diameter nail placed into the stud or floor joist respectively, and 0.47 or 0.48 for the 2.5-mm diameter nail when placed into the stud or floor joist respectively). k_3 equals 31.75 for the 3.3-mm diameter nail when placed into either the stud or floor joist, 27.42 for the 2.9-mm diameter nail when placed into either the stud or the floor joist, and 24.08 for the 2.5-mm diameter nail when placed into either the stud or the floor joist.

For the stapled connections, similar failure modes are assessed. The shear capacity, Z, of a stapled connection is given by:

I $$Z = \frac{2\,F_{es}\,l_s\,d}{K_D}$$ Eq. 20

II $$Z = \frac{2dF_{em}}{K_D}\left(\frac{l_m}{1+\frac{F_{es}}{F_{em}}}\right)\left[\left|\sqrt{\frac{F_{es}}{F_{em}}+2\left(\frac{F_{es}}{F_{em}}\right)^2\left[1+\frac{l_s}{l_m}+\left(\frac{l_s}{l_m}\right)^2\right]+\left(\frac{F_{es}}{F_{em}}\right)^3\left(\frac{l_s}{l_m}\right)^2-\frac{F_{es}}{F_{em}}\left(1+\frac{l_s}{l_m}\right)}\right|\right]$$ Eq. 21

III $$Z = \frac{2}{K_D}\left[\frac{-l_s F_{es} d}{2\frac{F_{es}}{F_{em}}+1}+F_{es}d\sqrt{\frac{{l_s}^2}{\left(2\frac{F_{es}}{F_{em}+1}\right)^2}+\frac{{l_s}^2}{2\frac{F_{es}}{F_{em}}+1}+\frac{4M}{F_{es}d\left(2\frac{F_{es}}{F_{em}}+1\right)}}\right]$$ Eq. 22

IV $$Z = \frac{4F_{em}d}{K_D}\sqrt{\frac{M}{F_{em}d\left(1+\frac{F_{em}}{F_{es}}\right)}}$$ Eq. 23

Where F_{em} is the dowel bearing strength for the main member (F_{em} = 29.3 MPa (4250 psi) given by ESR-1539 Table A), F_{es} is the dowel bearing strength of the side member (F_{es} = 426.4 MPa (61,850 psi) given by NDS (2018) Table 12.3.3) , d is the nominal wire diameter (d = 1.854-mm (0.073 in.) for the 15-gauge staple and 1.626-mm (0.064 in.) for the 16-gauge staple given by ESR-1539 Table 3.2), M is the minimum staple bending moment (M = 0.451 N-m (4.0 lbf-in) for 15-gauge staples and 0.407 N-m (3.6 lbf-in) for 16-gauge staples given by ESR-1539 Table 3.2), l_s is the length of the staple in the side member (l_s = 0.660-mm (0.026 in.)), l_m is the length of the staple in the main member (l_m = 63.5-mm (2.5 in.) or 38.1-mm (1.5 in.) for a 15-gauge staple when placed into the stud or floor joist respectively and 31.8-mm (1.25 in.) for a 16-gauge staple placed in either the stud or the floor joist) and K_D is the diameter coefficient (K_D = 2.2 given by ESR-1539). Many of the variables were defined for shear capacity of nailed connection, repeated here for clarity.

In addition to shear capacity, the strap may also control the capacity and subsequent failure mode of the W2F connection. This limit state is covered in Chapter D of the AISC Steel Construction Manual where the strap can either yield or rupture. If either the yield strength or rupture strength is lower than the shear strength of the connection, Z, as calculated above, the strength of the strap controls the capacity of the connection. The equations for steel in tensile yielding and rupture respectively, P_n, is given by:

$$P_n = F_y A_g$$ Eq. 24

$$P_n = F_u A_e$$ Eq. 25

Where A_e is the effective net area (A_e = 23.0 mm^2 (0.036 in^2) for the nails with a diameter of 3.3-mm, 23.3 mm^2 (0.036 in^2) for the nails with a diameter of 2.9-mm, 23.5 mm^2 (0.036 in^2) for the nails with a diameter of 2.5-mm, 22.7 mm^2 (0.035 in^2) for the 15-gauge staples, 23.1 mm^2 (0.036 in^2) for the 16-gauge staples), A_g is the gross area of the member (A_g = 25.2 mm^2 (0.039 in^2), F_y is the specified minimum yield stress (F_y = 227.5 MPa (33,000 psi)), and F_u is the specified

minimum tensile strength (F_u = 310.3 MPa (45,000 psi)). Because the nails and staples only create small holes in the strap, the effective area is too large for tensile rupture to control, so all values calculated are controlled by the tensile yield of the strap. When the yield strength is multiplied by the gross area, this maximum value computes to 5,725 N (1,287 lbf).

Each fastener pattern requires a unique calculation for each failure mode to determine theoretical capacities. For each of the eight fastener patterns selected for testing, these calculations were performed, and the results with applicable failure mode are tabulated in Table 7. The connections are paired by wall section, where the lower bound is presented first followed by the upper bound.

Table 7. W2F Connection Theoretical Design Capacities

Fastening Pattern	Wall Section	Capacity, N (lbf)	Failure Mode
(2) 15-Gauge Staples	Endwall	1,396.3 (313.9)	Mode III
(4) 2.5-mm (0.099 in.) Nails	Endwall	2,873.1 (645.9)	Mode IIIs
(4) 15-Gauge Staples	Endwall Opening	2,792.1 (627.7)	Mode III
(8) 2.5-mm (0.099 in.) Nails	Endwall Opening	5,724.9 (1,287.0)	Strap Yielding
(6) 3.3-mm (0.131 in.) Nails	Sidewall	5,724.9 (1,287.0)	Strap Yielding
(13) 16-Gauge Staples	Sidewall	5,724.9 (1,287.0)	Strap Yielding
(8) 16-Gauge Staples	Shearwall	4,927.7 (1,107.8)	Mode III
(7) 2.9-mm (0.113 in.) Nails	Shearwall	5,724.9 (1,287.0)	Strap Yielding

Monotonic Test for Wall to Floor Connection

For the wall to floor (W2F) connection tests, each connection was displaced until the connection had no remaining capacity. The maximum load achieved is documented as the measured capacity of the connection. For the 8 fastener combinations, each is tested with the row and stagger pattern resulting in 16 unique configurations. The mean capacity of each configuration including the specific pattern along with the coefficient of variation (COV) for each unique connection detail is recorded in Table 8. The tests are on-going at the time of this report, where the intention is to test at least three of each specimen. As shown in Table 8, the coefficient of variation ranged from 1% to 30% for the row pattern; however, the stagger pattern had a much smaller range of 1% to 12%. Although more consistent, the stagger pattern did not always have higher capacity than the row pattern. As shown in Table 8, the stagger pattern produced between a 15% to 42% higher capacity than the row pattern for each connection, except for the (4) 2.5-mm nails and (8) 16-guage staples, whereby Table 8 shows the row pattern produces between 3% to 6% higher capacity than the stagger pattern. Failure depends on the size of the fastener hole in the steel member and pitch of the stagger pattern, which may explain the atypical finding. Also evident in Table 8 is that the connection detail producing the lower bound capacity for each wall section was consistently lower

than the connection detail producing the higher bound capacity, except in the shearwall section detailed with the row pattern. In this case, the (8) 16-gauge staples were expected to produce a lower capacity than the (7) 2.9-mm nails. This is because the row pattern experienced a premature failure of the connection. The close spacing of the fasteners overloaded the wood fibers in a column and tore through the wood member. While the NDS does not specify required minimum spacing, the appendix provides information on recommended spacing. This recommended spacing allows staggered fasteners to be spaced closer together which explains why the stagger pattern achieved above the theoretical capacity.

Table 8. Uplift capacity of W2F connection

Fastener	Row Pattern			Stagger Pattern			Stagger to Row Mean Capacity Ratio
	# of tests	Mean Capacity, N (lbf)	COV	# of test	Mean Capacity, N (lbf)	COV	
(2) 15-Gauge Staples	4	2,549 (573)	0.30	3	3,163 (711)	0.08	**1.24**
(4) 2.5-mm (0.099 in.) Nails	3	4,448 (1,000)	0.14	3	4,184 (941)	0.04	**0.94**
Endwall Capacity Ratio		1.75			1.32		
(4) 15-Gauge Staples	3	4,139 (9,71)	0.20	3	5,439 (1,223)	0.07	**1.31**
(8) 2.5-mm (0.099 in.) Nails	3	4,684 (1,053)	0.07	3	6,070 (1,365)	0.03	**1.30**
Endwall Opening Capacity Ratio		1.13			1.12		
(6) 3.3-mm (0.131 in.) Nails	3	5,313 (688)	0.14	4	6,109 (1,373)	0.02	**1.15**
(13) 16-Gauge Staples	1	6,094 (1,370)	N/A	0	N/A	N/A	**-**
Sidewall Capacity Ratio		1.15					
(8) 16-Gauge Staples	3	5,439 (1,223)	0.01	4	5,260 (1,183)	0.12	**0.97**
(7) 2.9-mm (0.113 in.) Nails	3	4,276 (961)	0.09	2	6,081 (1,367)	0.01	**1.42**
Shearwall Capacity Ratio		0.78			1.16		

Figures 24 through 30 show the force-displacement (floor joist displacement) relationship for the W2F connection. The theoretical design capacity tabulated in Table 7 is marked with a horizontal dashed line and labeled as the nominal capacity on Figures 24 through 30. Because all fastener types were tested in a row and staggered pattern, the two different patterns are presented in blue and red, respectively. Figure 9 shows the results of the six tests performed on the two 15-gauge staples. As evident from Figure 9, the measured capacity was between 1.0 to 2.4 times higher than

the nominal capacity; this was true for the row and stagger pattern. After the peak, the load plateaus due to the nail pulling out of the floor joist, where the load plateaus in the range of the nominal capacity. The plateau is consistent with the bending of the fastener and local failure of the wood expected because the staples took on a hook shape as they failed. One specimen exhibited a much lower capacity than the other specimens, as shown on Figure 24, but it still peaked just higher than the nominal capacity. The premature failure was due to the strap failing around the staple which may have been weakened during placement.

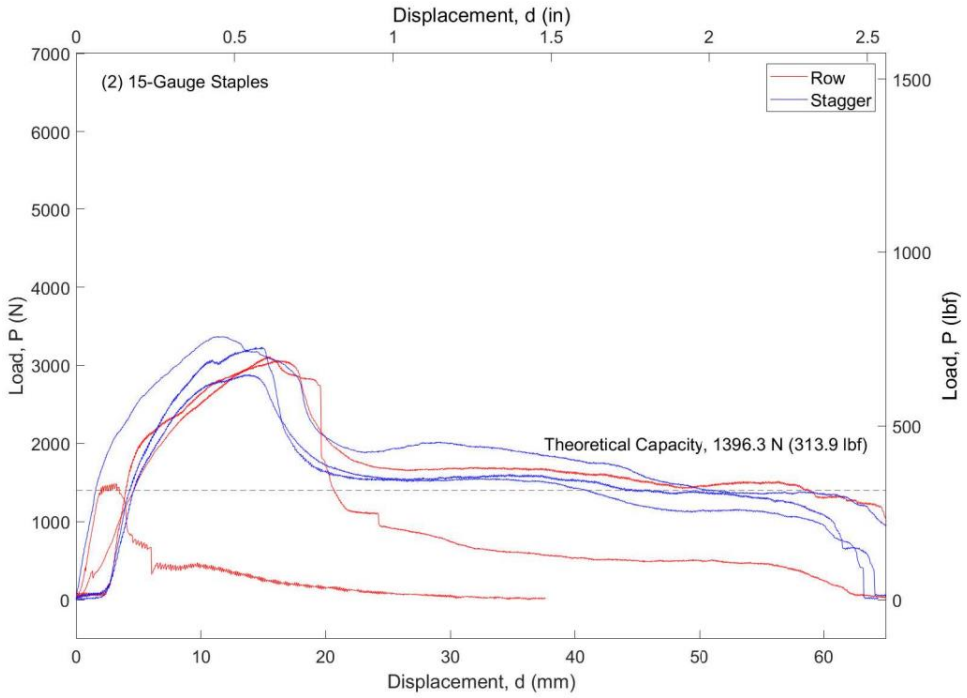

Figure 24. Monotonic load versus floor joist displacement for two 15-gauge staples

Figure 25 displays the results for the monotonic testing of the four 2.5-mm (0.099 in.) diameter nails, which peaked 1.4 to 1.7 times higher than the nominal capacity. Additionally, there is no discernable difference between the row and stagger pattern with both patterns reaching a peak value then tapering off in a consistent manner. Similar to the previous case, the four 2.5-mm (0.099 in.) diameter nail connection experienced failure by bending the nail. While the theoretical calculations indicated a failure of the side member, the steel strap, the tests resulted in the wood stud failing by pulling out columns of wood in the path of the nails. There is some bending damage seen in the steel strap, but the damage in the stud is consistent with failures seen in other connections.

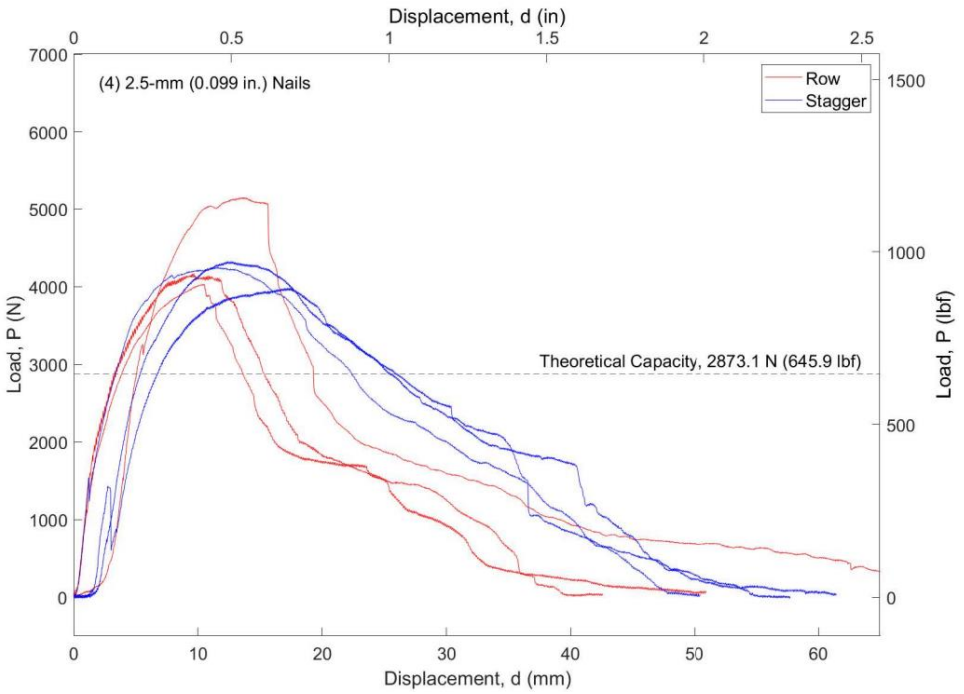

Figure 25. Monotonic load versus floor joist displacement for four 2.5-mm (0.099 in.) shank diameter nails.

Figure 26 shows results for the monotonic testing of the four 15-gauge stapled connection, where the loads were 1.1 to 2 times higher than the expected theoretical capacity. This connection displays a difference in performance for the stagger and row pattern. While the capacities are relatively similar, behavior of the failure changes substantially. As shown in Figure 26, the stagger pattern connections began to experience failures of the strap while the row patterns continued to bend and cause local failures of the wood around the staple. As evident in the trend lines, the row patterns load-displacement curves plateau and taper, whereas the stagger pattern sharply drop after the peak is reached.

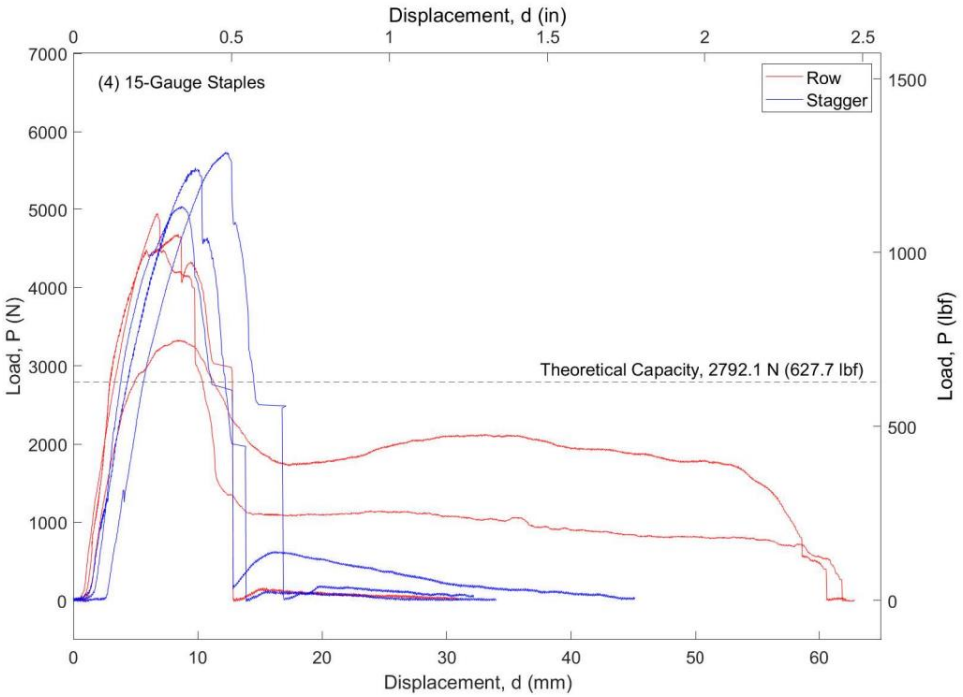

Figure 26. Monotonic load versus floor joist displacement for four 15-gauge staples

Figure 27 displays results of the monotonic testing of the eight 2.5-mm (0.099 in.) shank diameter nailed connection. This connection also demonstrates differences in failure modes and connection behavior between the row and stagger patterns. In this case, the row pattern fails to meet the nominal capacity, where the peak reaches between 78% to 87% of the nominal capacity. All the specimens that had the row pattern failed when the row of fasteners tore out the bottom of the stud. The stagger pattern connection peaks just exceed (by 6 to 10%) the nominal capacity All but one of the specimens with a stagger pattern experienced a failure in the strap. The one stagger pattern specimen that did not fail in this manner reached a comparable peak load before failure.

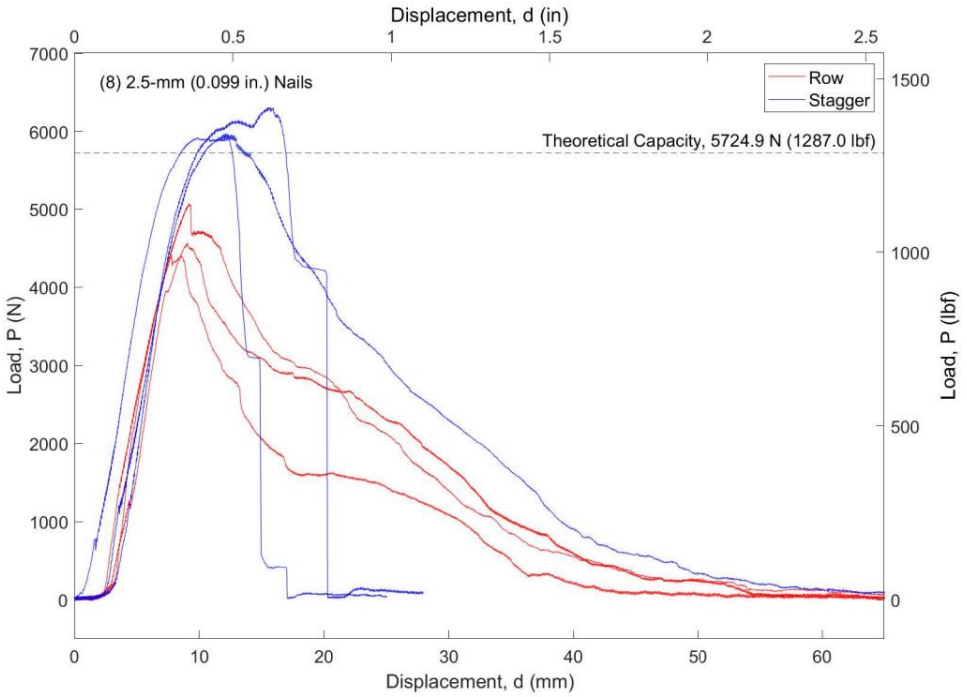

Figure 27. Monotonic load versus floor joist displacement for eight 2.5-mm (0.099 in.) shank diameter nails

Figure 28 provides the results of the monotonic testing of the six 3.3-mm (0.131 in.) shank diameter nailed connection. In this case, differences between stagger and row pattern behavior and failure mode are most apparent. All the stagger pattern specimens experienced failure in the strap, whereas the row pattern specimens experienced row tear out (as seen with the eight 2.5-mm (0.099 in.) shank diameter nail connection). The row pattern connections, and subsequent row tear out failures, reached a wide range of maximum loads before failure where all failed to meet the nominal capacity. The stagger pattern connections peaked at 1 to 1.13 times the nominal capacity.

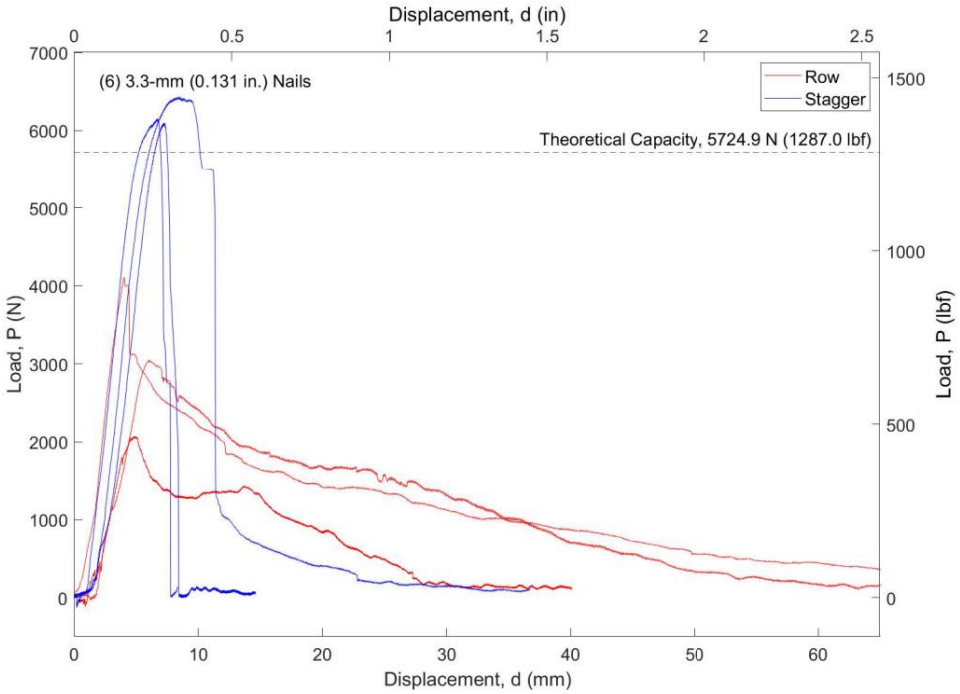

Figure 28. Monotonic load versus floor joist displacement for six 3.3-mm (0.131 in.) shank diameter nails

Figure 29 provides the monotonic test results of the eight 16-gauge stapled connection, where all six specimens experienced failure in the strap. With this connection all but one specimen reached a maximum load above the nominal capacity. Of note, strap failure is not the predicted failure mode. This deviation likely occurred since the nominal capacity is close to the yield limit of the strap, and any significant load above the nominal capacity causes a failure in the strap. Of note, the behavior of these strap failures differs from previous connections, particularly compared to the six 3.3-mm (0.131 in.) shank diameter nails (Figure 28). As shown in Figure 28, the nail connection has clear peaks with little capacity remaining after the maximum load is reached. However, in Figure 29, the staple connection has a stairstep trend after maximum load is reached. The stair stepping is due to the tear in the strap occurring at staple locations which allowed a portion of the strap to remain intact.

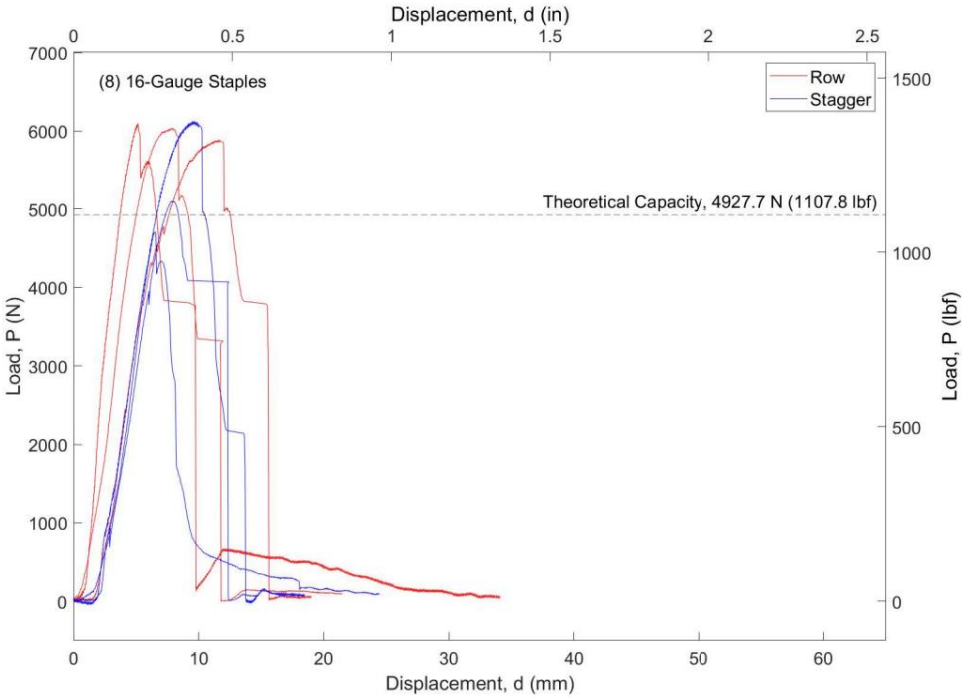

Figure 29. Monotonic load versus floor joist displacement for eight 16-gauge staples

Figure 30 displays the monotonic test results of the seven 2.9-mm (0.113 in.) shank diameter nailed connection. Here, the stagger pattern specimens peaked between 1 to 1.1 times the nominal capacity, whereas the row pattern specimens reached between 65% to 78% and thereby failing to reach the nominal capacity.

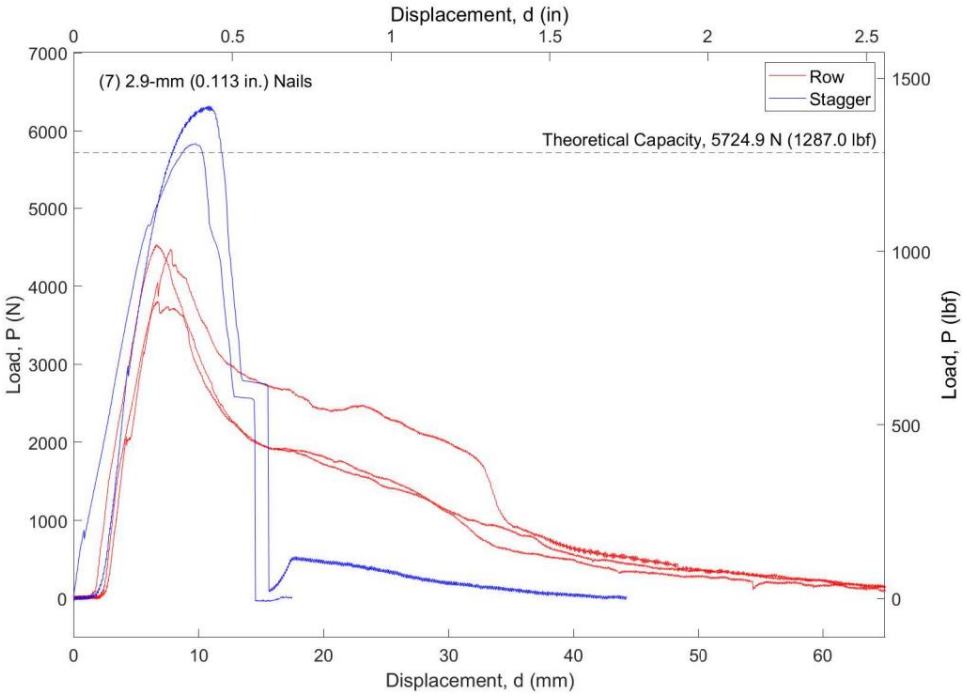

Figure 30. Monotonic load versus floor joist displacement for seven 2.9-mm (0.113 in.) shank diameter nails

Cyclic Test Results for Wall to Floor Connection

Cyclic testing is on-going, where only one specimen set has been tested at the time of the report. Figures 31 through 33 provide the load-displacement curves for the three (6) 3.3-mm diameter shank nailed specimens tested cyclically. Comparing monotonic to cyclic test results, the maximum (measured) capacity for this connection is slightly higher for the cyclic test. The failure modes are the same. During the cyclic tests, however, the nail was observed to slide in and out of the stud during the test causing compression during the unloading of the connection.

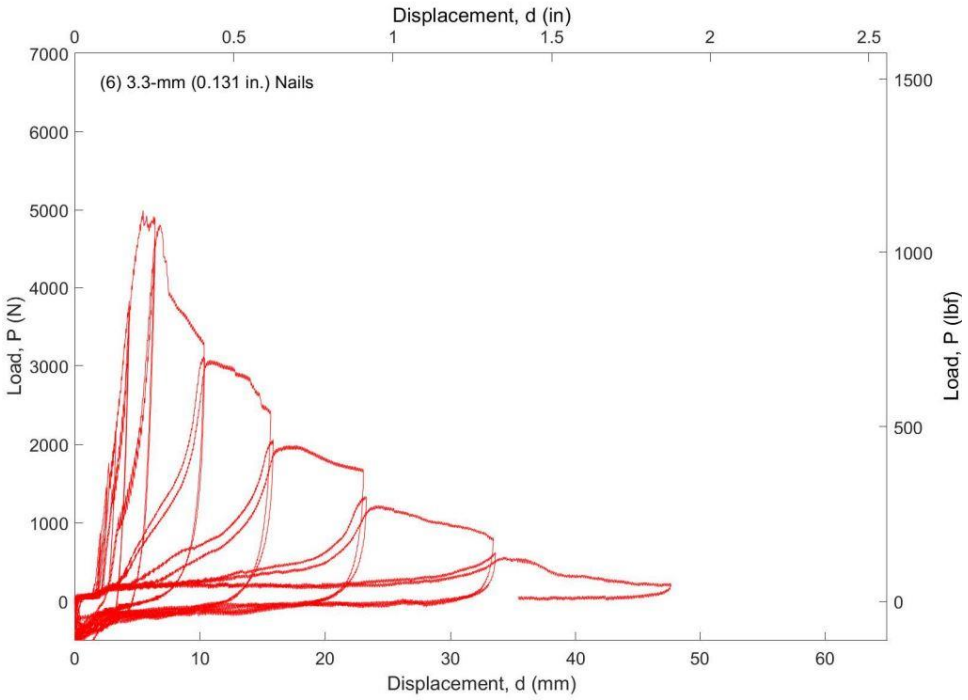

Figure 31. Cyclic force-displacement curve for (6) 3.3-mm (0.131 in.) diameter shank nails in a row pattern

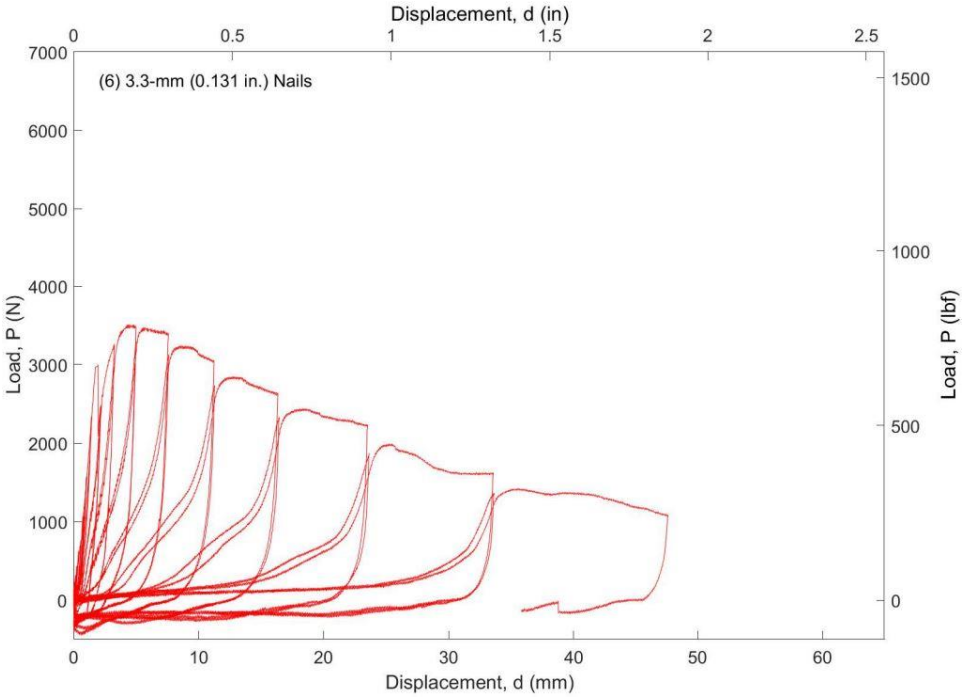

Figure 32. Cyclic force-displacement curve for (6) 3.3-mm (0.131 in.) diameter shank nails in a row pattern

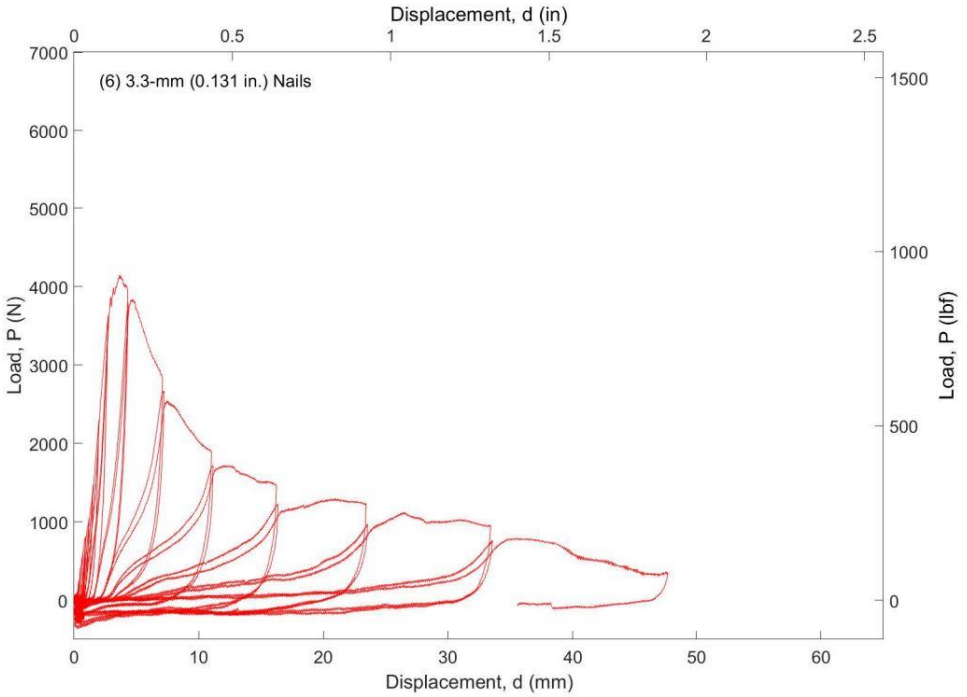

Figure 33. Cyclic force-displacement curve for (6) 3.3-mm (0.131 in.) diameter shank nails in a row pattern

Numerical Benchmark Study

For Wind Zone II, the county with the highest wind was St. Lucie County with a wind speed of 69.3 m/s (155 mph), and for Wind Zone III the maximum wind speed occurred in Monroe County with a wind speed of 76.4 m/s (171 mph). Despite Wind Zones II and III covering states all along the southeast coast of the U.S., these two counties represent the maximum wind speed for each wind zone in the state of Florida and for the entire wind zone. The well-known cities for each Wind Zone II and III were selected as Tallahassee and Miami, respectively. The basic wind speed for Tallahassee is 52.7 m/s (118 mph), and the basic wind speed for Miami is 75.5 m/s (169 mph). For Eq. (1), z_e = 5.8 m (19 ft) for St. Lucie County, 0 m (0 ft) for Monroe County, 65.2 m (214 ft) for Tallahassee, and 2.1 m (7 ft) for Miami. Using Eq. 3, the MWFRS velocity pressure for St. Lucie County is 2468.7 N/m^2 (51.6 psf), Monroe County is 3006.9 N/m^2 (62.8 psf), Tallahassee is 1422.0 N/m^2 (29.7 psf), and Miami is 2935.1 N/m^2 (61.3 psf). Tables 9 through 12 summarize the results of all four geographic locations for MWFRS and C&C wind pressures.

Tables 9 through 12 show the differences between the ASCE/SEI 7-22 and HUD Code MWFRS and C&C wind pressure calculations for the four locations in Florida. Tables 9 and 10 present the comparisons for St. Lucie County and Monroe County, respectively. Tables 11 and 12 present the comparisons for Tallahassee and Miami, respectively. The tabulated ASCE/SEI 7-22 wind pressures in Tables 9 through 12 present the pressures in two unit systems. In all cases, an ASD load factor of 0.6 was applied to the ASCE/SEI 7-22 pressures presented in brackets.

The ASCE/SEI 7-22 pressures generally produce a lower MWFRS pressure compared to the HUD Code. The MWFRS uplift pressures were consistently below those provided by the HUD Code, ranging from 37% to 79% difference. Similarly, the MWFRS lateral pressures for both the county and city in Wind Zone II are lower when calculated using ASCE/SEI 7-22 with percent differences of 95% and 55%, respectively. However, the lateral loads developed using ASCE/SEI 7-22 show an increase in pressure for both the county and city used for Wind Zone III.

The more significant difference across the comparisons is with the components and cladding pressures. Except for the study done for Tallahassee, Florida, all C&C pressures were higher for ASCE/SEI 7-22 compared to the HUD Code. C&C loads increased by a factor of 1.39 to 2.55. As observed in Tables 10 and 12, the locations in Wind Zone III had a greater difference with all ASCE/SEI 7-22 pressures exceeding HUD Code pressures at least a factor of 2. For the differing case of Tallahassee, the roof zone near the ridge and eaves resulted in an increase in ASCE/SEI 7-22 loads by a factor of 1.23 over what is required in the HUD Code. Two of the three remaining categories indicated a near similar load with a factor of 0.99 between the two loads. These areas represent the roof away from the ridge, eave, or gable. The remaining category presented in the C&C section is the area next to the gable end which has a lower pressure generated using ASCE/SEI 7-22 by a factor of 0.67.

Table 9. Load Comparison of ASCE 7-22 to HUD Code for St. Lucie County, FL (Wind Zone II)

Applicable Structure	**ASCE/SEI 7-22 Pressure, N/m^2 (psf)**	**HUD Code Pressure, N/m^2 (psf)**	**Ratio of ASCE/SEI 7-22 to HUD Code**
Main Wind Force Resisting System			
Shearwalls, Diaphragms	2,987.7 (62.4) [1790.7 (37.4)]	1,867.3 (39)	**1.60 [0.95]**
Ridge Beams, Main Roof Support Beams	-1,546.5 (-32.3) [-928.9 (-19.4)]	-1,436.4 (-30)	**1.08 [0.65]**
Components and Cladding			
Roof Trusses	-5,348.2 (-111.7) [-3212.8 (-67.1)]	-1,867.3 (-39)	**2.86 [1.72]**
Roof covering, Sheathing, Fastening	-5,348.2 (-111.7) [-3212.8 (-67.1)]	-1,867.3 (-39)	**2.86 [1.72]**
With 3’-0” of Gable End with No Overhang	-6,818.1 (-142.4) [-4093.8 (-85.5)]	-3,495.3 (-73)	**1.95 [1.17]**
With 3’-0” of Ridge and Eave	-8,709.4 (-181.9) [-5223.7 (-109.1)]	-2,441.9 (-51)	**3.57 [2.14]**

Table 10. Load Comparison of ASCE 7-22 to HUD Code for Monroe County, FL (Wind Zone III)

Applicable Structure	**ASCE 7-22 Pressure, N/m^2 (psf)**	**HUD Code Pressure, N/m^2 (psf)**	**Ratio of ASCE/SEI 7-22 to HUD Code**

Main Wind Force Resisting System			
Shearwalls, Diaphragms	3,643.7 (76.1) [2226.4 (45.6)]	1,867.3 (39)	**1.95 [1.17]**
Ridge Beams, Main Roof Stupoort Beams	-1,891.3 (-39.5) [-1134.8 (-23.7)]	-1,436.4 (-30)	**1.32 [0.79]**
Components and Cladding			
Roof Trusses	-6,516.5 (-136.1) [-3911.8 (-81.7)]	-1,867.3 (-39)	**3.49 [2.09]**
Roof covering, Sheathing, Fastening	-6,516.5 (-136.1) [-3911.8 (-81.7)]	-1,867.3 (-39)	**3.49 [2.09]**
With 3'-0" of Gable End with No Overhang	-8,307.2 (-173.5) [-4984.3 (-104.1)]	-3,495.3 (-73)	**2.38 [1.43]**
With 3'-0" of Ridge and Eave	-10,605.5 (-221.5) [-6363.3 (-132.9)]	-2,441.9 (-51)	**4.34 [2.61]**

Table 11. Load Comparison of ASCE 7-22 to HUD Code for Tallahassee, FL (Wind Zone II)

Applicable Structure	ASCE 7-22 Pressure, N/m^2 (psf)	HUD Code Pressure, N/m^2 (psf)	Ratio of ASCE/SEI 7-22 to HUD Code
Main Wind Force Resisting System			
Shearwalls, Diaphragms	1,718.9 (35.9) [1034.2 (21.6)]	1,867.3 (39)	**0.92 [0.55]**
Ridge Beams, Main Roof Support Beams	-890.6 (-18.6) [-536.3 (-11.2)]	-1,436.4 (-30)	**0.62 [0.37]**
Components and Cladding			
Roof Trusses	-3,078.7 (-64.3) [-1848.2 (-38.6)]	-1,867.3 (-39)	**1.65 [0.99]**
Roof covering, Sheathing, Fastening	-3,078.7 (-64.3) [-1848.2 (-38.6)]	-1,867.3 (-39)	**1.65 [0.99]**
With 3'-0" of Gable End with No Overhang	-3,926.2 (-82.0) [-2355.7 (-49.2)]	-3,495.3 (-73)	**1.12 [0.67]**
With 3'-0" of Ridge and Eave	5,013.1 (-104.7) [-3006.9 (-62.8)]	-2,441.9 (-51)	**2.05 [1.23]**

Table 12. Load Comparison of ASCE 7-22 to HUD Code for Miami, FL (Wind Zone III)

Applicable Structure	ASCE 7-22 Pressure, N/m^2 (psf)	HUD Code Pressure, N/m^2 (psf)	Ratio of ASCE/SEI 7-22 to HUD Code
Main Wind Force Resisting System			
Shearwalls, Diaphragms	3,557.5 (74.3) [-2135.5 (44.6)]	1,867.3 (39)	**1.91 [1.14]**
Ridge Beams, Main Roof Support Beams	1,843.4 (38.5) [-1106.0 (-23.1)]	-1,436.4 (-30)	**1.28 [0.77]**

Components and Cladding			
Roof Trusses	-6,363.3 (-132.9) [-3820.8 (-79.8)]	-1,867.3 (-39)	**3.41 [2.05]**
Roof covering, Sheathing, Fastening	-6,363.3 (-132.9) [-3820.8 (-79.8)]	-1,867.3 (-39)	**3.41 [2.05]**
With 3'-0" of Gable End with No Overhang	-8,110.9 (-169.4) [-4869.4 (-101.7)]	-3,495.3 (-73)	**2.32 [1.39]**
With 3'-0" of Ridge and Eave	-10,356.5 (-216.3) [-6214.9 (-129.8)]	-2,441.9 (-51)	**4.24 [2.55]**

Conclusions

Stakeholder Engagement

Manufactured home manufacturers continue to be challenging to connect with. Through conversations with federal and non-governmental agencies, there is significant interest in this research to quantify and improve the wind performance of manufactured homes, and in full-scale wind tunnel testing of a manufactured housing unit.

Components and Connection Testing Study

Fastener component monotonic testing informed cyclic testing protocols. Subsequent cyclic testing of various sheathing fastener configurations provided data that will be used in detailed finite element models of manufactured homes. As shown in the results of this report, the mean capacities for the nail connections in SYP lumber are substantially (2.5 to 3 times) less than the mean capacities for screw connections in SPF. Similarly, the COV was always 2.5 times higher for the nail connections in SYP compared with the screw connections in SPF. Given that nail connections are the more common connection used in the actual construction of Wind Zone II manufactured homes which have roof failure as the most common observed failure mode in the field, switching fasteners from nails to screws is expected to provide significantly higher performance. The study completed on common wall to floor connections shows that the expected capacity is often achieved for these connections. However, the pattern of the fasteners can make a critical difference, where the pattern was not specified in the documentation from HUD or the drawings our team received from a manufacturer. As observed in the field, stagger, row, random patterns are all common in practice. The stagger pattern is recommended as it distributes the load more evenly across a larger area of the wood member. More research is needed to understand this relationship for edge fasteners, as well as for the roof-to-wall connection. Additionally, more research is needed to understand the material and labor cost difference that is associated with (a) using screws instead of nails at the roof sheathing to rafter connection, and (b) staggering fasteners connecting the strap at the wall to floor connection.

Numerical Benchmark Study

The numerical benchmark study was performed to evaluate the differences in HUD Code wind loads with the wind loads specified in ASCE/SEI 7-22. As presented in Tables 9 through 12, there

were significant differences between the pressures calculated using the two provisions. ASCE/SEI 7-22 has gone through major revision over the past 35 years, continuously incorporating new findings, updated statistics, and the best science, whereas the HUD Code has remained stagnant. Based on the findings in the benchmark study, it may be the case that HUD Code wind pressures are conservative for MWFRS and unconservative for C&C. The significance in the difference in the C&C loads could be a source for the disparate failures of manufactured homes observed after major wind events.

Of note, the comparison only investigates one manufactured home geometry in four specific locations in Florida. More research is needed to investigate the range of manufactured home geometries for a larger geographic scope.

References

American Housing Survey (AHS) (2019). 2019 Florida – General Housing Data – All Occupied Units. Accessed July 24, 2022. https://www.census.gov/programs-surveys/ahs/data/interactive/ahstablecreator.html?s_areas=00012&s_year=2019&s_tablename=TABLE1&s_bygroup1=1&s_bygroup2=1&s_filtergroup1=1&s_filtergroup2=1

AF&PA. (2005). *National Design Specification for Wood Construction." Chapter 11: Dowel Type Fasteners, AF & PA American Wood Council,* Washington D. C.

American Society of Civil Engineers (ASCE) (2022). Minimum Design Loads for Buildings and Other Structures, Standard 7. American Society of Civil Engineers, Reston, VA.

American Society for Testing and Materials (ASTM) (2020). Standard Test Methods for Mechanical Fasteners in Wood and Wood-Based Materials, ASTM D1761. West Conshohocken, PA.

Clayton Homes. (2023). Manufactured Homes. Maryville, TN United States.

Douglas, B., Line, P., and Douglas, K. (2018). Evaluation of Fastener Head Pull-Through Strength of Wood. American Wood Council, Leesburg, VA.

Federal Emergency Management Agency (FEMA) (2007). Interim Testing Protocols for Determining the Seismic Performance Characteristics of Structural and Nonstructural Components, FEMA 461. Prepared by the Applied Technology Council for the Federal Emergency Management Agency, Washington, D.C.

Ferguson, W. (2022). 'Sitting on a time bomb': Mobile home park residents at risk in red-hot housing market. *Manufactured Home News*, published on April 27, 2022. https://www.manufacturedhomes.com/blog/red-hot-housing-market/

Hill, K. M. 2009. "Development of time-varying wind uplift test protocols for residential wood roof sheathing panels." Master's thesis, Dept. Of Civil and Coastal Engineering, Univ. of Florida.

Kallem, M. R. (1997). "Roof Sheathing Attachment for High Wind Regions: Comparison of Screws and Nails," MS Thesis, Clemson University, Clemson, SC.

Kerr, A., Sean, S., Prevatt, D. O. (2013). "Effects of installation Method on Nail Withdrawal Capacities." *Residential Building Design and Construction Conference*, 4(1), 183 – 191.

National Design Specification (NDS) (2018). National Design Specification for Wood Construction, 2018 Edition. ANSI/AWC-NDS 2018. American Wood Council, Leesburg, VA.

Sutley, E.J., Vazquez, K., Dao, T., Kim, J., Hunt, J., and Johnston, B. (2020). "Performance of Manufactured Housing during Hurricanes Irma and Michael." ASCE *Journal of Performance of Constructed Facilities*, 34(4). DOI 10.1061/(ASCE)CF.1943-5509.0001486.

U.S. Department of Housing and Urban Development (HUD) (2022). 24 Code of Federal Regulations Part 3280, Manufactured Home Construction and Safety Standards. Washington, D.C.

Appendix

Appendix A – Specimen-level Cyclic Results

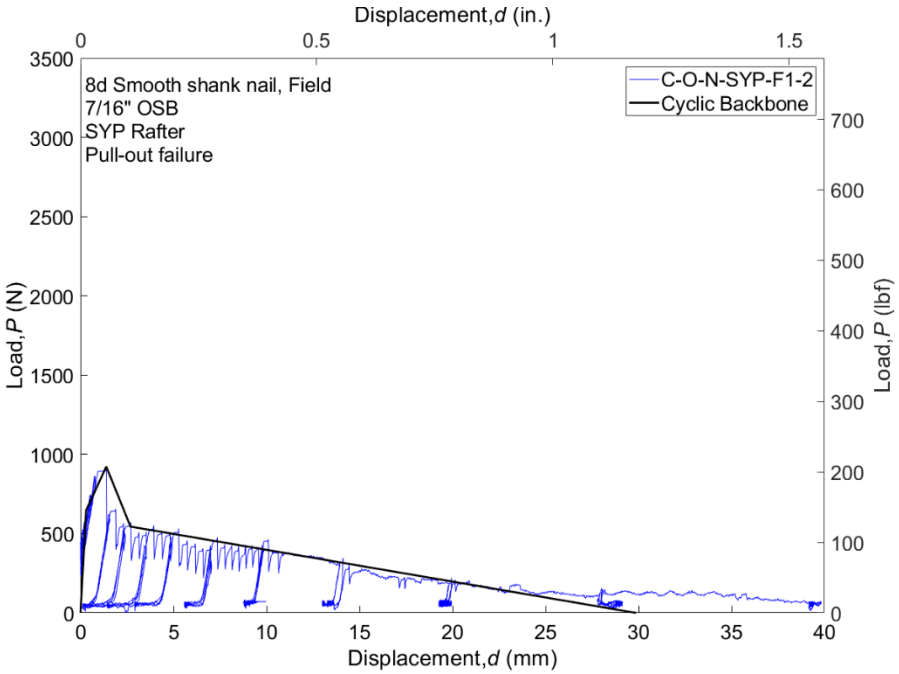

Figure C1. Cyclic force-deformation response for C-O-N-SYP-F1-2

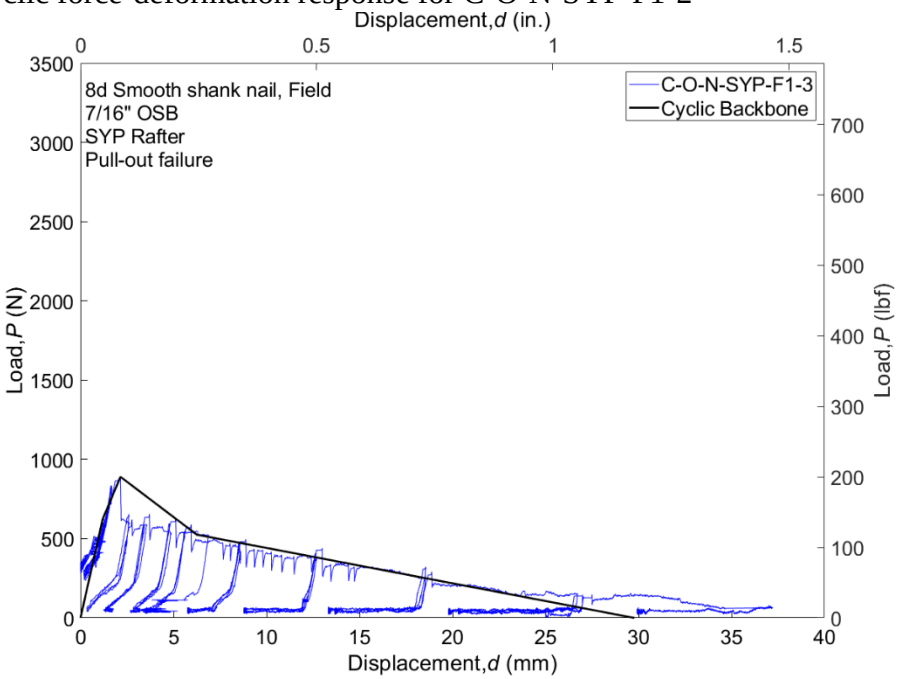

Figure C2. Cyclic force-deformation response for C-O-N-SYP-F1-3

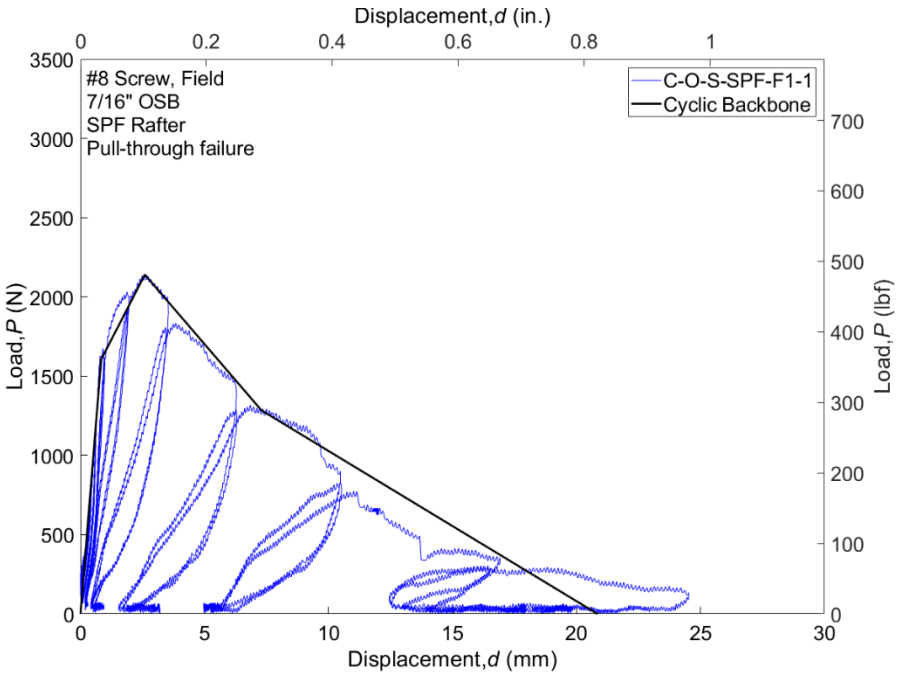

Figure C3. Cyclic force-deformation response for C-O-S-SPF-F1-1

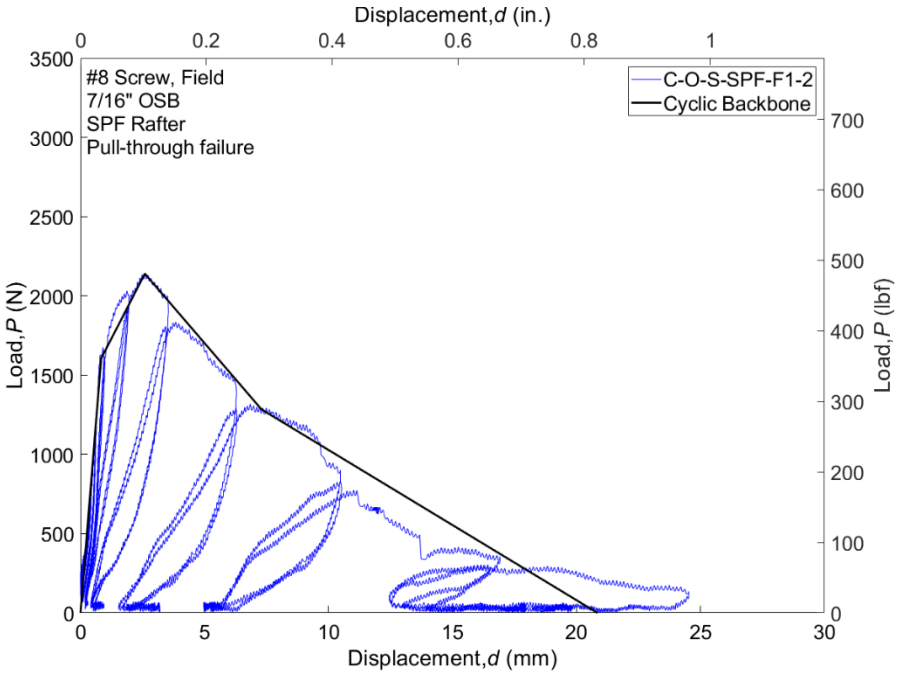

Figure C4. Cyclic force-deformation response for C-O-S-SPF-F1-2

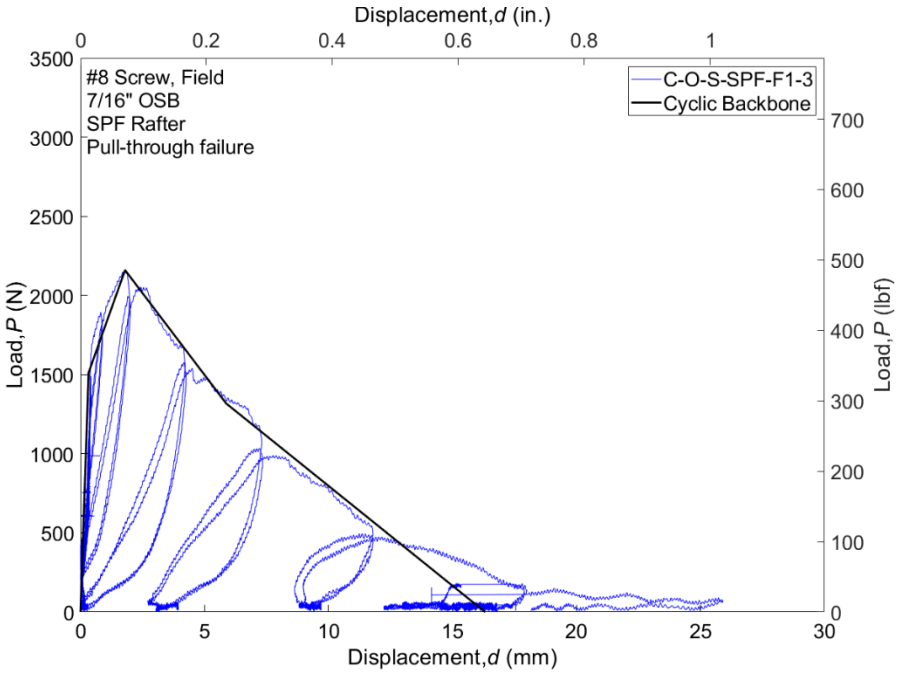

Figure C5. Cyclic force-deformation response for C-O-S-SPF-F1-3

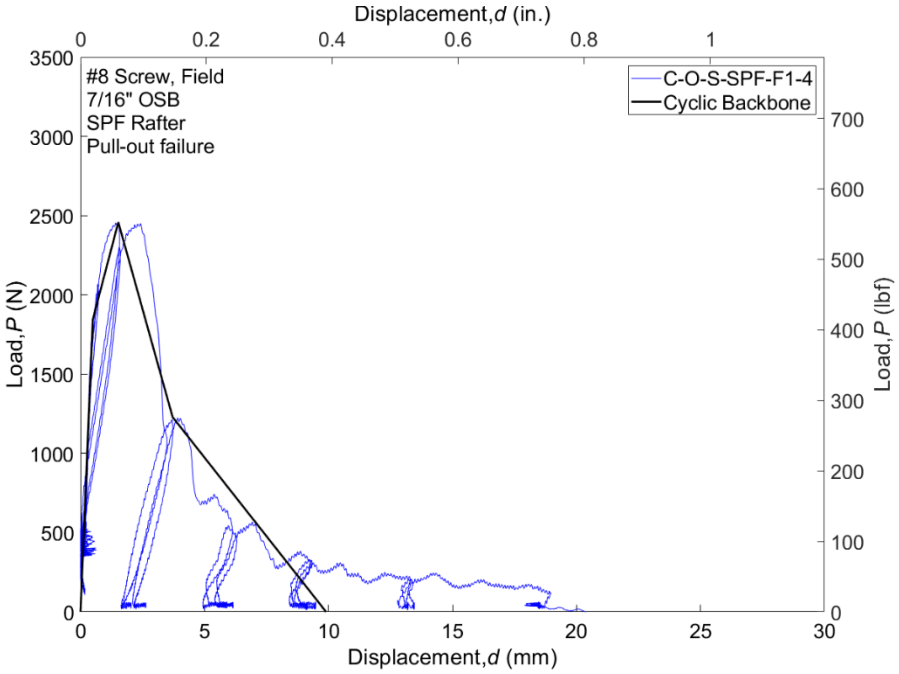

Figure C6. Cyclic force-deformation response for C-O-S-SPF-F1-4

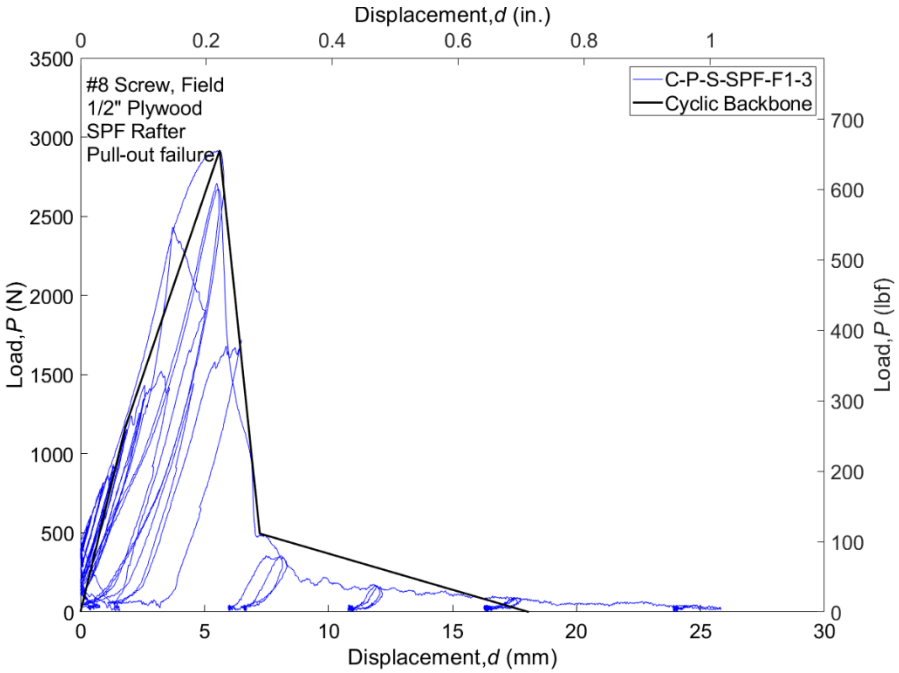

Figure C7. Cyclic force-deformation response for C-P-S-SPF-F1-3

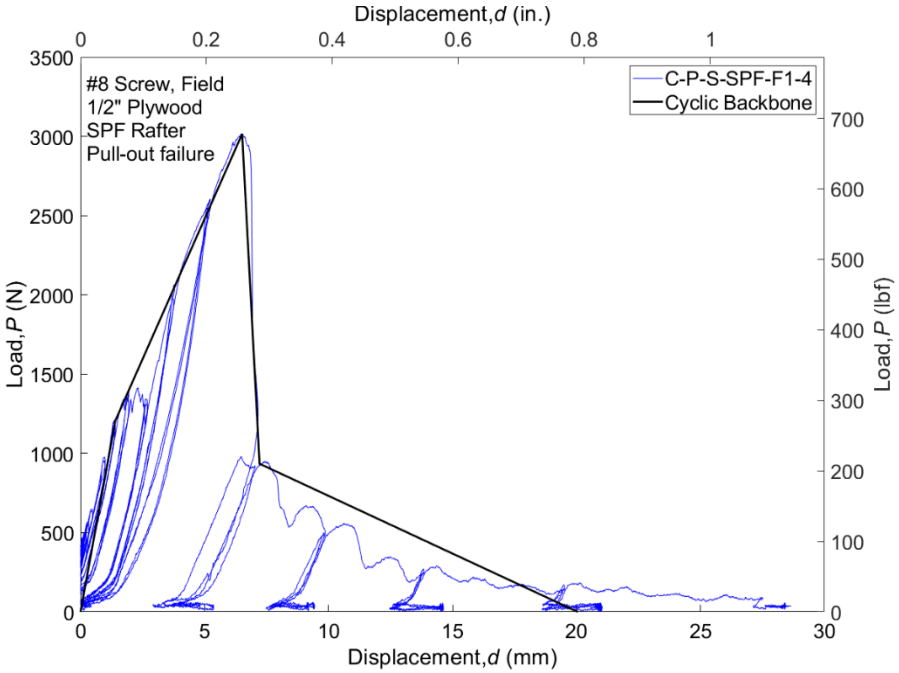

Figure C8. Cyclic force-deformation response for C-P-S-SPF-F1-4

SECTION 2 PART C:
NUMERICAL ANALYSIS OF MANUFACTURED HOMES UNDER HURRICANE EFFECTS

FINAL REPORT
(Period: 2023)

A Research Project Funded by:
The State of Florida Department of Emergency Management

Prepared by
Dr. Thang Dao

Graduate Student
Victor Onyia

Introduction

Hurricanes and windstorms pose a serious threat to manufactured housing units (MHUs). This study's main objective is to offer the fundamental and useful knowledge required to drastically decrease the physical susceptibility of manufactured homes to wind events. Although light-frame wood construction (LFWC) has been the subject of much investigation, little is known about MHUs. Although there is little research on anchorage systems, it does not account for many documented failure types, such as loss of roof and wall cladding. There is a significant knowledge vacuum on how hurricanes affect manufactured homes, as there are an estimated 2.7 million MHUs in mobile home parks across the U.S. (Ferguson 2022), including about 7% of Florida's households (AHS 2019). The novel methodologies offered have the potential to have transformative effects on both new and current mobile home parks as well as manufactured housing units through the generation of key foundational information that can alter code requirements, laws, and manufacturing processes. Manufactured homes are designed following the U.S. Department of Housing and Urban Development's Manufactured Home Construction and Safety Standards, Part 3280, (hereafter referred to as HUD Code). Notably, this code hasn't been substantially updated since 1994, and its hazard maps use lower wind speeds than the current ASCE-7 standard, stemming from the 1988 ASCE Standard 7. These manufactured housing units are the most susceptible residential structures to wind-related disasters, including hurricanes and tornadoes. Although these units employ wood frame construction, their structure differs significantly from traditional site-built homes, necessitating a distinct analysis. The HUD Code's design provisions are rather ambiguous, giving manufacturers a broad scope for interpretation. Our post-calamity field surveys show considerable inconsistency in the construction of manufactured homes, which corresponds to their performance, both within and across Wind Zones. Currently, there is no public information about the construction process of manufactured homes. However, our research team has acquired structural details from HUD and a leading U.S. manufacturer of these homes. Significant variability is present even within these documents. The actual structural design level(s) of manufactured homes remains a mystery; determining such is a critical initial step towards enhancing their resistance to wind damage.

The application of Finite Element Modeling (FEM) for seismic analysis of light-frame wood structures is a topic of significant interest within academic literature, same cannot be said about the use of FEM for wind analysis. A comprehensive review of light-frame wood structures' experimental and FEM studies under seismic loads created an analytical method for analyzing the behavior of light-frame wood constructions under static loads. In order to validate a sophisticated model made of superelements and quasisuperelements that represented the building's structural elements and linkages,

cyclic quasistatic loads were applied to a one-story wood-frame building (Kasal et al., 1994). Swansea and his team introduced two novel design strategies: the first approach integrates architectural components with structural ones to improve lateral strength and stiffness, while the second approach employs a cost-effective sliding base isolation system. Both design strategies aim to reduce earthquake damage in wood and cold-formed steel light-frame structures. For testing various increased details under reversed cyclic loading and pseudo-static cyclic loading, high-fidelity finite element models were created to simulate the behavior of light-frame sheathed walls. The findings were compared to fitted model component analysis behavior (Swensen et al., 2014).

Most of the hysteresis models found in literature focus on seismic analysis. A significant amount has not been done for wind analysis. To comprehend the dynamic properties of shear walls during repeated earthquakes, a shake table test of the shear walls of the Japanese post-and-beam building system was performed (Furuta & Nakao, 2023). The results of the shake table test are used to propose hysteresis models of the shear walls for earthquake response analysis. The impact of the cap beam on the seismic performance of traditional timber frames supported by stone was assessed (Wu et al., 2023). Four column foot and head joints were constructed in half and put through a reversed-cycling test. The joints' typical injury modes were discovered. To describe the rotational behavior of the joints, methods were put forth. Stone-supported traditional timber frames with or without cap beams were modeled using finite elements. Based on the generated models, lateral performance study was carried out on representative full-scale frames, and fragility analysis was then done to assess the seismic performance of the full-scale frames.

Foliente describes the general characteristics of the hysteretic behavior of wood joints and structural systems, and the hysteresis models for wood systems that are currently accessible are examined. In the nonlinear dynamic analysis of single-degree-of-freedom wood systems, a universal hysteresis model for wood joints and structural systems is described. It is based on a version of the Bouc-Wen-Baber-Noori model. The hysteretic constitutive rule generates a smoothly varying hysteresis that represents previously noticed behaviors of structural systems and wood joints, such as nonlinearity, degradation of strength and stiffness, and pinching (Foliente, 1995). On the other hand, a different analytical formulation of the pinching phenomena has been produced as a result of a critical examination of the hysteresis models of wooden connectors (Aloisio et al., 2020). The six-degrees-of-freedom formulation from the generalized Bouc-Wen model has been expanded to an eight-parameter formulation, which is a better representation of the connection's cyclical degradation. A true picture of the actual hysteresis cycles of wooden connections is provided by the data provided by the two extra

parameters as well as by the energy dependence of the parameters. The model was calibrated using experimental data after being identified using an Ordinary Least Squares (OLS) operator.

A computational model for predicting the behavior of wood shear walls under cyclic pressure is presented in another paper (Folz & Filiatrault, 2001). The model includes nonlinear connectors, linear elastic sheathing panels, and rigid framing components. It takes pinching behavior, strength degradation, and stiffness degradation into account. To evaluate the response of the wall, a displacement control approach is employed. The model is implemented using a computer software called CASHEW (Cyclic Analysis of Shear Walls), which is checked against experimental results. A single degree-of-freedom system can be calibrated using the program for predicting the nonlinear dynamic response of shear walls under seismic loading. In another paper, an 11-parameter model is used to fit hysteric behavior (Dao & van de Lindt, 2014), an improvement to the 10-paramter CASHEW model. Dao and van de Lindt presents numerical research on the seismic performance of a light-gauge cold-formed steel midrise building constructed with direct displacement design (DDD). The findings show that the structure, which uses a uniform truss construction system (UTCS), meets the necessary performance standards when subjected to cyclic loading and nonlinear time history analysis with 22 earthquakes.

In a recent study, Bai et al. investigates a novel fiber-reinforced polymer (FRP) material with a high tensile rupture strain of over 5% for seismic retrofitting of reinforced concrete (RC) square columns. A control column and nine RC square columns wrapped in different numbers and varieties of FRP were used in the investigation. By examining failure mechanisms, hysteretic behaviors, cumulative energy dissipation, and FRP strain progression, the seismic performance was evaluated. According to experimental findings, increasing confinement stiffness greatly increased specimen ductility while limiting and postponing longitudinal bar buckling. An LRS (Large-rupture-strain) FRP-confined concrete model and a reinforcing bar buckling model that took the FRP confining effect into account were used in the numerical analysis, which was done using OpenSees. For the columns with reduced confinement, results of the numerical simulation is consistent with the experimental curves. However, for FRP-wrapped columns with increased confinement, the envelope curves are slightly exaggerated. (Bai et al., 2023).

Another recent study presents a new analytical phenomenological-based hysteretic model called ASPID (Asymmetry, Pinching, and strength/stiffness Degradation) for timber members. In this study, ten physical-based hysteretic parameters for each loading direction and two force-displacement envelopes are used to model the asymmetric behavior (Chacón & Guindos, 2023). A novel generalized

fatigue evolution law is used to account for strength deterioration while a smooth piecewise function is used to account for pinching. Various key timber mechanical joints and assemblies can be simulated using the model. It is compared to three well-known hysteretic models and validated using six experimental benchmark tests. According to the findings, the ASPID model performs better than the competition in terms of accuracy, with low errors (less than 7.6%) in strength capacity and cumulative hysteretic dissipated energy (less than 2.9%). A trustworthy and efficient technique for simulating timber connections and assemblies is the ASPID model. Nonetheless, the model presented in this report more accurately predicts load response of a hysteric analysis than ASPID and other existing literature.

In this study, we introduce a general hysteresis model that can capture the cumulative damage of wood connections within the MHU. This new hysteresis model can be used for different types of connections by condensing the connection data using scattered data points and backbone curve of which the information can be extracted within the testing data. The curves are smoothed out by shape functions and average angle between adjacent segments. The details of the general hysteresis model are describe in the later section of this report.

Preliminary Wind Load Calculation

To determine the placements of the wind sensors, a model was utilized to estimate the preliminary wind load. The analysis offers a simplified and efficient method for estimating the forces acting on the model considering the dynamic behavior of substructures. Since at the time analysis was conducted, the roof-to-wall connection data were not available, a linear stiffness were assumed for those connections while non-linear behavior of sheathing fasteners were considered. From preliminary calculations, maximum forces in the connections are estimated and presented in Table 1.

The initial wind load calculation provides a starting point for additional study and design. The calculated load can be used to choose the best structural elements, identify the best materials, and improve the design through more in-depth computer simulations or experimental testing. It's vital to remember that the initial wind load determined by employing a linear model is only an estimate. Normally, safety factors are used to take uncertainties into account and guarantee the stability and safety of the construction. These elements consider things like the failure's consequences, the structure's dependability. From the results, in Table 1, sensors were recommended to be in the locations presented in Figure 1 (points circled with red). The final sensor locations were decided by FIU team and included inn the FIU report.

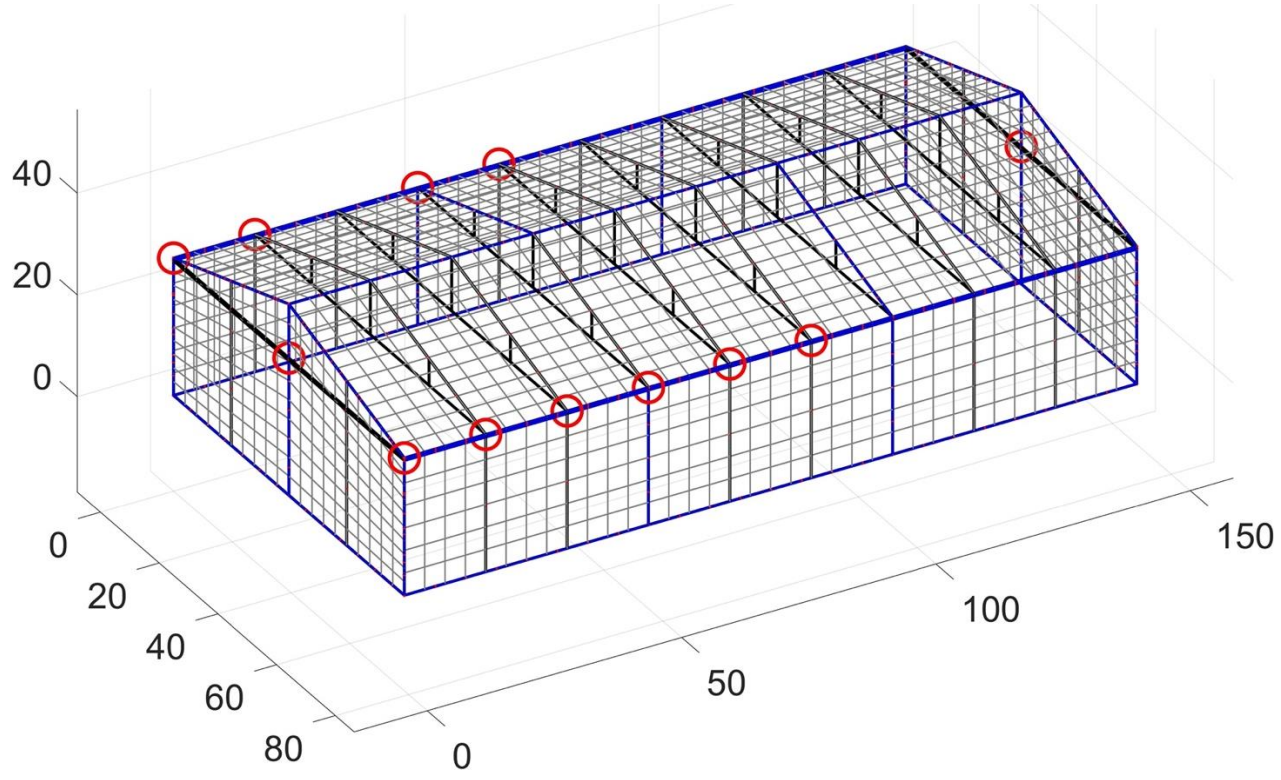

Figure 1(a): Roof-to-Wall Connection Displacement Measurement Locations

Table 1: Maximum Force in Connections

Connection Location	Wind Speed (mph)	Wind Diection to the Ridge (degrees)	Max in compression (kips)	Max in tesions (kips)	All case compression (kips)	All case tension (kips)
RTW Connections End Walls	60	0	-0.028	0.130	-0.665	1.187
		30	-0.034	0.114		
		45	-0.039	0.107		
		60	-0.063	0.066		
		90	-0.050	0.027		
	120	0	-0.185	0.574		
		30	-0.200	0.483		
		45	-0.321	0.590		
		60	-0.292	0.424		
		90	-0.318	0.197		
	160	0	-0.495	1.176		
		30	-0.598	0.979		
		45	-0.665	1.187		
		60	-0.551	0.770		
		90	-0.527	0.305		
RTW Connections Side Walls	60	0	-0.090	0.051	-0.177	0.648
		30	-0.006	0.06		
		45	-0.007	0.065		
		60	-0.012	0.075		
		90	-0.007	0.076		
	120	0	-0.060	0.209		
		30	-0.074	0.243		
		45	-0.051	0.309		
		60	-0.055	0.318		
		90	-0.072	0.298		
	160	0	-0.140	0.384		
		30	-0.164	0.445		
		45	-0.133	0.567		
		60	-0.177	0.648		
		90	-0.161	0.574		
WTF Connections	60	0	-0.056	0.036	-0.899	0.627
		30	-0.069	-0.037		
		45	-0.090	0.048		
		60	-0.078	0.047		
		90	-0.083	0.056		
	120	0	-0.301	0.209		
		30	-0.389	0.241		
		45	-0.480	0.335		
		60	-0.384	0.241		
		90	-0.472	0.368		
	160	0	-0.534	0.373		
		30	-0.714	0.526		
		45	-0.825	0.531		
		60	-0.899	0.591		
		90	-0.782	0.627		

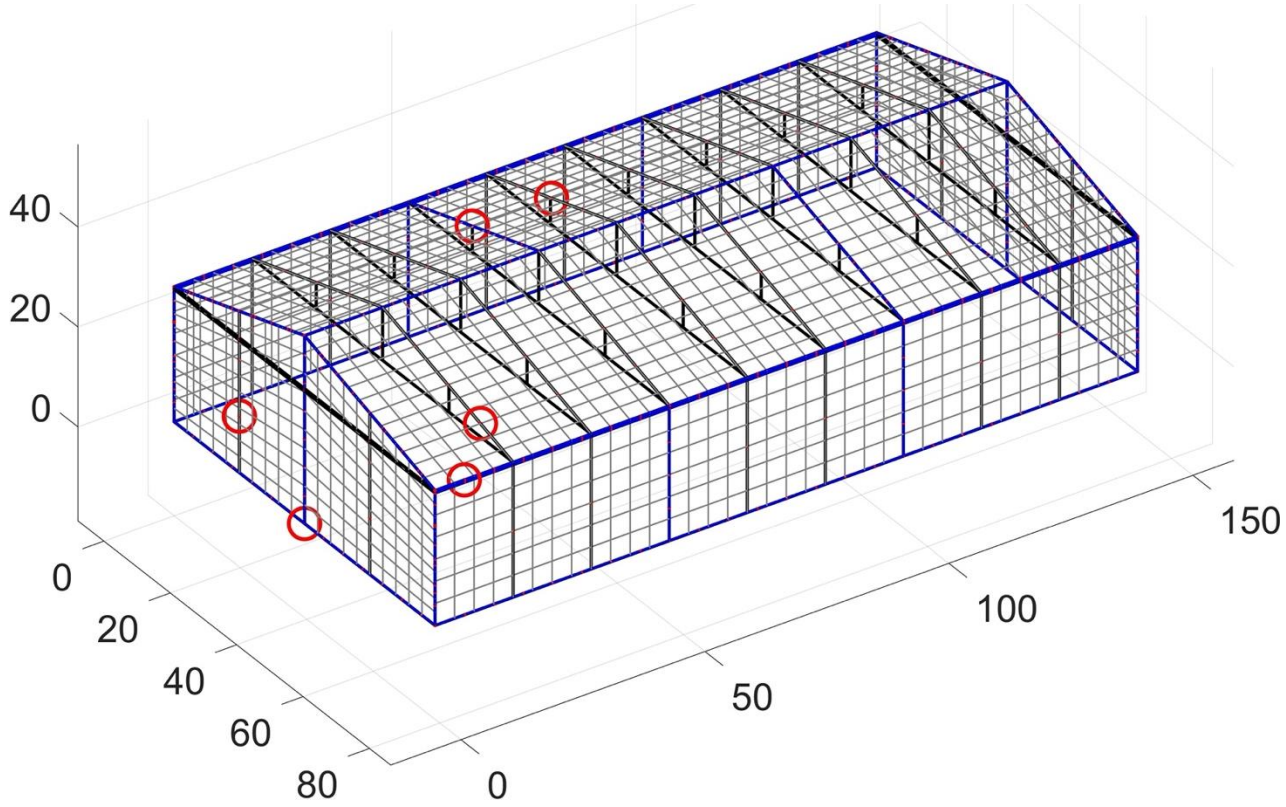

Figure 1(b): Sheathing Fastener Displacement Measurement Locations

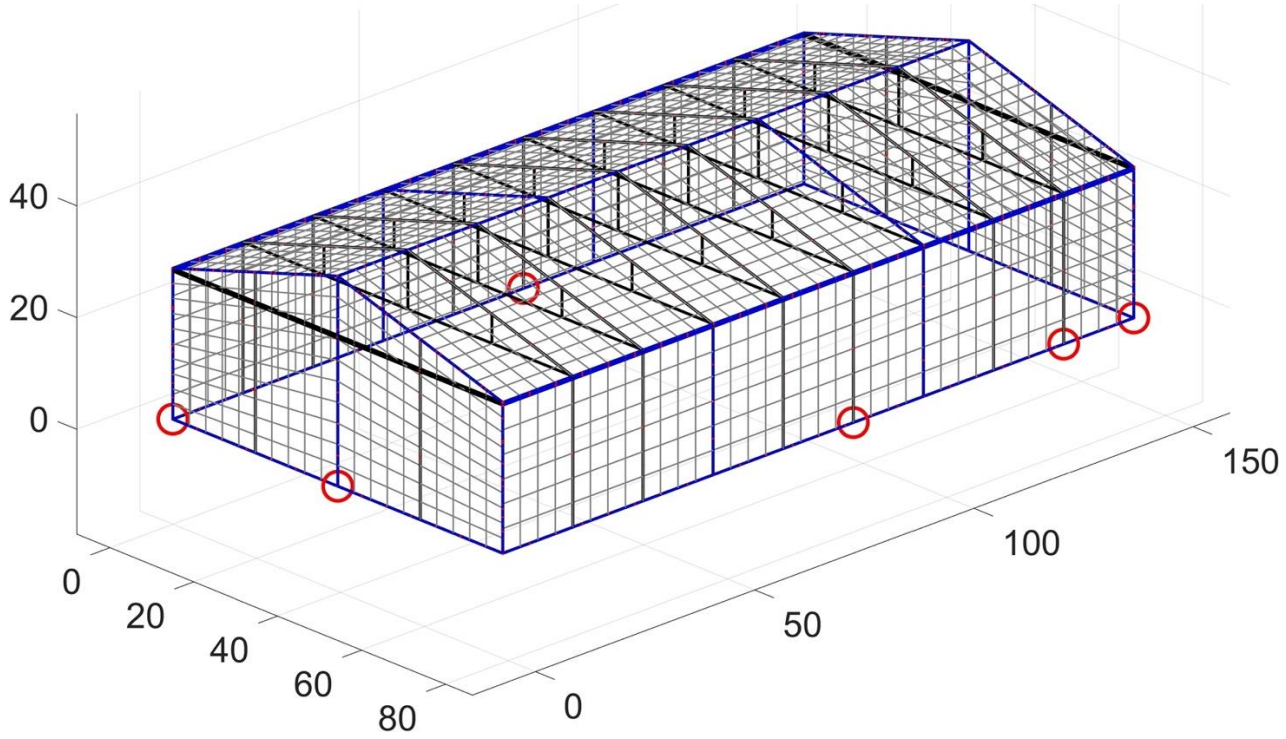

Figure 1(c): Wall-To-Foundation Force Measurement Locations

Hysteresis model for connections

Force (F) against displacements (X) were gotten from experiment conducted at Kansas State University. Tens of thousands of data points were collected during the hysteresis experiment. The data was first filtered to remove noise. After that, a threshold for X was set, below which were ignored for analysis purposes. This was done to eliminate irregularities arising from machine error at low displacements, of which the linear behavior of the connection is assumed. From the testing protocol and testing data, information about cycles were extracted. Figure 2 presents a plot of X.

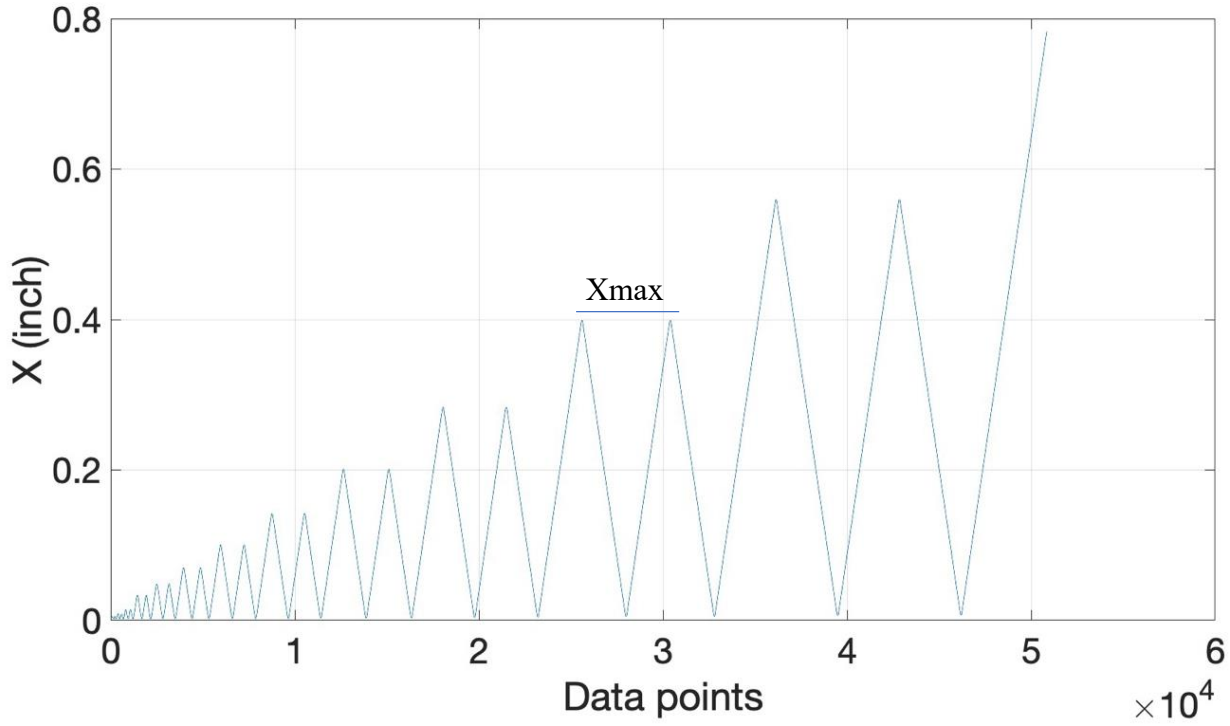

Figure 2: Loading protocols.

When the data was ready for analysis, backbone curve, loading curves and unloading curves were extracted for each cycle. Forty data points were selected at uniform interval from thousands of points to describe the hysteric behavior within each loading and unloading cycle. The more data points are selected, the better fit the loading and unloading curves fit to the data. However, it needs more memory to store those information during the analysis. Fmax for each cycle was calculated, with the maximum of all the Fmax being named Peak Fmax. To the right of the Peak Fmax, Fmax points were selected as points for the backbone curve. Whereas backbone curve to the right of Peak Fmax were at 40% and 75% way between Fmax and Xmax of each cycle. When these points are extracted, a shape function is used to join them smoothly. Figure 3 shows a plot of the data (F versus X) and the corresponding backbone curve (shown with red line).

The loading curve starts from point of zero displacement in each cycle up till Fmax, then for any further increase in X, it maintains the horizontal value of Fmax till it hits the backbone curve. For the unloading curve, the curve starts on the backbone curve, moves vertically downwards to meet Xmax point of the cycle in question and finally goes back to point of zero displacement. Just as in the backbone curve, loading and unloading curves are smoothed out using a shape function. Figure 4 shows a plot of the experimental data and shown in blue is the loading and unloading curves fitted with selected points.

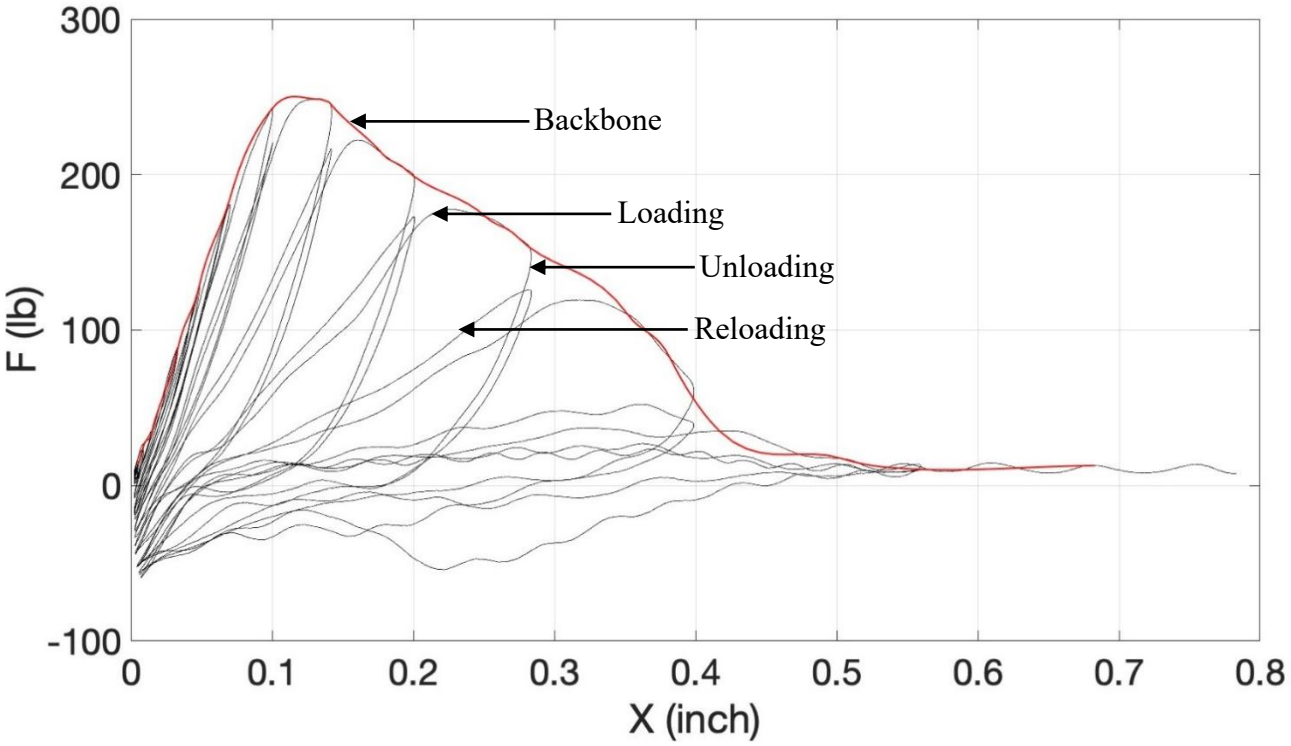

Figure 3: Experimental Data Plot and Backbone

The backbone curve defines the maximum possible force at each displacement level and is used to track the target displacement at each cumulative damage level of the connection under cyclic load. The experimental loading curves and unloading curves are extracted from experimental data. These curves are used to interpolate the loading curve and unloading curve at each target displacement, which is calculated based on damage level determined by cumulative energy dissipated under cyclic loading.

In the time history analysis, the information of experimental data is condensed into loading curves, unloading curves, and backbone curve. Each set of condensed information is presented for each connection test data; therefore, the model is accurately captured the cumulative damage at each connection.

In order to track the load and displacement, the loading and unloading curves at each target displacement is interpolated based on the loading and unloading curves extracted from the test data. Figure 4 shows how the loading curve and unloading curve of a target displacement are interpolated from extracted loading and unloading curves. The blue curves are extracted from experimental data while the green curves are interpolated from extracted curves.

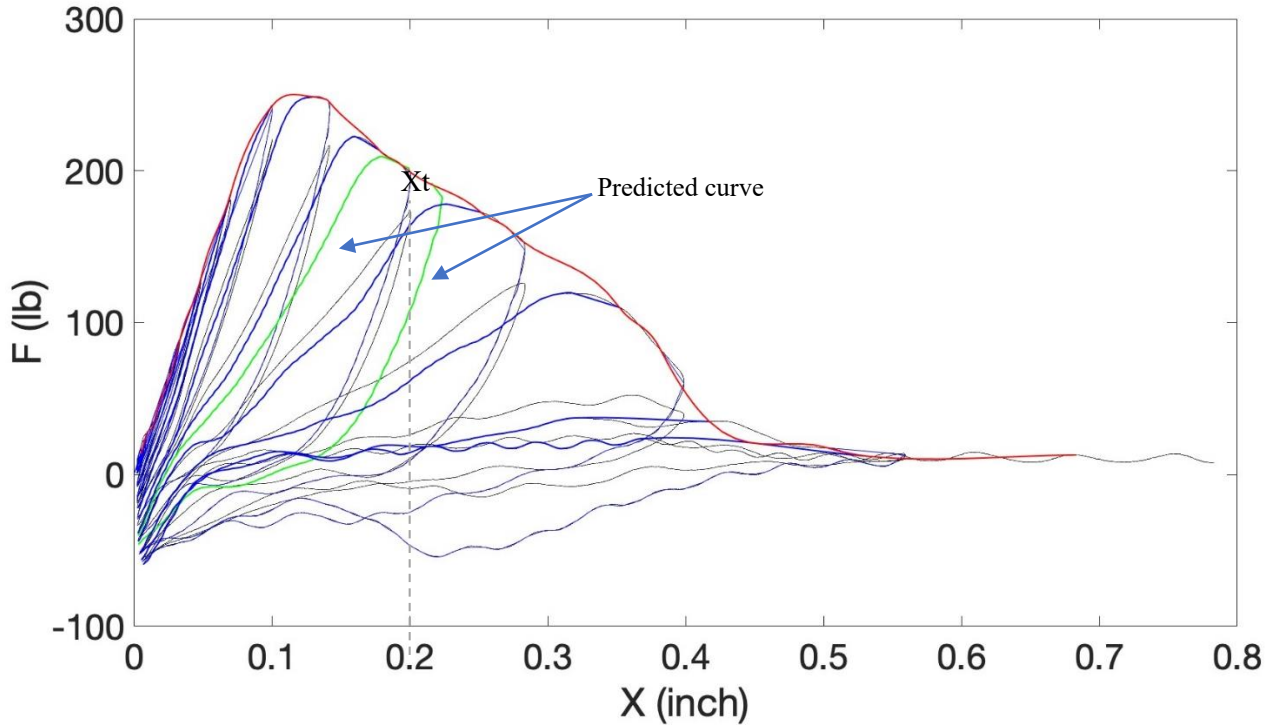

Figure 4: Curve for Target X

Figure 5 shows the extracted curves from experimental data for different connections. In the figure, the red curves are backbone curves, blue curves are the loading and unloading curves, and thin black curves are testing data. Figure 5 shows that the algorithm works well for different types of connection and different testing protocols, of which the extracted curves fit well with the experimental data.

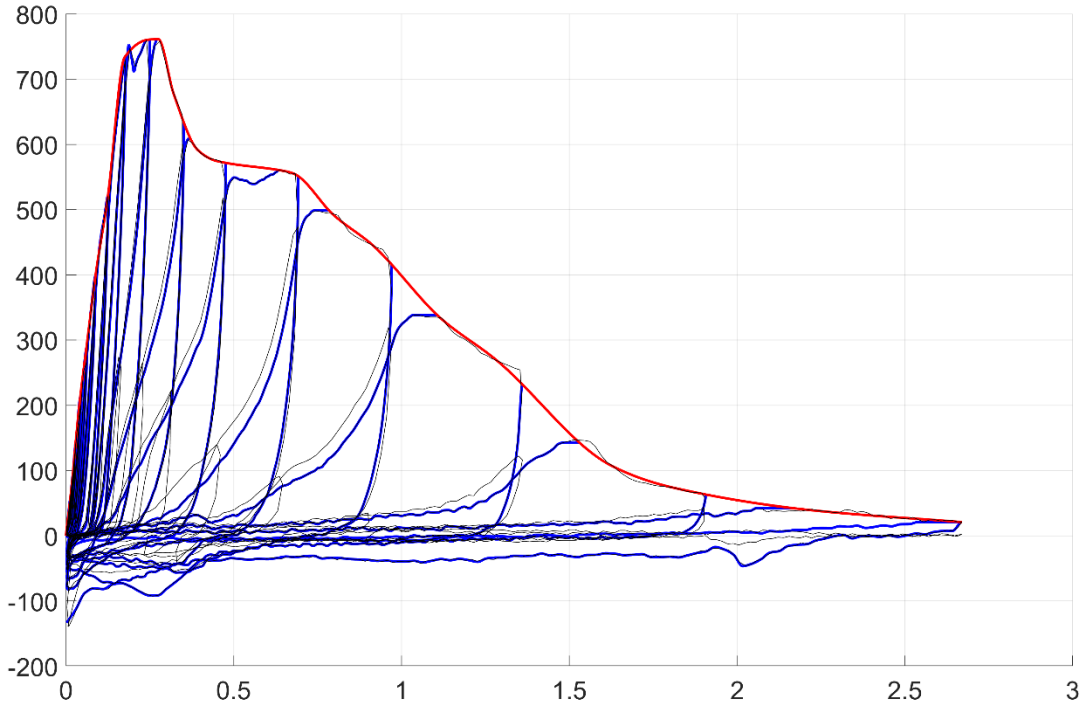

Figure 5a – Curves extracted for Wall-to-Floor connection.

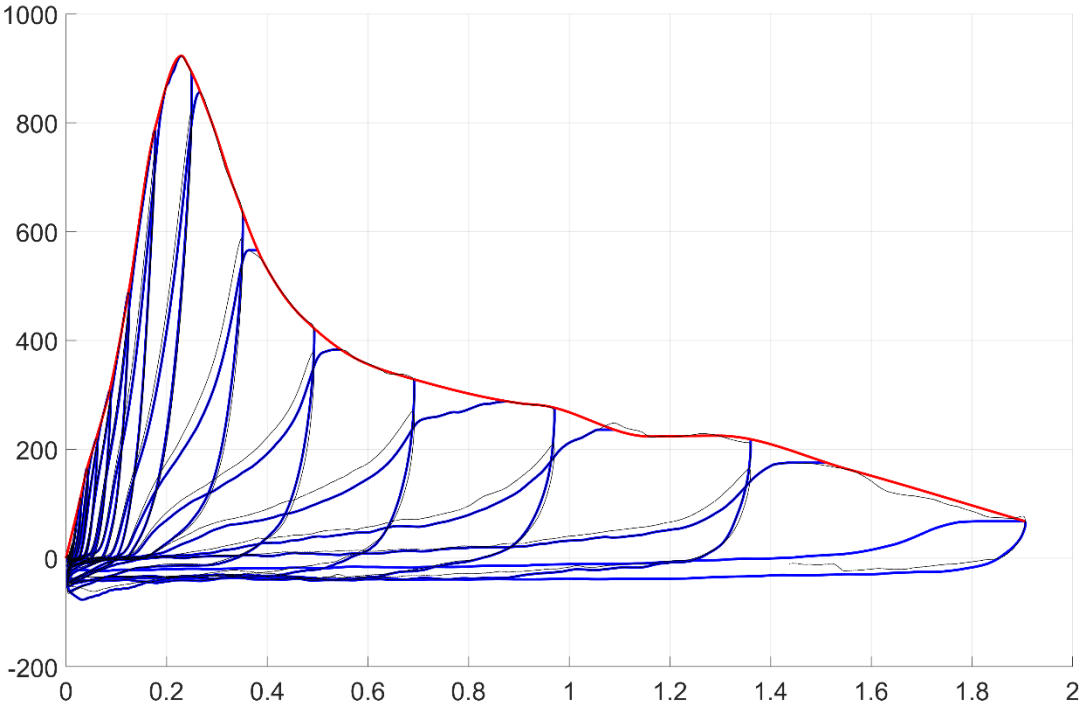

Figure 5b – Curves extracted for roof sheathing screw.

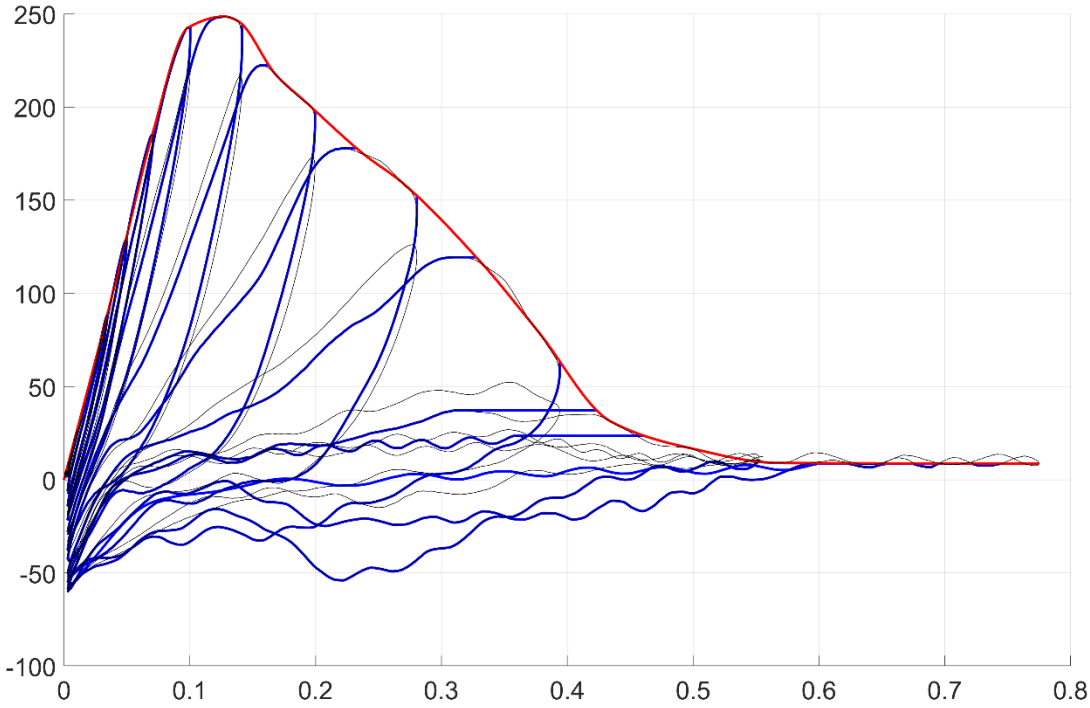

Figure 5c – Curves extracted for roof sheathing nail.

Analysis of Structure

Analysis commenced by drafting a detailed AutoCAD drawing of the model. After rigorous scrutiny, a final model was adopted (shown in Figure 5). The CAD drawing was exported to a DXF file and prepared for analysis, nodes, members, connections, material properties, etc. were all defined. Analysis was done using MATLAB program. At the time this report was created, the data for all connections and wind load measured from WOW experiments were not available, therefore the nonlinear analysis were not able to be completed. However, ongoing collaboration among the University of Alabama, Florida International University, and Kansas University keeps the work moving forward and further information and results will be included into next phase of reports.

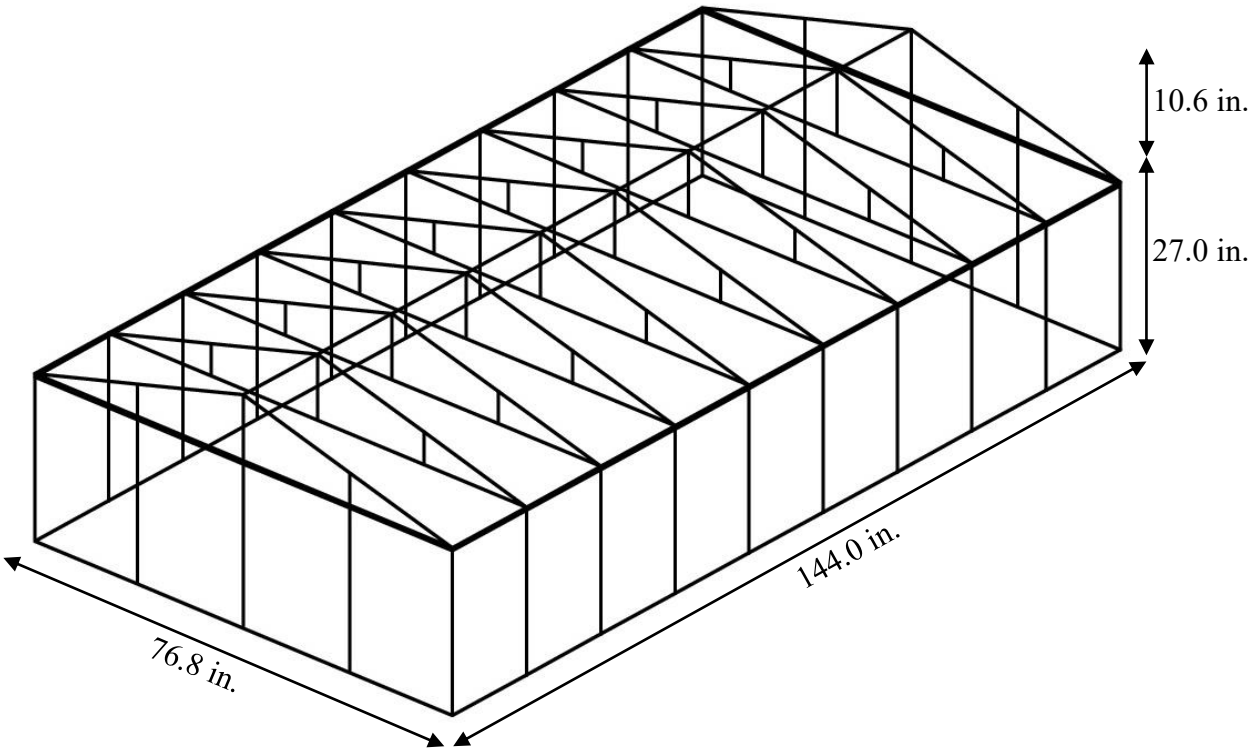

Figure 6: Structure Model

References

Aloisio, A., Alaggio, R., Köhler, J., & Fragiacomo, M. (2020). Extension of Generalized Bouc-Wen Hysteresis Modeling of Wood Joints and Structural Systems. *Journal of Engineering Mechanics*, *146*(3), 04020001.

Bai, Y.-L., Bai, S.-C., Mei, S.-J., Jia, J.-F., & Yang, K. (2023). Seismic behavior of RC square columns strengthened with LRS FRP under high axial load ratio. *Structures*, *56*, 104867. https://doi.org/10.1016/j.istruc.2023.07.057

Chacón, M., & Guindos, P. (2023). *Aspid: An Asymmetric Pinching Damaged Hysteresis Model for Timber Structures* (SSRN Scholarly Paper No. 4501163). https://doi.org/10.2139/ssrn.4501163

Dao, T. N., & van de Lindt, J. W. (2014). Numerical Seismic Performance of an Innovative CFS Midrise Building Designed Using DDD. *Journal of Performance of Constructed Facilities*, *28*(5), 04014018.

Foliente, G. C. (1995). Hysteresis Modeling of Wood Joints and Structural Systems. *Journal of Structural Engineering*, *121*(6), 1013–1022.

Folz, B., & Filiatrault, A. (2001). Cyclic Analysis of Wood Shear Walls. *Journal of Structural Engineering*, *127*(4), 433–441.

Furuta, T., & Nakao, M. (2023). *A Study on the Seismic Performance of Shear Walls under a Dynamic Load*.

Kasal, B., Leichti, R. J., & Itani, R. Y. (1994). Nonlinear Finite-Element Model of Complete Light-Frame Wood Structures. *Journal of Structural Engineering*, *120*(1), 100–119.

Swensen, S., Deierlein, G., Miranda, E., Fell, B., Acevedo, C., & Jampole, E. (2014). Finite element analysis of light-frame unibody residential structures. *NCEE 2014-10th US National Conference on Earthquake Engineering: Frontiers of Earthquake Engineering*.

Wu, Y.-J., Liu, C., Wang, L., Xie, Q.-F., & Zhang, L.-P. (2023). Seismic performance of stone supported traditional timber frames with or without cap beams. *Journal of Building Engineering*, *70*, 106395.

A Resource for the State of Florida

SECTION 3

Investigation and Incorporation of WOW testing outputs in the Florida Public Hurricane Loss Model

FINAL REPORT
(Period: 2022-2023)

A Research Project Funded by:
The State of Florida Department of Emergency Management

Investigators: Kurt Gurley, Ph.D.
Professor of Civil and Coastal Engineering
Engineering School for Sustainable Infrastructure and Environment
University of Florida
kgurl@ce.ufl.edu

Jean-Paul Pinelli, P.E., Ph.D.
Professor
Department of Civil Engineering
Florida Institute of Technology
pinelli@fit.edu

Graduate Students: *Christian Bedwell*
Zhuoxuan Wei

Executive Summary

An experimental study at the FIU WOW facility identified significant differences in roof overhanging sheathing when compared with ASCE 7 guidance. FIU published a paper (Mostafa et al. 2023) that included recommended changes to the roof overhand load coefficients. The Florida Public Hurricane Loss Model (FPHLM) explicitly accounts for overhanging sheathing wind loads, and thus offers an opportunity to investigate the influence of the FIU study on the outputs of a hurricane wind loss projection model. It was determined that, while the changes in loading resulted in larger mean losses to overhang roof sheathing over a range of strength models, the influence this had on overall building loss projections was negligible. However, since it reflects more accurately the actual wind-structure interaction than current ASCE 7 provisions, and given that it might be included in future ASCE provisions, formal inclusion of the WOW results in the FPHLM Unified Model, currently being validated, is warranted.

Overview & Motivation

In a recent experimental study, a series of WOW tests were performed by FIU faculty, students and staff to study the pressure profiles of roof overhangs varying in length and pitch. These tests culminated in a paper, "Codification of wind loads on hip roof overhangs of low-rise buildings" (Mostafa et. al, 2023), which specifically sought to evaluate the WOW data in light of ASCE 7 methods of calculating wind loads on roof overhangs and soffits. The paper investigated the assumption that the pressure acting on the wall adjacent to roof overhang is identical to the pressure acting on the soffit, the effect of overhang on corresponding pressure distributions, and the validity of ASCE 7-10, 7-16, and 7-22 roof overhang pressure coefficients.

One outcome of the FIU investigation is the validation of a methodology adopted by ASCE 7: that wind pressure acting on the top edge of walls can be appropriately assigned to adjacent soffits. Relative to the Florida Public Hurricane Loss Model (FPHLM) and the topic of this report, this methodology is also currently used in the FPHLM (as per ASCE 7 guidance), this therefore did not prompt a change in the FPHLM.

A second and more significant FIU finding is that ASCE 7 pressure coefficients for roof overhangs did not coincide with their experimental results. That is, the WOW experimental net pressure on the roof sheathing that covers the roof overhang did not align with ASCE 7 guidance. Figure 1 presents the current ASCE 7 values (left) and the FIU developed a new values (right) of roof overhang pressure coefficients. It is observed that the magnitudes of the FIU coefficients are larger than the current ASCE 7 values, resulting in larger wind uplift loads on overhang roof sheathing and potentially more vulnerability to damage. In the context of this current investigation, this led the FPHLM team to develop a version of their model which utilized the new experimental FIU roof overhang pressure coefficients and then analyze their effects on the vulnerability of the model.

While it is anticipated that loss of roof sheathing will increase under the new loading scheme, the influence this has on the overall losses ratios is unknown prior to a full simulation over the range of structural models in the FPHLM. This comparison study was conducted for the base weak, medium and strong models, representing the full range of older poor-quality construction to modern housing built to current standards.

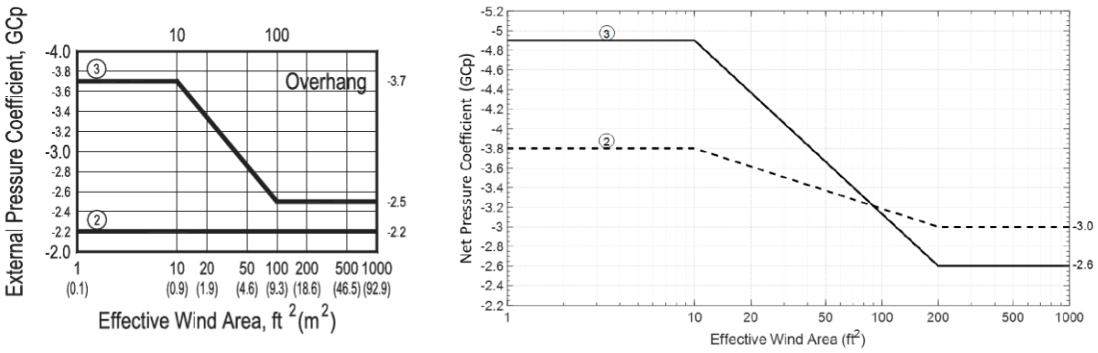

Figure 1. Net pressure coefficient charts for hip roof overhangs according to ASCE 7-10 (left), Mostafa et. al. (right).

FPHLM study

A beta-version of the FPHLM vulnerability model was developed using the pressure coefficients developed in response to the WOW tests (Figure 1 – right). To replicate the structure used in the WOW test, a single-story, timber-frame, hip-roof model building was modeled. Table 1 lists the pressure coefficients used for Zones 2 & 3 using ASCE 7-10, and using the pressure coefficients developed by Mostafa et. al (using an effective wind area of 32 ft^2 for a 4x8 ft sheathing panel). The coefficients are a direct multiplier in the equation that determines the force being applied to the building component. Thus, for zone 3, the change from -3.09 to 4.01 represents an increase in loading by a factor of 4.01/3.09. While this significant increase of ~33% in loading should increase overhang sheathing damage, the portion of the roof that constitutes Zone 3 on the overhand is small, particularly considering that the wind directionality approach in the model only applies Zones 2 and 3 to the windward portions of the roof, while other portions are considered Zone 1.

Table 1. Roof Overhang Pressure Coefficients

Overhang Zone	ASCE 7-10	Mostafa et. al.
Zone 2	-2.20	-3.49
Zone 3	-3.09	-4.01

To analyze the influence of these differing coefficients over a variety of model strengths, tests were performed using the base weak, medium, and strong models. Changing these models affects the capacity of various structural components. Most relevant to this study are the changes in uplift capacity for roof sheathing and roof cover (Table 2).

Table 2. Roof Component Capacities of FPHLM Models

Component	Weak Model	Medium Model	Strong Model
Roof Sheathing (psf)	55	80	130
Roof Cover (psf)	51	51	70

The Weak, Medium, and Strong models were run through the FPHLM Unified Model using the ASCE 7-10 & WOW roof overhang pressure coefficients separately to allow a side-by-side comparison. The mean damage to roof overhang sheathing as function of 3-second gust wind speed was plotted directly (Figure 2), and averaged over all 8 wind directions the simulations are conducted for. The results demonstrate that the increase in roof pressure coefficients results in a maximum of 2% change to overhand sheathing damage. The next phase of the work is to investigate the influence this change has on the overall building loss ratios for building damage and content losses.

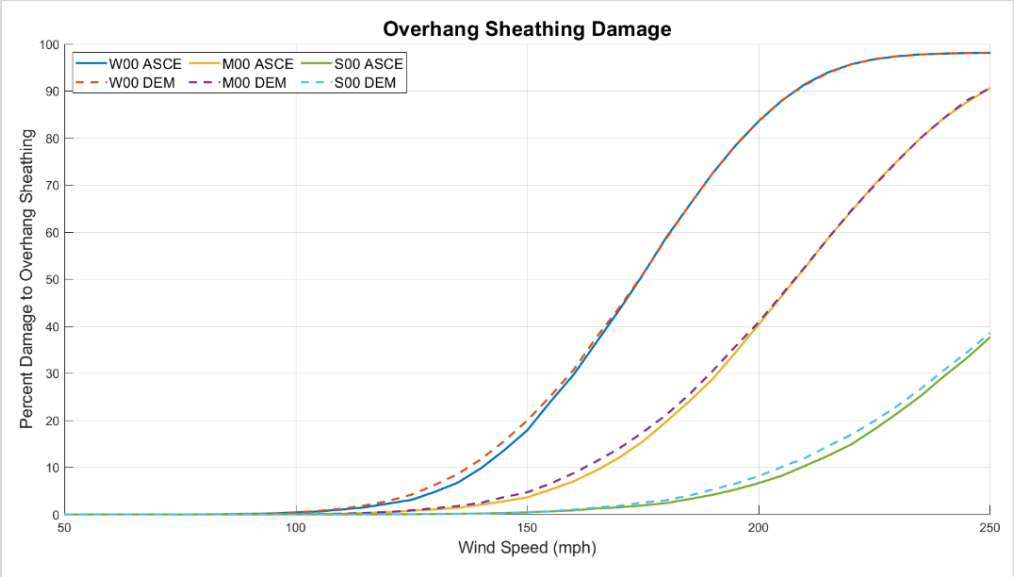

Figure 2. Roof overhang sheathing damage curves for weak, medium, strong models under ASCE 7-10 & DEM (Mostafa et al.) roof overhang pressure coefficients.

The vulnerability curves that are outputs from the FPHLM vulnerability module represent financial losses due to building repair as a function 3-second gust wind speed. The financial losses are quantified as a Damage Ratio (DR), which is the cost of repair in ratio with the value of the building. These DR vs wind speed plots are determined for the physical building damage and the building content damage (mostly damage from water ingress) separately, although content loss is certainly correlated with physical building damage. For example, more broken windows equal more water ingress and content damage.

Comparative vulnerability curves for building damage and content damage were produced in Figures 3 & 4, respectively. Following Figure 2, weak, medium and strong results are presented for both the current sheathing overhang loading scheme and the scheme suggested by Mostafa et al. (FIU WOW study, Figure 1). These demonstrate that the increase in pressure coefficients on roof overhang sheathing have negligible impact on the overall vulnerability of the model.

Analysis: In the model used, the roof overhang accounts for 16% of the roof area, and while the increase in pressure coefficients is significant (58% increase for Zone 2, 33% increase for Zone 3), the effected area and its contribution to building damage is small enough that it does not meaningfully modify the vulnerability of the building. The influence of the Zone 2 and Zone 3 coefficient updates is further reduced by the scheme used to account for wind direction approach. Figure 5 illustrates that, for any given approach wind direction, the portion of the overhang roof that is actually in Zones 2 or 3 is significantly less than the 16% overhang portion of the entire roof. In fact, the portion of the roof affected by the Zone 2 & 3 changes is less than 8% for any given direction.

It is concluded that the influence of the FIU WOW study on overhang roof sheathing does not alter the FPHLM outputs significantly. However, since it reflects more accurately the actual wind-structure interaction than current ASCE 7 provisions, and given that it might be included in future ASCE provisions, formal inclusion of the WOW results in the FPHLM Unified Model, currently being validated, is warranted.

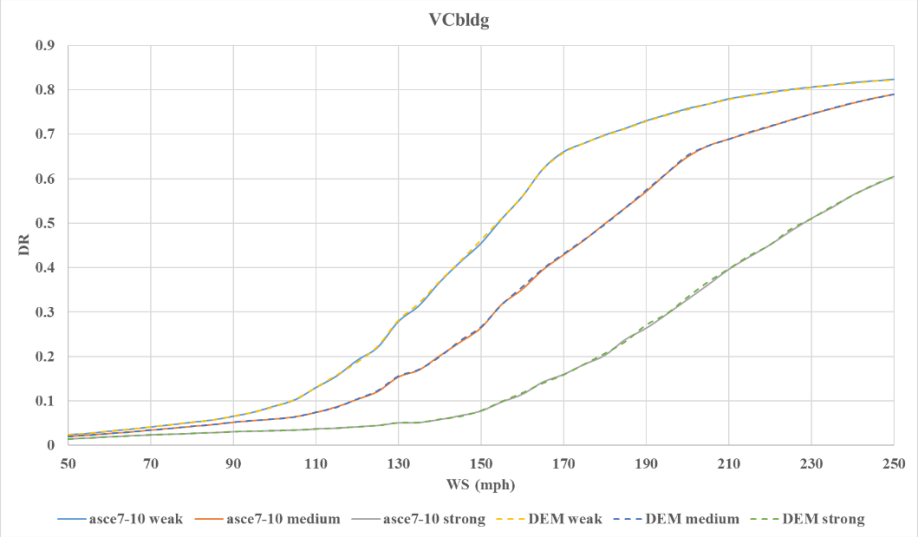

Figure 3. Building damage vulnerability curves for weak, medium, strong models under ASCE 7-10 & DEM (Mostafa et al.) roof overhang pressure coefficients.

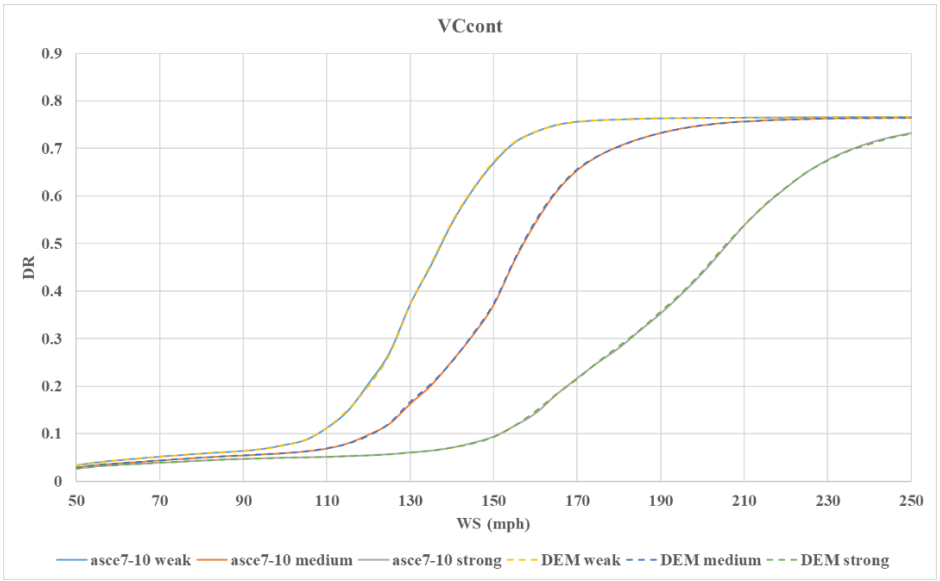

Figure 4. Content damage vulnerability curves for weak, medium, strong models under ASCE 7-10 & DEM (Mostafa et al.) roof overhang pressure coefficients

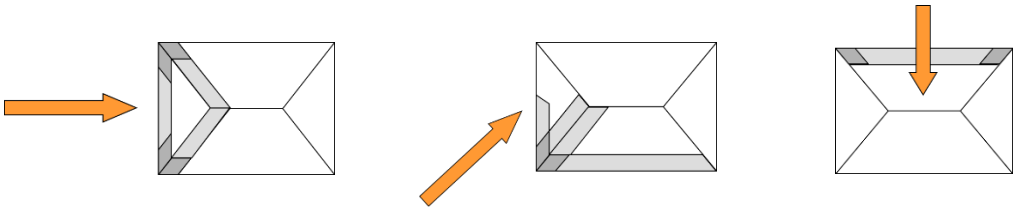

Figure 5. Directionalized roof pressure coefficients: White – Zone 1, Light Gray – Zone 2, Dark Gray – Zone 3.

References

Aly, A. M., Chowdhury, A. G., & Bitsuamlak, G. (2011). Wind profile management and blockage assessment for a new 12-fan Wall of Wind facility at FIU. *Wind & Structures*, 14(4), 285-300.

Baheru, T., Chowdhury, A. G., Bitsuamlak, G., Masters, F. J., & Tokay, A. (2014, a). Simulation of wind-driven rain associated with tropical storms and hurricanes using the 12-fan Wall of Wind. *Building and Environment*, 76, 18-29.

Baheru, T., Chowdhury, A. G., Pinelli, J. P., & Bitsuamlak, G. (2014, b). Distribution of wind-driven rain deposition on low-rise buildings: Direct impinging raindrops versus surface runoff. *Journal of Wind Engineering and Industrial Aerodynamics*, 133, 27-38.

Baheru, T., Chowdhury, A. G., & Pinelli, J. P. (2015). Estimation of wind-driven rain intrusion through building envelope defects and breaches during tropical cyclones. *Natural Hazards Review*, 16(2), 04014023.

Chowdhury, A. G., Bitsuamlak, G. T., Fu, T. C., & Kawade, P. (2011). Study on roof vents subjected to simulated hurricane effects. *Natural Hazards Review*, 12(4), 158-165.

Gan Chowdhury, A., Zisis, I., Irwin, P., Bitsuamlak, G., Pinelli, J. P., Hajra, B., & Moravej, M. (2017). Large-scale experimentation using the 12-fan wall of wind to assess and mitigate hurricane wind and rain impacts on buildings and infrastructure systems. *Journal of Structural Engineering*, 143(7), 04017053.

Eamon, C. D., Fitzpatrick, P., & Truax, D. D. (2007). Observations of structural damage caused by Hurricane Katrina on the Mississippi Gulf Coast. *Journal of Performance of Constructed Facilities*, 21(2), 117-127.

Johnson, T., Pinelli, J. P., Baheru, T., Chowdhury, A. G., Weekes, J., & Gurley, K. (2018). Simulation of rain pene-tration and associated damage in buildings within a hurricane vulnerability model. *Natural Hazards Review*, 19(2), 04018004.

Kennedy, A., Copp, A., Florence, M., Gradel, A., Gurley, K., Janssen, M., ... & Silver, Z. (2020). Hurricane michael in the area of mexico beach, florida. *Journal of Waterway, Port, Coastal, and Ocean Engineering*, 146(5).

Mileti, D. (1999). *Disasters by design: A reassessment of natural hazards in the United States*. Joseph Henry Press.

Mostafa, K., Zisis, I., & Stathopoulos, T. (2023). Codification of wind loads on hip roof overhangs of low-rise buildings. *Engineering Structures*, 288.

Mullens, M., Hoekstra, B., Nahmens, I., & Martinez, F. (2006). Water intrusion in central Florida homes during Hurricane Jeanne in September 2004. *UCF Housing Constructability Lab*, Orlando.

Pinelli, J. P., Roueche, D., Kijewski-Correa, T., Plaz, F., Prevatt, D., Zisis, I., Elawady, A., Haan, F. Pei, S., Gurley, K. & Rasouli, A. (2018). Overview of damage observed in regional construction during the passage of Hurricane Irma over the state of Florida. *Proc., ASCE Forensic*, 18.

Pita, G., Pinelli, J. P., Cocke, S., Gurley, K., Mitrani-Reiser, J., Weekes, J., & Hamid, S. (2012). Assessment of hurricane-induced internal damage to low-rise buildings in the Florida Public Hurricane Loss Model. *Journal of wind engineering and industrial aerodynamics*, 104, 76-87.

Pita, G. L. (2012). Hurricane vulnerability of commercial-residential buildings (Vol. 73, No. 289, p. 2012).

Pita, G. L., Pinelli, J. P., Gurley, K., Weekes, J., Cocke, S., & Hamid, S. (2016). Hurricane vulnerability model for mid/high-rise residential buildings. *Wind and Structures*, 23(5), 449-464.

Raji, F. (2018). Interior damage of residential building due to wind-driven rain intrusion.
Raji, F., Zisis, I., & Pinelli, J. P. (2019, September). Intrusion and propagation of hurricane induced rain water in building interior. *In Proc., 15th Int. Conf. on Wind Engineering. Kanagawa, Japan: International Association for Wind Engineering*.
Raji, F., Zisis, I., & Pinelli, J. P. (2020). Forthcoming "A wind tunnel study to quantify the wind-driven rain propagation in the interior of residential structures,". *ASCE Journal of Structural Engineering*, 146(7).
USGS. (2019) Rainfall calculator, metric units How much water falls during a storm?. https://water.usgs.gov/edu/activity-howmuchrain-metric.html#:~:text=Slight%20rain%3A%20Less%20than%200.5,than%208%20mm%20per%20hour : retrieved 07/25/2022

A Resource for the State of Florida

SECTION 4

Education and Outreach Programs to Convey the Benefits of Various Hurricane Loss Mitigation Devices and Techniques

A Report Submitted to:
The State of Florida Division of Emergency Management

Prepared By:
Erik Salna

The International Hurricane Research Center (IHRC)
Florida International University

July 31, 2023

Executive Summary:

The FIU International Hurricane Research Center developed and coordinated education and outreach activities to build on the foundation of previous work under this grant and showcased the hurricane-loss mitigation objectives of the RCMP.

For the 2022-2023 performance period, the below mentioned educational partnerships, community events, and outreach programs were developed:

Executive Summary:

Wall of Wind Mitigation Challenge (WOW! Challenge): Wednesday, March 15th, 2023
The International Hurricane Research Center (IHRC), located on the campus of Florida International University (FIU), has developed the Wall of Wind Mitigation Challenge (WOW! Challenge), a judged competition for South Florida high school students. As the next generation of engineers to address natural hazards and extreme weather, this STEM education event features a competition between high school teams to develop innovative wind mitigation concepts and real-life human safety and property protection solutions. The mitigation concepts are tested live at the FIU NSF-NHERI Wall of Wind (WOW) Experimental Facility (EF), located on FIU's Engineering Campus.

- The objective for the 2023 Wall of Wind (WOW) Mitigation Challenge was to reduce the wind-induced uplift force on a building's roof, by optimizing its overall shape. Solutions demonstrated a sound comprehension of aerodynamic principles.
- The high school teams prepared three components for the competition: a physical test, an oral presentation, and a written technical paper.
- The competition involved teams from eight South Florida high schools, including about 100 students and eight teachers.
- *First Place* was awarded to TERRA Environmental Research Institute.
  Second Place was awarded to Booker T. Washington Senior High School.
  Third Place was awarded to G. Holmes Braddock Senior High School.
- A complete scoring summary can be found on the following link: https://www.ihrc.fiu.edu/wp-content/uploads/2023/04/2023_WOW_CHALLENGE_RESULTS_SUMMARY.pdf

Media exposure resulted in great positive visibility for the IHRC, FIU and FDEM's message of mitigation:

- FOX Weather Network: https://www.youtube.com/watch?v=cXKl1cgiBp0
- WOW Challenge Highlights Video: https://youtu.be/W2pInso5IXk
- FIU News: https://news.fiu.edu/2023/wall-of-wind-challenge-is-launching-pad-for-high-school-students

Eye of the Storm (Science, Mitigation & Preparedness) In-Person Event: May 20th, 2023
The Museum of Discovery & Science (MODS), located in Fort Lauderdale, FL, assisted the IHRC in planning, coordinating, and facilitating this free admission public education event that showcased special hands-on, interactive activities and demonstrations teaching hurricane science, mitigation and preparedness. There was also the opportunity for visitors to support recovery efforts for the April flooding event in Fort Lauderdale through volunteering or monetary donations.

- A record 4,900 visitors attended Eye of the Storm, showcasing special interactive activities and demonstrations teaching hurricane science, mitigation and preparedness.
- A Participant Post Survey showed 80.2% of respondents increased their knowledge about wind engineering and mitigating hurricane damage and 81.4% will be taking steps to mitigate hurricane damage.
- Media Release and Flyer: 2023 Eye of the Storm – Hurricane (Science, Mitigation & Preparedness) Free Museum Event, Saturday, May 20th, 10am to 5pm | IHRC Website (fiu.edu)

Special Guest:

- Grant Goodwin, HLMP Program Manager, Florida Division of Emergency Management

Media exposure resulted in great positive visibility in the community for the IHRC, FIU and FDEM's message of mitigation.

- Museum of Discovery and Science 'Eye of the Storm' Event – NBC 6 South Florida (nbcmiami.com)

NOAA Hurricane Awareness Tour: IHRC did not participate because the stop in Marathon, Florida was cancelled due to aircraft mechanical problems.

Get Ready, America! The National Hurricane Survival Initiative: Cancelled due to lack of sponsorships.

Education and Outreach Programs:

Wall of Wind Mitigation Challenge (WOW! Challenge): Wednesday, March 15th, 2023

Overview of Wall of Wind Mitigation Challenge:
The International Hurricane Research Center (IHRC), located on the campus of Florida International University (FIU), has developed the Wall of Wind Mitigation Challenge (WOW! Challenge), a judged competition for South Florida high school students. As the next generation of engineers to address natural hazards and extreme weather, this STEM education event features a competition between high school teams to develop innovative wind mitigation concepts and real-life human safety and property protection solutions. The student teams prepare three components for the competition: a physical test, an oral presentation, and a written technical paper. The mitigation concepts are tested live at the FIU NSF-NHERI Wall of Wind (WOW) Experimental Facility (EF), located on FIU's Engineering Campus.

The WOW! Challenge requires problem solving, teamwork, and creativity, and it includes aspects of science, technology, engineering, mathematics, architectural design, and business entrepreneurship. The high school students are inspired to pursue STEM education and careers in wind engineering and hurricane mitigation. The competition has real world applications and benefits society by developing hurricane mitigation techniques that can lead to enhanced human safety, property loss reduction, insurance cost reduction, and a culture of hurricane preparedness. There is no other competition like it in the entire country, and it's a once in a lifetime opportunity for the high school students – *an experience they never forget*.

"The WOW! Challenge is a platform to educate high school students in our community with regards to hurricane engineering and community resilience. Student teams are given real-world wind engineering problems and they conceive and validate wind mitigation concepts to solve such problems. The WOW! Challenge informs students about the importance of mitigation and community resilience to prepare them as future leaders in disaster mitigation. We see these young students become motivated toward STEM careers and possibly enrolling at FIU with the dream of performing research at our national NSF-NHERI Wall of Wind Experimental Facility." Arindam Gan Chowdhury, professor of civil and environmental engineering and director of the NHERI Wall of Wind Experimental Facility.

2023 Wall of Wind Mitigation Challenge:

The objective for the 2023 Wall of Wind (WOW) Mitigation Challenge was to reduce the wind-induced uplift force on a building's roof, by optimizing its overall shape. (A schematic diagram of this interaction is shown in Figure 1 below.) Solutions will demonstrate a sound comprehension of aerodynamic principles. Teams were tasked with developing a roofing solution to improve the aerodynamic performance of the roof, with the goal of reducing the roof-to-wall forces and moments on a scaled-down model of the roof concept. The roof models were tested by the NSF-NHERI Wall of Wind at FIU to evaluate the effectiveness of the mitigation solution.

Teams from eight South Florida high schools participated in the competition involving about 100 students and eight teachers. They were from Booker T. Washington Senior High School, Florida Christian School, G. Holmes Braddock Senior High School, Jose Marti MAST Academy, J. P. Taravella High School, North Miami Senior High School, St. Brendan High School, and TERRA Environmental Research Institute.

Student teams prepared three components for the competition: a written technical paper, an oral presentation, and a physical test of their roof model. All the details of the rules and guidelines for the three required components are on the WOW Mitigation Challenge web page located at: http://www.ihrc.fiu.edu/outreach-education/wall-of-wind-challenge/.

Written technical papers and oral presentations had to include the following:

- Effectively communicate some scientific process or analysis and include any scientific or mathematical analysis involved with the development of their hurricane wind mitigation solution for their roof model.
- What is hurricane wind mitigation?
- What is the importance of hurricane wind mitigation?

- How is hurricane wind mitigation being addressed with your roof model?
- In addition to wind engineering, other disciplines could be included, such as architecture, business, economics, finance, marketing, geosciences, insurance, political science, sociology, and urban planning.
- Details for the written technical paper guidelines can be found at: https://www.ihrc.fiu.edu/wp-content/uploads/2023/02/2023_WOW_CHALLENGE_GUIDELINES_TECHNICAL_PAPER.pdf

The Oral Presentation Description:

- Oral presentations were done live at FIU to a panel of judges who then computed a score for the Team.
- Oral presentations could not exceed 7 minutes and were strictly enforced.
- Judges had some follow-up questions for each high school team after their oral presentation.
- Details for the oral presentation guidelines can be found at: https://www.ihrc.fiu.edu/wp-content/uploads/2023/02/2023_WOW_CHALLENGE_GUIDELINES_ORAL.pdf

The Physical Test Description:

- Each high school team designed and constructed a model of their roof design (physical guidelines described below) and had it tested by the NSF-NHERI Wall of Wind.
- The goal was to construct a roof model that would remain in place on a base structure to the highest possible wind speed, without permanently lifting.
- The roof models were tested at two wind directions, determined by the judges, between +/- 90 deg. (Refer to Figure 4 below for example wind directions.)
- The wind speed for each of the two directions were gradually increased until the roof model permanently lifted up. The higher the wind speed at which that happened resulted in a higher score for the team.
- The scoring for the wind testing was calculated as follows: Permanent lift-off wind speeds were recorded for each team's roof model at the two wind directions. The team's score was the mean of the two recorded wind speeds.
- Details for the physical test guidelines can be found at: https://www.ihrc.fiu.edu/wp-content/uploads/2023/02/2023_WOW_CHALLENGE_GIUDELINES_PHYSICAL_02-13-2023.pdf

There was a cumulative and weighted scoring point scale for the written technical paper (25%), oral presentation (25%), and physical test of the roof model (50%) to determine the top three winning teams:

- *First Place* was awarded to TERRA Environmental Research Institute.
- *Second Place* was awarded to Booker T. Washington Senior High School.
- *Third Place* was awarded to G. Holmes Braddock Senior High School.

A complete scoring summary can be found on the following link: https://www.ihrc.fiu.edu/wp-content/uploads/2023/04/2023_WOW_CHALLENGE_RESULTS_SUMMARY.pdf

All three required components of the competition were judged and scored by a combination of IHRC NSF-NHERI Wall of Wind faculty, Florida Division of Emergency Management, FIU wind engineering alumni, local emergency management, community educators, partners, and media:

- Grant Goodwin, HLMP Program Manager, Bureau of Mitigation, Florida Division of Emergency Management
- Steven W. Diaz, PhD, PE, Program Director/Site Operations Manager, NSF-NHERI Wall of Wind Experimental Facility, International Hurricane Research Center, Extreme Events Institute, Florida International University
- Manuel A. Matus M.Sc., Research Specialist, NSF-NHERI Wall of Wind Experimental Facility, International Hurricane Research Center, Extreme Events Institute, Florida International University
- Dejiang Chen, Ph.D., Research Specialist, NSF-NHERI Wall of Wind Experimental Facility, International Hurricane Research Center, Extreme Events Institute, Florida International University
- Melody Gonzalez (FIU Alum), E.I., Project Engineer - Operations, Civil Department, Black & Veatch
- Luis A. Silva (FIU Alum), PE, Principal, Aluces Corporation
- Johnny Estephan (FIU Alum), Ph.D., E.I., Engineer, Bliss & Nyitray, Inc.
- Ziad Azzi (FIU Alum), PhD, PE, Principal Forensic Engineer, DDA Forensics
- Adrian Robaina (FIU Alum), PE, Principal, Project Manager, CONNECT Engineering
- Carlos de la Camara, Director, Science Curriculum Support Specialist, HS, Department of Mathematics and Science, Miami-Dade County Public Schools
- JP Keener, Science Department, Broward County Schools
- Robin Yang, MA, FPEM, EM Planner, Miami-Dade County, Department of Emergency Management
- Hidsa Carozzo, Planning Intern, Department of Emergency Management, Division of Operations and Safety, Florida International University
- Brandy Campbell, Multimedia Journalist - Miami Based, FOX Weather National Network

Wall of Wind Mitigation Challenge media exposure resulted in great positive visibility for the IHRC, FIU and FDEM's message of mitigation:

- FOX Weather Network: https://www.youtube.com/watch?v=cXKl1cgiBp0
- WOW Challenge Highlights Video: https://youtu.be/W2pInso5IXk
- FIU News: https://news.fiu.edu/2023/wall-of-wind-challenge-is-launching-pad-for-high-school-students

Evaluation and Assessment:

- All teachers gave an overall rating of *Good to Excellent* for the competition experience.
- Teachers rated all aspects of the Wall of Wind Mitigation Challenge – materials, communication, educational value - from *Good to Excellent.*
- Teachers said that the Wall of Wind Mitigation Challenge contributed to an increase in knowledge of wind engineering.

- Students expressed considerable interest in studying wind engineering at the college level.

The Wall of Wind Mitigation Challenge received positive feedback from the teachers, students, judges, and alumni:

- *"The STEAM holisticness of the FIU WOW challenge makes it an excellent STEAM integration activity, easy to adapt into existing FDOE science and engineering curriculum. WOW helped me foster meaningful hands-on, project base learning, that allowed my students to engage in realistic learning, and the importance of hurricane and natural hazard preparedness. Hence, I strongly advocate that we keep FIU WOW challenge going strong years to come."* Mr. Bidokwu D.O, Chemistry, Physics and Engineering Teacher, Booker T. Washington Senior High School
- *"The sponsors [of] this program are building a stronger bridge for future scientists and engineers, especially for us minority students that would likely not have had this opportunity and experience anywhere else. For this unique chance alone, we cannot thank you enough. Please continue to inspire those down the path of STEM, as your support has inspired me to pursue a STEM career after high school*." Jeremiah Duarte, a senior at Booker T. Washington Senior High School
- *"I have competed with my students in the challenge for the last three years, and every year I can see the exceptional change in their problem-solving skills [and] in their wind engineering interest and knowledge as well," she said. "As a teacher, we are constantly looking for real life scenarios [and] challenges to push our students to think critically and problem solve. I am proud to be an FIU alumna and am so grateful that we have great community partners like FIU to be able to have our students compete in events such as the Wall of Wind challenge."* Lacey Simpson, Science Department, G. Holmes Braddock Senior High School
- *"I really enjoyed the challenge," said "It helped us learn the basics of mechanical engineering and what the process for designing and creating a reliable structure is like."* Luke Penafiel, a junior at TERRA Environmental Research Institute
- *"Learning the intricacies of writing a technical report based on the research and experiments done on prototypes was very interesting," he said. "These skills will definitely be useful later on as an engineer."* Liam Huang, a junior at TERRA Environmental Research Institute.
- *"I was transported to the future. The students from Miami Dade County Public Schools were like executives and engineers. What a truly impressive experience. The Wall of Wind Challenge created an opportunity for students to compete while finding solutions that will directly impact their community. Our future in South Florida is bright indeed."* Carlos de la Camara, Director, Science Curriculum Support Specialist, HS, Department of Mathematics and Science, Miami-Dade County Public Schools
- *"Great to be back at Florida International University - College of Engineering & Computing as a judge for the WOW Challenge. The WOW has a special place in my heart as it was my first professional experience, and by managing the Engineers on Wheels program, I developed a profound understanding of the importance of K-12 outreach to fuel the next generation of STEM professionals."* Melody Gonzalez, E.I., Project Engineer - Operations, Civil Department, Black & Veatch

The Wall of Wind Mitigation Challenge also received sponsor support for awards, trophies, lunch, event video, and additional materials and supplies for each high school team. The sponsor support came from the FIU alumni serving as judges and their companies: DDA Forensics, Bliss & Nyitray, Inc., CONNECT Engineering, Black & Veatch and The Biltmore School.

Roof model requirements and restrictions described for the student teams:

- The roof model will be constructed on a 36 x 24 x 3.5 in (L x W x H) base frame, which will be supplied to each team by FIU (see Figure 2).
- The roof model shall NOT interfere with the lower 2.0 inches along the outer perimeter of the provided base frame. This region is needed for attachment of the roof to the base structure (see Figure 3). Pivot hinges will be affixed to either of the 36-inch sides, at the discretion of the Wall of Wind team.
- The entire roof structure, including the base frame, shall not exceed 11.5 inches in height (i.e., the roof may extend a maximum of 8.0 inches above the TOP of the provided base frame).
- The weight of the roof model must be no less than 35 lbs., and no greater than 45 lbs., including the provided base frame. The submitted roof's center of gravity must be directly above the center of the 24-inch and 36-inch base dimensions (+/- 1.0 inches). See Figure 2.
- Above the lowest 2.0 inches of the provided base, any roof shape may be used as long as it always has a minimum solid width of 24 inches and 36 inches when viewed from respective directions (see Figure 3).
- The roof can be any shape but must be designed as if to prevent water from entering the base structure. Cladding and/or mitigation elements can be attached to the roof structure.
- The roof must include an overhang of at least 1 inch, and not exceeding 3 inches on all sides (see Figure 3).
- All roof models will be tested at two wind directions between +/- 90 deg. Refer to Figure 4 for example wind directions.
- Details for the physical guidelines for the roof model can be found at: https://www.ihrc.fiu.edu/wp-content/uploads/2023/02/2023_WOW_CHALLENGE_GIUDELINES_PHYSICAL_02-13-2023.pdf

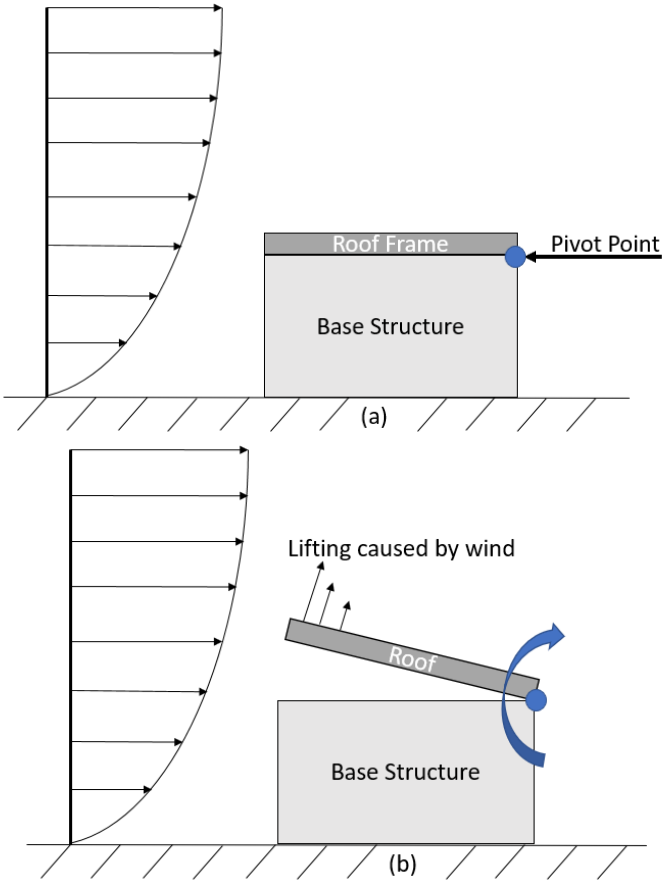

Figure 1: Simplified two-dimensional schematic diagram of wind acting on roof model: (a) view before permanent liftoff and (b) view after permanent liftoff.

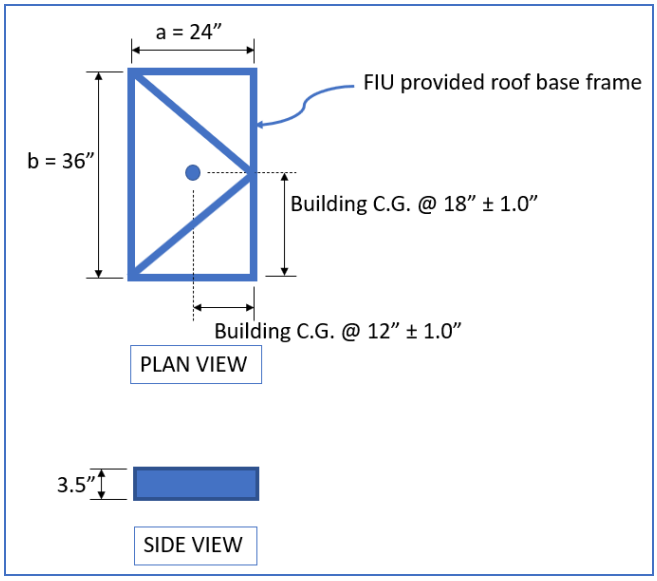

Figure 2: Roof base frame provided to each school and center of gravity requirements.

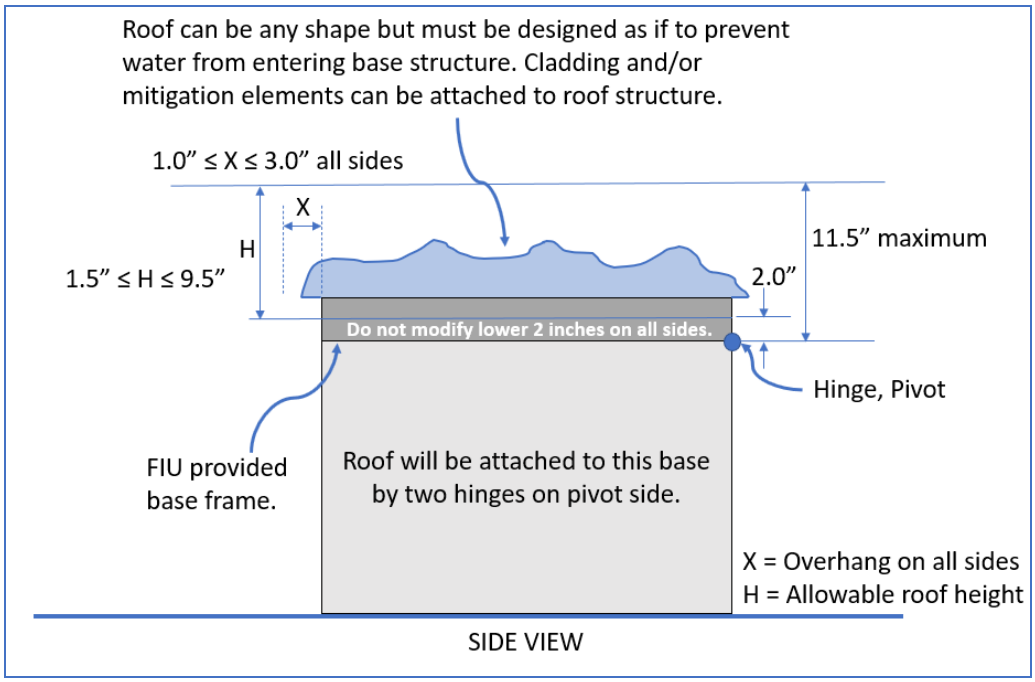

Figure 3: Schematic drawing showing build parameters.

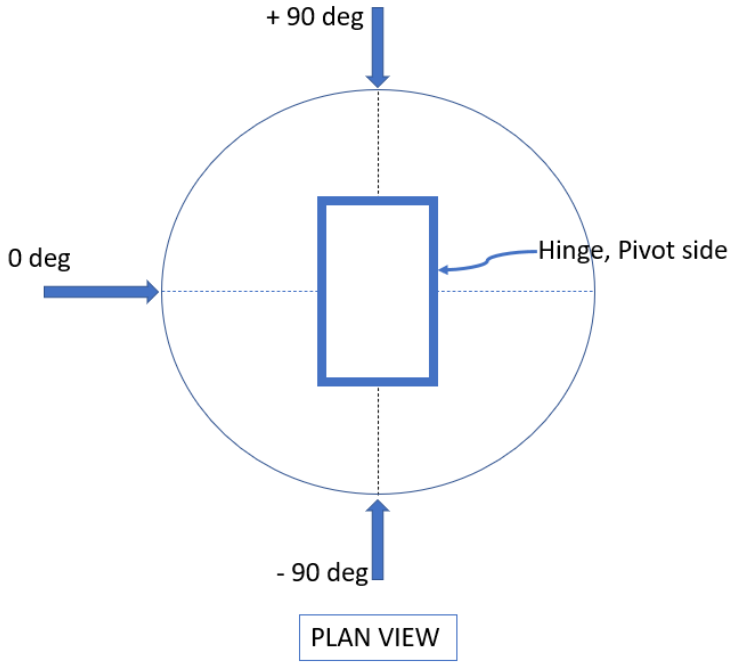

Figure 4: Wind Direction naming convention. The roof models will be tested at two wind directions between +/- 90 deg.

Engineering Dean Volakis speaks to teams.

FOX Weather interviews TERRA E.R.I.

G. Holmes Braddock H. S. oral presentation.

North Miami H. S. watching live wind test.

Jose Marti MAST 6-12 Academy roof.

J. P. Taravella H. S. team and roof.

St. Brendan H. S. team and roof.

North Miami H. S. team and roof.

1st Place Team: TERRA Env. Res. Inst.

2nd Place Team: Booker T. Washington H.S.

3rd Place Team: G. Holmes Braddock H.S

Judges for oral presentations.

Eye of the Storm (Science, Mitigation & Preparedness) Event: May 20th, 2023

Overview:
The Museum of Discovery & Science (MODS), located in Fort Lauderdale, FL, assisted the IHRC in planning, coordinating and facilitating this free admission public education event. A record 4,900 visitors attended Eye of the Storm, showcasing special interactive activities and demonstrations teaching hurricane science, mitigation and preparedness. This included special learning activities for parents and children providing family fun throughout the day. There was also the opportunity for visitors to support recovery efforts for the April flooding event in Fort Lauderdale through volunteering or monetary donations.

- Media Release and Flyer: 2023 Eye of the Storm – Hurricane (Science, Mitigation & Preparedness) Free Museum Event, Saturday, May 20th, 10am to 5pm | IHRC Website (fiu.edu)

Key Messages Communicated to the Public:
1. Know Your Risk
2. Know Your Evacuation Zone
3. Complete Your Hurricane Plan
4. Address Any Special Needs
5. Assemble Your Supply Kit
6. Prepare Your Pets
7. Get an Insurance Check-Up
8. Protect Your Home
9. Help Your Neighbor

This collaborative community education outreach project partnered the IHRC and MODS with:

- Florida Division of Emergency Management
- Broward County Emergency Management
- Broward County CERT
- Broward County Office of Resilience
- City of Fort Lauderdale Emergency Management
- City of Fort Lauderdale Fire Rescue and Fire Explorers
- City of Fort Lauderdale Police Department
- NOAA National Hurricane Center
- NOAA Atlantic Oceanographic and Meteorological Laboratory and Hurricane Research Division
- NOAA National Weather Service – Miami Office
- BECON-TV (Broward Education Communications Network)
- International Hurricane Protection Association
- Florida Power & Light
- American Red Cross
- Humane Society of Broward County
- Many other organizations and non-profits

Special guest:

- Grant Goodwin, HLMP Program Manager, Bureau of Mitigation, Florida Division of Emergency Management

Various distinguished hurricane experts participated:

- Neal Dorst, Hurricane Researcher, NOAA/AOML/HRD
- Stanley B. Goldenberg, Research Meteorologist, NOAA/AOML/HRD
- Robert Molleda, Warning Coordination Meteorologist, National Weather Service-Miami

Special interactive exhibits and demonstrations included:

- IHPA Live Air Cannon Demonstrations Showing Debris Impact of Shutters and Windows
- BECON-TV Hurricane Broadcast Center
- FIU NSF-NHERI Wall of Wind Exhibit and Researcher Talks
- FIU Meteorology Student Demonstrations
- MODS Live Weather Science Demonstrations
- MODS Windy Weather Activities for Kids
- Special Showings of Built to Last? Resilience Documentary in IMAX Theater
- Weather Jeopardy Game
- Touch a Truck – Emergency Response and Recovery Vehicles

Special live interactive theater presentations:

- Tsunami Tim Live Weather Education Theater Shows
- Mike Mogil How the Weather Works Live Weather Education

Partner Mascots:

- *Sparky the Fire Dog* - City of Fort Lauderdale Emergency Management
- *Joey the Otter* - Museum of Discovery and Science Joey the Otter Mascot
- *Dazzlers Spirit Team* - Florida International University

Assessment Activities:
Participant Post Survey Questions for Event Attendees:

1. Did you attend the 2023 Eye of the Storm event?
2. To what extent did this event increase your knowledge about how wind engineering can mitigate hurricane damage?
3. To what extent are you interested in learning more about wind engineering?
4. To what extent will you be taking to steps to mitigate hurricane damage to your property?
5. How many times have you attended the Eye of the Storm Event?

Positive Survey Results:

- 80.2% increased their knowledge about wind engineering and mitigating hurricane damage.
- 73.6% would like to learn more about wind engineering.
- 81.4% will be taking steps to mitigate hurricane damage.
- 81.4% were first time attendees of the event.

Message Board #1 During Event:
What did you learn today about protecting your home from hurricanes?

- *I learned that I need to shut my shutters.*
- *A hip roof is the best type of roof to protect from hurricanes.*
- *No tape on the windows.*
- *I learned that you need to have shutters on your window because if not your window will break.*
- *I would need to do research to find assistance/guidance in preparing for hurricane season.*
- *I learned you need to stock up food that does not need to be refrigerated in case of power outages.*
- *Be prepared early.*
- *Put up shutters and use bags of sand for flood.*

Message Board #2 During Event:
Would you like to study wind engineering in school?

- *Yes, I want to study wind engineering.*
- *I think wind engineering would be a good thing to teach kids about in school because it can lead to better engineers in the future, especially in architecture. I also think it sounds interesting.*

Message Board #3 During Event:
What are your thoughts on today's events?

- *Super awesome fun day. I loved it. Thank you, MODS.*
- *Today's events were very important and interesting.*
- *My thoughts on today's events were informative, fun, and educational.*
- *I absolutely love this event. It gives kids the opportunity to grow their knowledge and make something beautiful out of it. I also love the rides.*
- *Loved it!*
- *Great ! I've learned so much so far and making so many memories. I love this museum and I hope everyone loves it too!*
- *I loved Tsunami Tim show.*
- *Awesome.*
- *My thoughts – This is amazing ! Teaching kids science is so important.*
- *I really love The Eye of the Storm Event.*
- *Today's events were nice because the kids got exposed to different situations and how to prepare for them.*
- *My thoughts on today's events are that today was the best day of my life !!!*

Kahoot! Education Quiz Questions Before Live Theater Shows:

- The Florida Division of Emergency Management recommends Florida residents do what for hurricane season?
- In what year did Hurricane Andrew make landfall over South Florida?
- What type of shutter is strongest against flying hurricane debris?

- Florida has seen the most hurricane landfalls in what month?
- Which roof shape is best in a hurricane wind?
- What items should you have in your disaster supply kit?
- What category of hurricane can tape be used to protect a window?
- When is it OK to open a window just a little bit before a hurricane?
- What do wind engineers do?
- What is the purpose of the NSF-NHERI Wall of Wind at Florida International University?
- What is the highest hurricane category the NSF-NHERI Wall of Wind at FIU can generate?

Weather Jeopardy Categories:

- Hurricanes 101
- Know Your Zone
- Don't Blow Away
- Whacky Weather

The Eye of the Storm received great coverage by the local South Florida media. This resulted in great positive visibility in the community for IHRC, FIU and FDEM's message of hurricane preparedness and mitigation.

- Museum of Discovery and Science 'Eye of the Storm' Event – NBC 6 South Florida (nbcmiami.com)

The following local South Florida media representatives participated in person:

- Phil Ferro, Chief Meteorologist, WSVN-TV (FOX)
- Vivian Gonzalez, Meteorologist, WSVN-TV (FOX)
- Betty Davis, Chief Meteorologist, WPLG-TV (ABC)
- Brandon Orr, Meteorologist, WPLG-TV (ABC)

Digital Marketing Campaign Summary

- Impressions: 8,353,528+

Facebook Posts

- Impressions: 272,580+

Twitter Posts

- Impressions: 90,158+

Instagram Posts

- Impressions: 55,651+

LinkedIn Posts

- Total Impressions: 649

Print and Digital:
Total: Visitors/Viewership: 2,001,022

- Eye of the Storm | Visit Lauderdale Website | April 5, 2023 | Unique Monthly Visitors: 35,280

- Eye of the Storm | Living FLA Website | April 5, 2023 | Unique Monthly Visitors: 2,130
- Eye of the Storm | Sun Sentinel Website | April 10, 2023 | Unique Monthly Visitors: 1,540,420
- Eye of the Storm | Patch Website | April 10, 2023 | Unique Monthly Visitors: 1,352,021
- Eye of the Storm | WPLG Website | April 10, 2023 | Unique Monthly Visitors: 552,990
- Eye of the Storm | Macaroni Kid Website | April 10, 2023 | Unique Monthly Visitors: 63,810
- Eye of the Storm | South Florida on the Cheap Website | April 10, 2023 | Unique Monthly Visitors: 36,780
- Eye of the Storm | Boca Raton Observer Website | April 10, 2023 | Unique Monthly Visitors: 15,210
- Eye of the Storm | CitySpark Website | April 10, 2023 | Unique Monthly Visitors: 14,580
- Eye of the Storm | GoRiverwalk Website | April 10, 2023 | Unique Monthly Visitors: 13,580
- Eye of the Storm | South Florida Family Life Website | April 10, 2023 | Unique Monthly Visitors: 6,390
- Eye of the Storm | OutClique Magazine Website | April 20, 2023 | Unique Monthly Visitors: 8,070
- Eye of the Storm | Fort Lauderdale Magazine Website | April 20, 2023 | Unique Monthly Visitors: 7,290
- Eye of the Storm | Miami Moms Website | April 21, 2023 | Unique Monthly Visitors: 11,400
- Eye of the Storm | Easy 93.1 Website | May 14, 2023 | Unique Monthly Visitors: 26,690
- Eye of the Storm | Hits 97.3 Website | May 14, 2023 | Unique Monthly Visitors: 23,800
- Eye of the Storm | WTVJ-NBC | May 12, 2023 | Nielsen Audience: 12,105 | Calc Publicity Value: $1,680
- Eye of the Storm | NBC Miami Website | May 12, 2023 | Unique Monthly Visitors: 706,654
- Eye of the Storm | Moody Radio Website | May 18, 2023 | Unique Monthly Visitors: 64,680
- Eye of the Storm | 99 Jamz Website | May 18, 2023 | Unique Monthly Visitors: 9,120
- Eye of the Storm | WSVN Website | May 20, 2023 | Unique Monthly Visitors: 339,777
- Eye of the Storm | WSVN-FOX | May 20, 2023 | Nielsen Audience: 34,257 | Calc Publicity Value: $3,200
- Eye of the Storm | WPLG-ABC | May 21, 2023 | Nielsen Audience: 53,839 | Calc Publicity Value: $12,915

2020 Virtual Eye of the Storm: Update as of June 6th, 2023

The 2020 virtual Eye of the Storm, the 12-episode "evergreen" video series, was re-promoted in conjunction with the Eye of the Storm in-person event on May 20th. The video series continues to be promoted during the current hurricane season by MODS, IHRC, and many of the partners who attended on May 20th.

All the videos are listed on the MODS virtual Eye of the Storm webpage and YouTube page:
Virtual Eye of the Storm - Museum of Discovery & Science | IMAX AutoNation (mods.org)
Eye of the Storm 2020 - YouTube
All the videos are also listed on the following MyFloridaCFO web-page:
Plan Prepare Protect: Are You Disaster Ready? Resources (myfloridacfo.com)

The virtual Eye of the Storm has resulted in a hugely successful digital marketing campaign and has expanded the reach and impact beyond South Florida to other states on the Gulf of Mexico and the U.S. eastern seaboard at risk of a hurricane landfall.

The Eye of the Storm virtual series continues to be an outstanding success:

- A reach of more than 133,510,220+ impressions for the entire digital marketing and public relations campaign.
- Social media channels included Facebook, Twitter, Instagram, LinkedIn, and YouTube.
- The Museum utilized Google Display and Search Ads and My Business Posts.
- Museum marketing included slides in the AutoNation IMAX Theater, article in the Museum's What Will You Discover? magazine, emails to 88,000+ subscribers, webpage with link to videos and Facebook event page.
- Calendar listings and articles were featured in fifty publications and media with a circulation of 45,328,368.

Fort Lauderdale First Responder Vehicles

Live Weather Safety Theater Shows

FIU Wall of Wind Exhibit & FIU Dazzlers

BECON-TV Hurricane Broadcast Center

Florida Division of Emergency Management

Broward County Emergency Management

Humane Society of Broward County

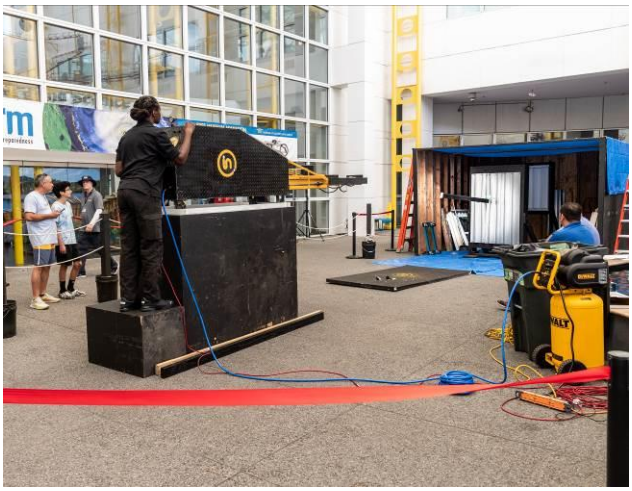

Live Air Cannon Missile Demonstrations

Fort Lauderdale Emergency Management

Fort Lauderdale Police

Families Building Houses for Wind Testing

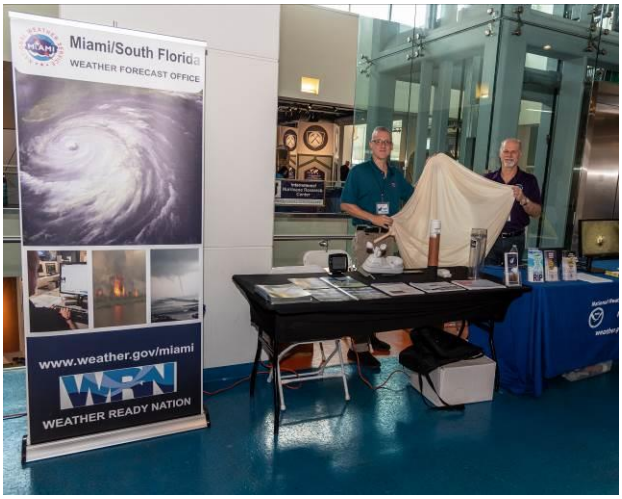

National Hurricane Center & NWS-Miami

Important Preparedness Messages

City of Hollywood CERT Team

United Way of Broward County

NOAA Hurricane Research Division

Broward County Office of Resilience

MODS Exploding Cloud Demonstration

WLRN Public Media

WPLG-TV Local 10 News